MODELING *DEPDC5* MUTATIONS IN EPILEPSY USING PATIENT-DERIVED CELLS AND A GENETIC MOUSE MODEL

By

Lindsay K. Klofas

Dissertation

Submitted to the Faculty of the

Graduate School of Vanderbilt University

in partial fulfillment of the requirements

for the degree of

DOCTOR OF PHILOSOPHY

in

Neuroscience

June 30, 2020

Nashville, Tennessee

Approved:

Rebecca A. Ihrie, Ph.D. (Committee Chair)

Bruce Carter, Ph.D.

Jeffrey Rathmell, Ph.D.

Kevin C. Ess, M.D., Ph.D. (Co-Mentor)

Robert P. Carson, M.D., Ph.D. (Mentor)

Copyright © 2020 by Lindsay K. Klofas
All Rights Reserved

ACKNOWLEDGMENTS

Thank you to my mentor, Dr. Rob Carson, for giving me the opportunity to shape this new project and for giving me the independence in lab that allowed me to build my critical thinking skills. Your continual pursuit of translationally-relevant research questions is an inspiration.

Thank you to my co-mentor, Dr. Kevin Ess, for the support, encouragement, and feedback throughout the years. You have helped me hone my ability to critically evaluate scientific work and taught me about the nuances of the physician-scientist career path.

To John Snow, I have been so lucky to have gone through this process with you across the lab. You are a meticulous, thoughtful scientist and I benefit from your example. Thank you for forging the path with neuronal differentiation protocols and MEA analysis and for always being generous of your time to discuss new data and important trivia questions.

To the resident amateur ornithologist, Brittany Parker Short, this work truly would not have been possible without you. Your enthusiasm for science is infectious and you are always willing to go above and beyond in the lab. You have been the best benchmate, color-coder, tube labeler, and mouse handler I could have ever asked for. You are the perfect balance to this introvert.

To Grant Westlake, Lord of Stonehenge, thank you for helping me find reagents, for teaching me the basics of stem cell culture, for always keeping highly secret backups of nearly all reagents and consumables, and for the laughs along the way.

Thank you to all the other past and present members of the Carson, Ess, and Fu labs for your support and encouragement, and, very importantly, for feeding cells when I was away.

Thank you to the Vanderbilt MSTP, especially to Dr. Terry Dermody, the MSTP director upon my admission to Vanderbilt, and to Dr. Chris Williams, the current MSTP director, who both have given generously of their limited time to mentor and advise students. To my entering MSTP class, the laughs and commiserations helped me get through the toughest parts of graduate school.

Thank you to my committee members, Dr. Bruce Carter and Dr. Jeff Rathmell for their support, guidance, and collaboration. Thank you to Dr. Rebecca Ihrie, who I first met during my Vanderbilt interview in 2013, for serving as my committee chair but also as a guide, mentor, role model, and collaborator throughout this process, and who has also given generously of her time.

To my parents, who were supportive when I told them I had decided to move to Tennessee for a decade and have patiently waited for me to return to New England ever since, who have been supportive through our daily phone calls and are never disappointed when the answer to "Did you make progress today?" is always, at best, "Incremental."

To my son, Addison, who always put a smile on my face when I came home after even the most trying of days, because he knows that doctors say "No no!" (to monkeys jumping on the bed). Thank you to our nanny, Maggie McDaniel, whose care of Addison let me spend my days in lab thinking about science and performing experiments, confidently knowing that my son was in excellent hands.

To my husband, Krystian, thank you for your constant unwavering support. I love that we have similar career paths and that we can come home at the end of the day and enthusiastically discuss mundane experimental issues like the proper number of technical replicates, express frustration over experimental failures, and excitedly speculate when new potential hypotheses arise. You have been so helpful through this process, from the best days of graduate school to the worst, and I could not have done it without you.

TABLE OF CONTENTS

Page

ACKNOWLEDGMENTS ..... **iii**

LIST OF FIGURES ..... **vi**

LIST OF TABLES ..... **vii**

LIST OF ABBREVIATIONS ..... **viii**

CHAPTER

1. Introduction to Epilepsy, mTOR signaling, and the GATOR1 complex **1**

Background and History of Epilepsy 1
Characterization of Clinical Epilepsy 2
Definition of epilepsy 2
Genetic causes of epilepsy 4
Cortical Development and Mechanisms of Epilepsy 6
The mTOR Signaling Pathway 8
Discovery of mTOR 8
mTORC2 9
mTORC1 10
Upstream regulation of mTORC1 12
Identification and function of the GATOR1 complex 15
Mutations in *DEPDC5* as a Cause of Epilepsy 18
Role of mTOR in Neurodevelopment and Neurological Disease 22
Developmental windows of mTOR regulation 23
mTOR role in dendritic arborization, synaptic regulation 24
mTORC1 role in regulation of cell size and neuronal migration 25
Autophagy in neurons 26
DEPDC5 Mutations and Epilepsy: Current Models and Mechanisms 26
Expression of DEPDC5 and GATOR1 in the brain and during development: 26
Impact of GATOR1 loss of function 27
Effects in heterozygous animal models 27
Conditional animal models 29
Summary and Project Rationale 30

2. *DEPDC5* haploinsufficiency drives increased mTORC1 signaling and abnormal morphology in human cortical neurons **33**

Abstract 33
Introduction 33
The need for human models of *DEPDC5* mutation 34
Induced pluripotent stem cells: value in studying neurological disease 35
Results 38
Generation of iPSCs from epilepsy patients with *DEPDC5* mutations. 38
Validation of iPSCs 42
Decreased *DEPDC5* mRNA and NPRL2 protein in *DEPDC5*$^{+/-}$ iPSCs suggests impaired GATOR1 expression 42
Increased activation of mTORC1 signaling in iPSCs from patients with *DEPDC5*-related epilepsy 49
Dynamics of mTOR signaling activity in response to rapamycin and nutrient-stimulation differ in *DEPDC5*-mutant cells. 52
Therapeutic potential of drugs promoting readthrough of premature termination codons 58
Derivation of neuroprogenitor cells and neurons from induced pluripotent stem cells 60
Cytomegaly and increased mTORC1 activation in *DEPDC5*-mutant neuroprogenitor cells. 63

Cytomegaly in *DEPDC5*$^{+/-}$ neurons is ameliorated by mTORC1 inhibition with rapamycin 63
Cytomegaly persists in post-mitotic neurons heterozygous for *DEPDC5* mutation 64
Post-mitotic neurons have elevated mTORC1 activity that persists after amino acid deprivation 68
Discussion 71
Methods 74
Generation and validation of iPSCs from epilepsy patients with *DEPDC5* mutations. 74
mRNA quantification. 75
Immunofluorescence 76
Immunoblotting 76
Doubling time assays. 79
Flow cytometry – iPSCs. 79
Generation of cortical neural progenitor cells and neurons from iPSCs 80
Neuronal size analysis. 80
Nutrient starvation assays. 81
Statistical analysis and controls 81

3. Prevention of premature death and seizures in a Depdc5 mouse epilepsy model through inhibition of mTORC1 83

Abstract 83
Introduction 84
Results 86
Generation of *Depdc5-Emx1*-Cre CKO transgenic mice 86
Depdc5-CKO mice have decreased life expectancy with terminal seizures 86
Depdc5-CKO mice have abnormally thickened cortex with cytomegalic neurons 90
Depdc5-CKO astrocyte cultures demonstrate increased mTORC1 activation 94
Depdc5-CKO mice show alterations of inhibitory neurotransmission 96
Rapamycin extends survival of *Depdc5*-CKO mice and reduces seizure frequency, even after withdrawal 98
Discussion 100
Materials and Methods 103
Generation of CKO mouse model 103
Genotyping 103
Seizure threshold testing with flurothyl 104
Immunofluorescence 104
Cell size 105
Rapamycin treatment 105
Immunoblotting 105
Primary mouse astrocyte cultures 106
Semi-quantitative RT-PCR from primary mouse astrocyte cultures 107
Brain slice preparation and whole-cell recordings 107

4. Future Directions and Discussion 110

Summary 110
The role of gene dosage in *DEPDC5*-related epilepsy and potential brain-specific effects 110
Functional evaluation of neurons: alternative differentiation protocols 115
mTORC1 and epileptogenesis: defining specific mechanisms 116
Therapeutic use of mTOR inhibitors for epilepsy patients 120
Conclusion 121

References 122

LIST OF FIGURES

Figure **Page**
Figure 1-1. Diagram of generalized-onset versus focal-onset seizures. 6
Figure 1-2. Unique components define mTOR complex 1 and mTOR complex 2. 9
Figure 1-3. Simplified diagram of major pathways downstream of mTORC1. 11
Figure 1-4. Activation of mTORC1 is dependent on detection of both amino acids and growth factors. 13
Figure 1-5. Upstream regulators of mTORC1. 14
Figure 1-6. GTPase-activating proteins (GAPs) increase the rate of GTP hydrolysis by G proteins. 16
Figure 1-7. DEPDC5 serves as a scaffold to facilitate interaction of NPRL2 and NPRL3 with the Rag GTPases. 18
Figure 1-8. Timeline of clinical and biochemical discoveries related to the GATOR1 complex, its function as a regulator of mTORC1, and its link to epilepsy. 19
Figure 1-9. Neuronal consequences of hyperactive mTORC1 signaling. 22
Figure 2-1. Dual SMAD inhibition drives differentiation of pluripotent cells toward a neuronal fate. 37
Figure 2-2. Pedigrees of epilepsy patient families suggest an autosomal dominant inheritance pattern. 39
Figure 2-3. Locations of mutation variants in iPSCs generated from patients with epilepsy and *DEPDC5* mutations. 40
Figure 2-4. Validation of control induced pluripotent stem cell lines. 44
Figure 2-5. Validation of patient-derived induced pluripotent stem cell lines. 45
Figure 2-6. PluriTest results indicate passing pluripotency scores in all lines yet borderline novelty scores in three lines. 46
Figure 2-7. iPSCs generated from epilepsy patients with *DEPDC5* mutations demonstrate decreased *DEPDC5* mRNA expression. 47
Figure 2-8. NPRL2 expression is decreased in $DEPDC5^{+/-}$ patient iPSCs. 48
Figure 2-9. Elevated mTORC1 signaling in $DEPDC5^{+/-}$ patient iPSCs. 50
Figure 2-10. $DEPDC5^{+/-}$ patient iPSCs demonstate a more rapid doubling time that is slowed with rapamycin. 51
Figure 2-11. Experimental and gating strategy for flow cytometry studies. 54
Figure 2-12. Divergent responses to rapamycin and nutrient stimulation in $DEPDC5^{+/-}$ iPSCs. 55
Figure 2-13. Temporal response of iPSCs to refeeding after nutrient starvation. 56
Figure 2-14. Biaxial plots demonstrate mTOR pathway changes following rapamycin treatment specific to $DEPDC5^{+/-}$ iPSCs. 57
Figure 2-15. Forced pharmacologic readthrough of a premature translation codon attenuates mTORC1 activity in $DEPDC5^{+/-}$ iPSCs with R874X mutation. 59
Figure 2-16. Differentiation of cortical neurons from iPSCs. 61
Figure 2-17. Immunofluorescent images of neuroprogenitor cells and physical synapses. 62
Figure 2-18. $DEPDC5^{+/-}$ patient neuroprogenitor cells (NPCs) are cytomegalic with increased mTORC1 signaling. 65
Figure 2-19. Cytomegalic $DEPDC5^{+/-}$ neurons are sensitive to mTORC1 inhibition. 66
Figure 2-20. Post-mitotic neurons haploinsufficient for *DEPDC5* continue to display larger cell size. 67
Figure 2-21. $DEPDC5^{+/-}$ neurons have elevated mTORC1 activity at baseline but remain sensitive to starvation. 69
Figure 2-22. P-S6 (S240/244) in $DEPDC5^{+/-}$ neurons is further decreased after two hours of nutrient starvation. 70
Figure 3-1. Generation of Depdc5F/FEmx1-Cre CKO mice and genotyping strategy. 88
Figure 3-2. *Depdc5-Emx1* CKO mice display changes in gross brain/body weight and demonstrate both seizures and reduced survival. 89
Figure 3-3. Neurohistologic abnormalities in CKO animals. 91
Figure 3-4. Immunofluorescent staining with the layer II-IV marker Cux1 demonstrates a greater number of ectopic neurons present in the CKO than the control. 92
Figure 3-5. CKO mice at P19 do not demonstrate increased astrogliosis. 93
Figure 3-6. Astrocyte cultures from CKO mice display increased mTORC1 activation. 95
Figure 3-7. Brain slice cultures from CKO mice demonstrate increased capacitance and changes in inhibitory neurocircuitry. 97
Figure 3-8. Rapamycin treatment prolongs survival even after withdrawal. 99
Figure 4-1. Changes in protein expression in GABAergic neurons heterozygous for *DEPDC5* mutation. 114
Figure 4-2. Using MEA analaysis to assess functional impacts of *DEPDC5* haploinsufficiency. 116
Figure 4-3. Correction of the 2620C>T mutation in iPSCs restores wild-type levels of DEPDC5 mRNA expression. 118

LIST OF TABLES

Table **Page**
Table 1-1. Definition of epilepsy according to the International League of Epilepsy. 3
Table 1-2. Seizure classification by region of onset according to the International League of Epilepsy, 2017....3
Table 1-3. Effects of mTOR hyperactivation at various time points during cortical development. 24
Table 1-4. Summary of heterozygous phenotypes seen in published genetic animal models of *Depdc5* loss. 29
Table 2-1. Additional characteristics of patients with *DEPDC5* mutations and epilepsy from whom iPSC lines were generated. 41
Table 2-2. *DEPDC5* sequencing primers. 75
Table 2-3. Assays used for quantitative RT-PCR. 76
Table 2-4. Antibodies used for immunocytochemistry (IF), immunoblot (WB), and flow cytometry (FC). 77
Table 2-5. Specific iPSC clones used in individual experiments. 82
Table 3-1. *Depdc5*^{Emx1} mice are born at a Mendelian ratio. 86
Table 3-2. List of primary antibodies. 106

LIST OF ABBREVIATIONS

CASTOR	Cellular arginine sensor for mTORC1
DEP	Disheveled, Egl-10, and Pleckstrin
DEPDC5	DEP domain-containing protein 5
DEPTOR	DEP domain containing mTOR-interacting protein
DMEM	Dulbecco's modified Eagle's medium
E#	Embryonic day of life #
ESC	Embryonic stem cell
EMX1	Empty spiracles homeobox 1
FCD	Focal cortical dysplasia
FGF2	Fibroblast growth factor 2
FKBP12	12-kDa FK506-binding protein
FLCN/FNIP	Folliculin/folliculin-interacting protein
GAP	GTPase activating protein
GATOR	GAP activity toward Rags
GEF	Guanine exchange factor
GTP	Guanosine triphosphatase
iPSC	Induced pluripotent stem cell
IRS1	Insulin receptor substrate 1
KICSTOR	KPTN, ITFG2, C12orf66, and SZT2-containing regulator of mTORC1
mEPSC	Miniature excitatory postsynaptic current
mIPSC	Miniature inhibitory postsynaptic current
mLST8	Mammalian lethal with sec13 protein 8
mSIN1	Mammalian stress-activated MAP kinase-interacting protein
mTOR	Mechanistic target of rapamycin
mTORC1	Mechanistic target of rapamycin complex 1
mTORC2	Mechanistic target of rapamycin complex 2
NPC	Neuroprogenitor cell

NPRL2	Nitrogen permease regulator-like 2
NPRL3	Nitrogen permease regulator-like 3
P#	Postnatal day of life
PBS	Phosphate buffered saline
PFA	Paraformaldehyde
PRAS40	Proline-rich Akt substrate of 40 kDa
PROTOR	Proteins observed with rictor
PTEN	Phosphatase and tensin homolog
p-4E-BP1	Phosphorylated eukaryotic translation initiation factor 4E (eIF4E)-binding protein 1
p-AKT	Phosphorylated Akt
p-S6	Phosphorylated ribosomal protein S6
RAPTOR	Regulator-associated protein of the mammalian target of rapamycin
RHEB	Ras homolog enriched in brain
RICTOR	Rapamycin-insensitive companion of mTOR
shRNA	Short-hairpin ribonucleic acid
SAMTOR	S-adenosylmethionine sensor upstream of mTORC1
SUDEP	Sudden unexpected death due to epilepsy
SYN1	Synapsin 1
TSC	Tuberous sclerosis complex

CHAPTER I

INTRODUCTION TO EPILEPSY, MTOR SIGNALING, AND THE GATOR1 COMPLEX

Background and History of Epilepsy

Epilepsy, a disorder of recurrent seizures, originates from the word "epilepsia," meaning "to take hold" of or "to seize." This is a reference to the original conception of epilepsy, several millennia ago, as a disorder of spiritual possession. Indeed, a Babylonian tablet details various types of seizures that are clinically recognized today, with each type attributed to a different demon or spirit (Wilson and Reynolds, 1990). The view of epilepsy as an intrinsic brain disorder did not take hold until much later. While the physician or group of physicians known as Hippocrates suggested as much in 400 B.C., it was thought to be a revolutionary idea at the time. It was not until the 19th century that the physician John Hughlings Jackson[1] proposed that seizures were caused by "nervous discharges" in the brain, discharges that he thought to be of chemical origin (York and Steinberg, 2007).

These sudden, excessive discharges in the brain were further characterized as electrochemical with the advent of the electroencephalogram, or EEG, developed in the 1920s, which allowed physicians to directly witness the aberrant electrical firing in the brain leading to seizures. The first clinical anti-seizure drugs were also developed in the early 20th century: phenobarbital and phenytoin, which pharmacologically modulate different ion channels in the brain to reduce excitability (Brodie, 2010). The modern use of the ketogenic diet was also developed around this time, with Drs. Stanley Cobb and W.G. Lennox noting that starvation seemed to induce an improvement in seizures (reviewed in D'Andrea Meira et al. (2019). Development of neuroimaging techniques much later eventually led to the identification of structural brain lesions, which were posited to be causative or contributive to epilepsy; indeed, the link between structural brain lesions and epilepsy will be discussed further below.

[1] Of "Jacksonian march" fame, also a contemporary of Charles Brown-Séquard (Brown-Séquard syndrome) and Paul Broca (Broca's area of language comprehension), Jonathan Hutchinson ("Hutchinson's teeth," a sign of congenital syphilis), and Robert Bentley Todd ("Todd paralysis"), reflecting the extraordinary advances occurring in the understanding of neurobiology and neurological disease at the time. Hughlings Jackson's life's work on evolutionary neurophysiology and the theory of cerebral localization is reviewed in York, G.K., and Steinberg, D.A. (2007). An Introduction to the Life and Work of John Hughlings Jackson: Introduction. Med Hist Suppl, 3-34.

In recent years, we are within a modern revolution in the understanding of epilepsy as we begin to acknowledge the genetic origins of many epilepsies. If epileptic convulsions are, as Hughlings Jackson posited, 'the result of experiments made by disease on the brain of man," the genetic alterations that occur are these experiments (Pierce, 2002). In the following chapters, I delve into one specific molecular pathway, mutations in which are responsible for greater than 10% of localized epilepsies.

The story of the discovery of the role of the GATOR1 (GAP activity toward Rags) complex is a harmony of clinical research studies and biochemical mechanistic discoveries. The GATOR1 complex (consisting of proteins DEPDC5, NPRL2, and NPRL3) was identified in 2013 by Bar-Peled *et al*. of the David Sabatini laboratory, who himself was one of the first scientists to characterize the mammalian/mechanistic target of rapamycin (mTOR) kinase. That same year, multiple reports were published identifying *DEPDC5* mutations as causative for focal epilepsies, with subsequent identification of *NPRL2* and *NPRL3* mutations as well. The GATOR1 complex was ultimately shown to act as a GTPase-activating protein toward the RagA/B GTPases. The Rag GTPases are critical modulators of mTOR signaling that recruit mTORC1 to the lysosome when amino acids are present, where it can then be activated by Rheb, another small GTPase originally defined as Ras homolog enriched in brain. Dysregulated mTOR signaling is a well-known causal and contributory factor of neurological disease (Lipton and Sahin, 2014). Thus, GATOR1 loss-of-function mutations join the class of neurological diseases known as "mTORopathies," diseases due to dysregulated and increased signaling of mTOR.

Characterization of Clinical Epilepsy

Definition of epilepsy

Epilepsy is a condition of recurrent, unprovoked seizures (**Table 1-1**) (Fisher et al., 2014). As one of the most common brain disorders, epilepsy affects close to 1% of the world's population (Thijs et al., 2019). Seizures describe spontaneous bursts of electrical activity in the brain and can manifest in diverse forms, ranging from brief "absence" seizures to prolonged convulsions. Epilepsies are categorized in several different ways, with classifications most recently revised by the International League of Epilepsy in 2017 (**Table 1-2**) (Fisher et al., 2017; Scheffer et al., 2017). The starting point of

the epilepsy classification scheme is the location from which seizures originate in the brain. From this, epilepsy types can be described and classified into various epilepsy syndromes, each with diverse etiologies.

Definition of epilepsy:
1) At least two unprovoked (or reflex) seizures occurring more than 24 hours apart
2) One unprovoked (or reflex) seizure and a probability of further seizures similar to the general recurrence risk (at least 60%) after two unprovoked seizures, occurring over the next ten years
3) Diagnosis of an epilepsy syndrome

Table 1-1. Definition of epilepsy according to the International League of Epilepsy.
(Fisher et al., 2014).

Generalized onset	Focal onset	Unknown onset
Motor	**(Aware vs. impaired awareness)**	**Motor**
Tonic-clonic	**Motor**	Tonic-clonic
Tonic	Automatisms	Epileptic spasms
Clonic	Atonic	**Non-motor**
Myoclonic	Clonic	Behavior arrest
Myoclonic-tonic-clonic	Epileptic spasms	
Myoclonic-atonic	Hyperkinetic	
Atonic	Myoclonic	
Epileptic spasms	Tonic	
Non-motor (absence)	**Non-motor**	
Typical	Autonomic	
Atypical	Behavior arrest	
Myoclonic	Cognitive	
Eyelid myoclonia	Emotional	
	Sensory	

Table 1-2. Seizure classification by region of onset according to the International League of Epilepsy, 2017
(Fisher et al., 2017; Scheffer et al., 2017).

Seizures are classified as either generalized or focal. Generalized seizures arise in both hemispheres of the brain simultaneously, demonstrating "ictal" activity in all EEG leads (**Figure 1-1A**). Generalized seizures, by definition, involve impairment of consciousness but can have a wide range of manifestations. For example, in absence seizures, consciousness is suddenly but briefly impaired, whereas in tonic-clonic seizures, sometimes referred to as "grand mal," patients have a loss of consciousness accompanied by tonic stiffening, followed by motor jerking activity. Focal seizures initiate in localized networks in the brain that are spatially limited, thus EEG demonstrates abnormalities in only those leads (**Figure 1-1B**). The semiology, or symptomatic manifestations, of focal seizures depends on the location. For

example, seizures involving motor activity are likely to originate from the contralateral frontal lobe, whereas seizures with oral automatisms (lip-smacking, etc.) likely originate from the temporal lobe. Focal seizures have the potential to progress to generalized seizures, however it is important to distinguish between focal seizures with secondary generalization and generalized seizures.

Seizure classification provides a framework for diagnosis and treatment and allows for the defining of epilepsy syndromes, which can help guide potential pharmacological therapies. While epilepsies comprise differing groups of syndromes with various etiologies, at the core, epilepsy is thought to be due to an imbalance between excitatory and inhibitory cellular inputs, resulting in aberrant network hyperexcitability. An abundance of excitatory inputs or a paucity of inhibitory inputs contributes to a hyperexcitable state resulting in seizures. Different mechanisms can contribute to different sides of this equation. Acquired causes include infection, stroke, trauma, neoplasms, and autoimmune diseases, however this dissertation will focus on genetic and inherited rather than acquired causes of epilepsy.

Genetic causes of epilepsy

As little as thirty years ago, an epileptologist would not have been expected to have a grasp of genetics. With current knowledge that epilepsies can be inherited or due to a sporadic mutation, epilepsy sequencing panels in 2020 now include hundreds of genes. In the era of genetic sequencing, it is becoming standard of care to sequence blood or tissue from patients suspected to be carrying an epilepsy-causing mutation.

Multigenerational families with epilepsy led to the identification of the first epilepsy-related genes, including *SCN1A*, *CHRNA4*, *KCNQ2*, *KCNQ3*, and *SCN2A*. Notably, almost all inherited mutations are in ion channels, which regulate the electrical homeostasis of the cell. For example, mutations have been identified in the GABA receptor, various sodium channels, subunits of the nicotinic acetylcholine receptor, and various potassium channels. Mutations in non-ion channel proteins are less common. For example, mutations in *LGI1*, which encodes leucine-rich glioma inactivated 1, a protein involved in cell adhesion as well as in synaptic maturation, cause a rare familial lateral temporal lobe epilepsy (Fukata et al., 2017). Mutations in proteins that form the GATOR1 complex, a negative regulator of mTOR which this chapter will discuss in detail, are also non-ion channel mutations that are causative for a variety of focal epilepsies.

Most of the anti-seizure medications available target ion channels in order to reduce the hyperexcitability and synchronicity that leads to seizures. These medications are sufficient to achieve long-term remission in over two-thirds of patients with epilepsy (Thijs et al., 2019). While symptomatic modulation of seizures is certainly achieved in most cases, it is possible that these medications are less effective when the pathophysiology of the epilepsy is not directly due to a mutation in an ion channel. Patients with GATOR1 mutations, for example, have been reported to have an especially high rate of drug resistance, up to 78% (Baulac et al., 2015; Picard et al., 2014). In these cases, alternative therapeutic strategies may be more successful. For example, in epilepsies due to GATOR1 mutations, modulating the characteristic hyperactive mTOR signaling may be an effective approach.

In the general population of individuals with epilepsy, one-third of patients have drug-resistant epilepsy in which they continue to have seizures despite trials of multiple anti-seizure medicines. Aside from a greatly diminished quality of life, uncontrolled epilepsy also conveys a higher risk of sudden unexpected death in epilepsy (SUDEP) (Nashef et al., 2012). The cause of SUDEP remains elusive, but some evidence from video-EEG studies suggests that SUDEP is the result of a convulsive seizure followed by apnea and asystole (Ryvlin et al., 2013). While the incidence of SUDEP is relatively low (about 1 per 1000 person-years), the peak age of incidence is quite young, between 20 and 40 years of age (Sveinsson et al., 2017; Thijs et al., 2019). Because of this, death due to SUDEP ranks only behind stroke in number of years of potential life lost due to neurologic disease, representing a significant public health burden (Thurman et al., 2014). GATOR1 mutations in particular have been linked to an increased risk of SUDEP (Bagnall et al., 2016; Bagnall et al., 2017; Nascimento et al., 2015). Because of the link to drug-resistant epilepsy and SUDEP, the discovery of new therapeutic strategies for GATOR1-related epilepsies would significantly improve public health. In order to identify novel pharmacological targets, an understanding of the underlying mechanisms that result in epileptogenesis is essential.

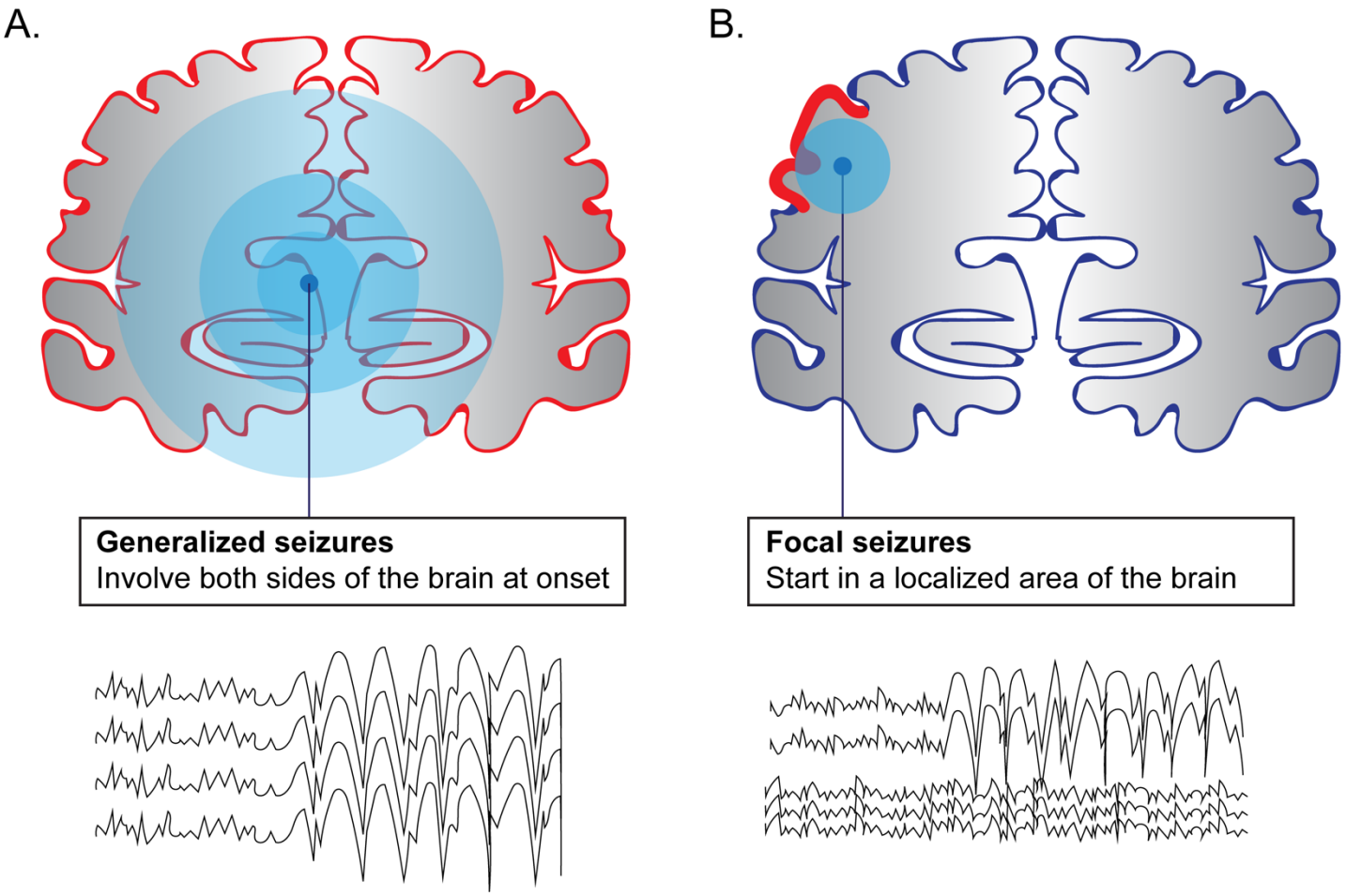

Figure 1-1. Diagram of generalized-onset versus focal-onset seizures.
(A) In seizures with generalized onset, abnormal electrical activity is detected in all areas of the cortex simultaneously. The trigger likely originates in the thalamus or reticular formation of the brainstem (represented generally by the central dark blue dot). Generalized-onset seizures thus involve loss of consciousness. Aberrant electrical activity is detected in all EEG leads. (B). Seizures with focal onset begin in a defined area of the cortex and are characterized by their initial manifestations. Aberrant electrical activity is thus only detected in EEG leads corresponding to the location of seizure onset. Patients with focal-onset seizures can go on to have secondary generalization of their seizures.

Cortical Development and Mechanisms of Epilepsy

This section will focus on mechanisms of epileptogenesis with particular attention to developmental and inherited causes. Acquired epilepsies are reviewed in Pitkanen et al. (2016) (epilepsy following ischemic stroke), Van Loo and Becker (2020) (ion channelopathies in acquired epilepsies), and Goldberg and Coulter (2013) (neural circuit dysfunction in acquired epilepsies). In order to discuss the neurodevelopmental origins of some epilepsies, it is important to briefly overview human cortical development (reviewed in greater detail elsewhere, such as Sun and Hevner (2014) and Fernández et al. (2016).

The nervous system originates from the neuroectoderm, which invaginates to form the neural tube during embryogenesis. The anterior portion of the neural tube forms the forebrain, from which the telencephalic vesicles rapidly expand to eventually become the cortex. Cortical development then occurs in three general phases: proliferation, migration, and functional maturation. First, stem/progenitor cells located in the ventricular zone (VZ) and subventricular zone (SVZ) proliferate and differentiate to generate neural precursor cells and glial cells. As the neural progenitor pool expands in the VZ/SVZ, changes in the pattern of cell division occur such that progenitors begin to divide asymmetrically. This division produces another neural progenitor cell in addition to one further differentiated cell that is committed to a specific neuronal fate. These committed cells follow along the path marked by the processes of radial glial cells, migrating toward the cortical plate as they reference specific molecular cues. The six-layered cortex is then generated "inside-out", with deep layers forming first and outer layers forming last. Each cortical layer has distinct markers by which resident neurons can be identified. This process generates the vast majority of neurons in the cortex, namely excitatory glutamatergic projection neurons. The remaining ~20% of neurons are GABAergic inhibitory interneurons, which regulate activity of local excitatory neurons through synaptic contacts. GABAergic interneurons are generated in the ganglionic eminences and initially migrate tangentially until they enter the cortical plate to find their final destinations. Following neuronal migration, cortical circuits are finely tuned by a combination of programmed apoptosis and synaptogenic events, which ultimately regulate the final number of neurons and their synaptic connections.

Disruption of any of these phases can have deleterious consequences, reviewed in detail in Bozzi et al. (2012). For example, if the neural precursor population is exhausted early in development, microcephaly will result (Kassai et al., 2014). Disruptions in migration can cause cortical malformations; for example, mutations in the extracellular glycoprotein protein Reelin result in lissencephaly (a smooth cortex lacking the typical folds called gyri) with cerebellar hypoplasia (D'Arcangelo, 2006; Guerrini and Parrini, 2010). Finally, defects in the remodeling of post-mitotic neuronal circuits can result in hyperexcitability. For example, *Lgi1*-mutant mice do not properly form glutamatergic synapses in the hippocampus, resulting in immature dendrites with a high density of branching and spines, which ultimately lowers the seizure threshold of these mice (Zhou et al., 2009b). A key signaling pathway in modulating aspects of all three phases of cortical development is the mTOR signaling pathway. Disruption of mTOR signaling during neurodevelopment can cause cortical malformations, synaptic dysregulation, and epilepsy (D'Gama et al., 2015; D'Gama et al., 2017; Kassai et al.,

2014). Even following normal development, dysregulated mTOR signaling in post-mitotic neurons can cause neurological dysfunction and epilepsy. The mTOR pathway in relation to neurologic disease will be further discussed next.

The mTOR Signaling Pathway

The mTOR signaling pathway is a central regulator of growth and proliferation and is dysregulated in various disease conditions, including cancers, brain malformations, and neurodegenerative diseases. Various diseases caused by dysfunction of the mTOR signaling axis have epilepsy as a feature, including tuberous sclerosis, focal cortical dysplasia, non-lesion focal epilepsies, and post-traumatic epilepsies (Lipton and Sahin, 2014). I will describe the regulation of the mTOR pathway with particular attention to the control of mTORC1 by nutrients. I will then focus on the role of mTOR signaling during neurodevelopment and how its dysregulation can contribute to brain malformations and epilepsies.

Discovery of mTOR

The discovery of an antifungal macrolide produced by soil bacteria on the Polynesian island called Rapa Nui (also known as Easter Island), eponymously christened 'rapamycin', led to the initial discovery and characterization of mTOR. The history of the discovery of mTOR is reviewed in further detail by one of the scientists fundamental in its initial characterization (Sabatini, 2017). Rapamycin was shown to have antigrowth and antiproliferative properties toward multiple different cell types, including human cells. We now know the mTOR signaling pathway to be a crucial nexus linking nutrient availability and organismal growth.

mTOR kinase is a large, highly-conserved serine-threonine kinase that is ubiquitously expressed in eukaryotic cell types and is a key controller of cell growth and proliferation (Lipton and Sahin, 2014). mTOR is the catalytic subunit of at least two distinct protein complexes, mTOR complex 1 (mTORC1) and mTOR complex 2 (mTORC2) (**Figure 1-2**). mTORC1 and mTORC2 have unique drug sensitivities, upstream regulators, downstream targets, and complexed proteins. Components common to both mTORC1 and mTORC2, in addition to mTOR, are mLST8 and DEPTOR. The defining component of mTORC1 is Raptor (regulatory protein associated with mTOR) (Hara et al., 2002; Kim et al., 2002). Other components include proline-rich Akt substrate of 40 kDa (PRAS40) and FKBP12, the latter of which inhibits mTORC1

when complexed with rapamycin (Sabatini et al., 1994; Sancak et al., 2007). The analogous defining component of mTORC2 is Rictor (rapamycin insensitive companion of mTOR); other unique components are proteins observed with rictor 1 and 2 (Protor1/2) and mammalian stress-activated MAP kinase-interacting protein 1 (mSin1) (Sarbassov et al., 2004).

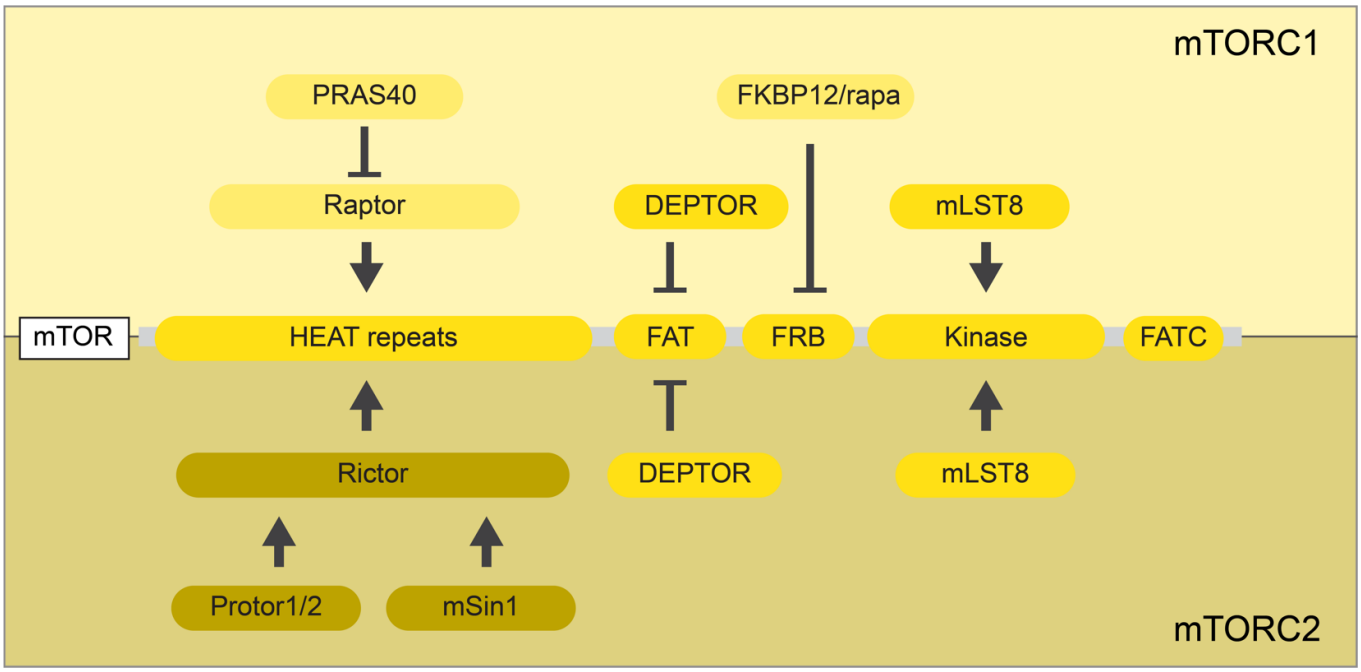

Figure 1-2. Unique components define mTOR complex 1 and mTOR complex 2.
mTOR kinase nucleates two distinct complexes, mTORC1 (top) and mTORC2 (bottom). mTOR has a domain of HEAT repeats, which interfaces with Raptor to form mTORC1 and Rictor to form mTORC2.

mTORC2

mTORC2 regulates cell proliferation and survival, including control of the actin cytoskeleton and thus cell remodeling and migration (Jacinto et al., 2004; Liu et al., 2010; Liu et al., 2019). mTORC2 also has a significant role in activating the PI3K/Akt pathway by phosphorylation of Akt at serine 473 (Sarbassov et al., 2005). Phosphorylated Akt can then engage in crosstalk with the mTORC1 signaling axis by inhibiting TSC2/tuberin, an upstream regulator of mTORC1 through Rheb (Inoki et al., 2002). mTORC2 signaling can in turn be regulated by mTORC1 signaling through insulin/PI3K signaling via mTORC1-induced phosphorylation and activation of Grb10, a negative regulator of insulin/IGF-1 signaling upstream of PI3K/Akt (Hsu et al., 2011; Yu et al., 2011). S6K1, a downstream effector of mTORC1, can also suppress mTORC2 by phosphorylating insulin receptor substrate 1 (IRS1), a positive upstream regulator of PI3K/Akt, leading to its

degradation (Harrington et al., 2004; Shah et al., 2004). Thus, it is possible for dysregulation of mTORC1 signaling to have reciprocal effects on mTORC2 signaling.

A defining feature of mTORC2 is its insensitivity to rapamycin, except perhaps when administered in a chronic fashion (Lamming et al., 2012; Sarbassov et al., 2006). Prolonged rapamycin treatment is hypothesized to diminish mTORC2 signaling due to the accumulation of FKBP12-rapamycin-mTOR complexes, which then may be unable to nucleate new mTORC2 complexes (Sarbassov et al., 2006). The impact of chronic rapamycin administration on mTORC2 is cell-type specific and may depend on baseline expression of mTOR (Sarbassov et al., 2006).

As the target of the GATOR1 complex, the remainder of this dissertation will largely focus on mTORC1. mTORC2 is extensively reviewed in other sources (Gaubitz et al., 2016; Liu and Sabatini, 2020; Saxton and Sabatini, 2017).

mTORC1

To grow and proliferate, cells must synthesize proteins, lipids, and nucleotides while concurrently inhibiting competing processes such as autophagy. Because biosynthesis is a highly energy-demanding process, it is important that it only occur under conditions of sufficient nutrient availability. mTORC1 senses and synthesizes multiple different inputs, including oxygen, glucose, amino acids, energy, and insulin, in order to determine nutrient sufficiency. When active, mTORC1 phosphorylates effectors that drive many anabolic processes, including protein, lipid, and nucleotide synthesis as well as ribosome and lysosome biogenesis (**Figure 1-3**).

One of the first identified downstream targets of mTORC1 was eukaryotic translation initiation factor 4E (eIF4E)-binding protein 1 (4E-BP1), which is a regulator of cap-dependent translation of mRNA (Beretta et al., 1996). Most mRNAs have a 5'-cap consisting of a methylated guanine repeat. 4E-BP1 binds to this cap, preventing translation initiation factors from accessing it. When phosphorylated by mTORC1, p-4E-BP1 dissociates from the cap, allowing eIF4E to access the cap and recruit other initiators of translation, including the RNA helicase eIF4A (Lipton and Sahin, 2014; Ma and Blenis, 2009). This ultimately allows cap-dependent translation to proceed. p70S6 Kinase 1 (S6K1) is another downstream factor that promotes protein synthesis (Chung et al., 1992). When activated by mTORC1, S6K1 phosphorylates and activates ribosomal protein S6 to promote mRNA translation initiation and elongation. The phosphorylation site at Ser240/244 is

specific for S6K1, thus experimental detection of p-S6 S240/244 allows direct evaluation of upstream mTORC1 activity (Pende et al., 2004; Roux et al., 2007). As cells accumulate mass through increased protein synthesis, they must also generate lipids for membrane expansion. mTORC1 drives lipid synthesis through control of two transcription factors, sterol regulatory element binding protein 1/2 (SREBP1/2) and peroxisome proliferator-activated receptor γ (PPARγ) (Laplante and Sabatini, 2009). Additionally, mTORC1 regulates the availability of substrates for nucleotide synthesis (Liu and Sabatini, 2020).

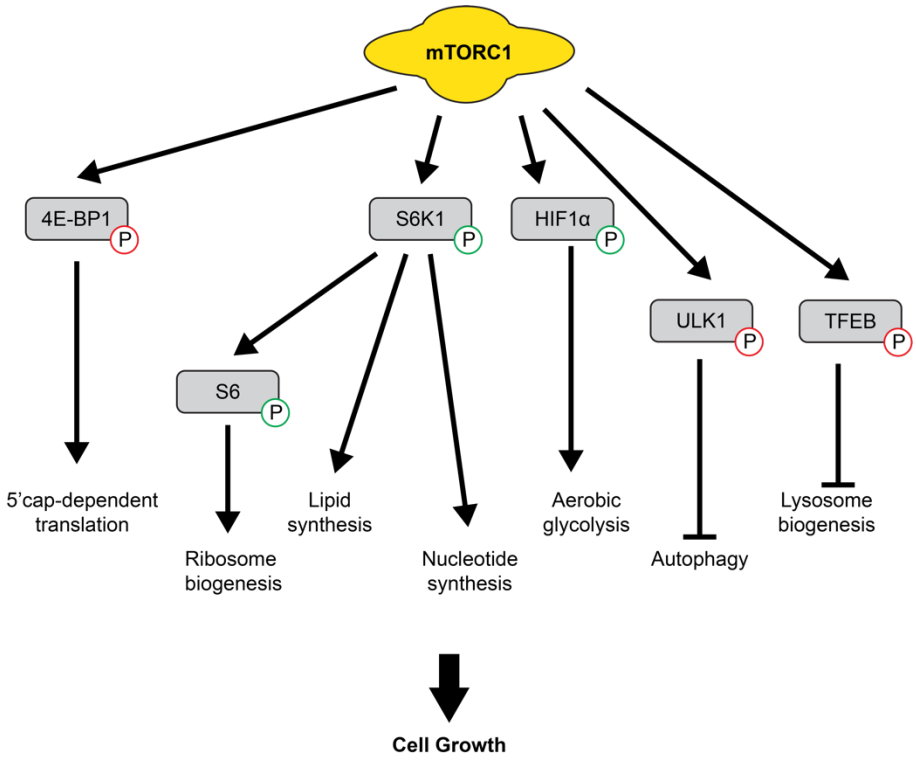

Figure 1-3. Simplified diagram of major pathways downstream of mTORC1.
mTORC1 is a central regulator of cell growth, driving anabolic processes and inhibiting catablic processes. Activating phosphorylations are indicated in green, inhibitory phosphorylations in red.

While driving anabolic processes, mTORC1 also inhibits protein catabolism, most significantly by repressing autophagy Autophagy is a catabolic pathway by which intracellular proteins and organelles are degraded by targeting them to the lysosome for destruction (Galluzzi et al., 2017). Autophagy begins with the formation of an isolation membrane, or phagopore, around the components to be degraded. The phagopore develops into a double membrane, forming an autophagosome, which then fuses with a recruited lysosome to create an autolysosome. Components inside the autolysosome are then degraded due to the acidic nature of the lysosomal lumen. AMPK activates ULK1 (unc-51-like

autophagy-activating kinase), a kinase that forms a complex with ATG13 (mammalian autophagy-related gene 13), ATG101 (mammalian autophagy-related gene 101, and FIP200 (200 kDa focal adhesion kinase family-interacting protein) to drive autophagosome formation. When active, mTORC1 performs an inhibitory phosphorylation of ULK1, preventing its activation by AMPK and thus inhibiting initiation of autophagy (Ganley et al., 2009; Hosokawa et al., 2009; Jung et al., 2009). mTORC1 also inhibits the nuclear translation of TFEB, a transcription factor that drives lysosomal biogenesis, further suppressing the autophagy machinery (Martina et al., 2012; Sardiello et al., 2009; Settembre et al., 2012). Under low nutrient conditions, mTORC1 is inhibited, thus allowing autophagy initiation and lysosomal biogenesis in order to recycle cellular components and organelles.

Unlike mTORC2, mTORC1 is highly sensitive to treatment with rapamycin, with nanomolar concentrations usually sufficient to completely inhibit phosphorylation of downstream targets. Mechanistically, the rapamycin-FKPB12 complex partially occludes substrates from the active site of mTORC1 (Yang et al., 2013). Interestingly, rapamycin differentially inhibits phosphorylation of mTORC1 targets (Thoreen and Sabatini, 2009). For example, phosphorylation of S6 kinase is dramatically decreased, but other targets, like p-4E-BP1 and p-ULK1, are not as drastically affected. Other competitive inhibitors (e.g. Torin1, PP242) inhibit the phosphorylation of all mTORC1 targets (Feldman et al., 2009; Kang et al., 2013; Thoreen et al., 2009)

Upstream regulation of mTORC1

Activation of mTORC1 is dependent on coordinated activation by two different inputs that act as a 'coincidence detector': mTORC1 needs to be in the right place (at the lysosome) at the right time (when Rheb is bound to GTP) in order to be activated (**Figure 1-4**). These separate arms are controlled by the presence of nutrients and growth factors, respectively. The Rag GTPases translocate mTORC1 from the cytoplasm to the lysosome when upstream nutrient sensors detect amino acids (Sancak et al., 2008). Lysosomal-bound Rheb, when activated itself by upstream detection of growth factors, can then activate mTORC1 (Long et al., 2005). The tuberous sclerosis complex, consisting of TSC1, TSC2, and TBC1D7, acts upstream of Rheb to suppress mTORC1 in the absence of growth factors.

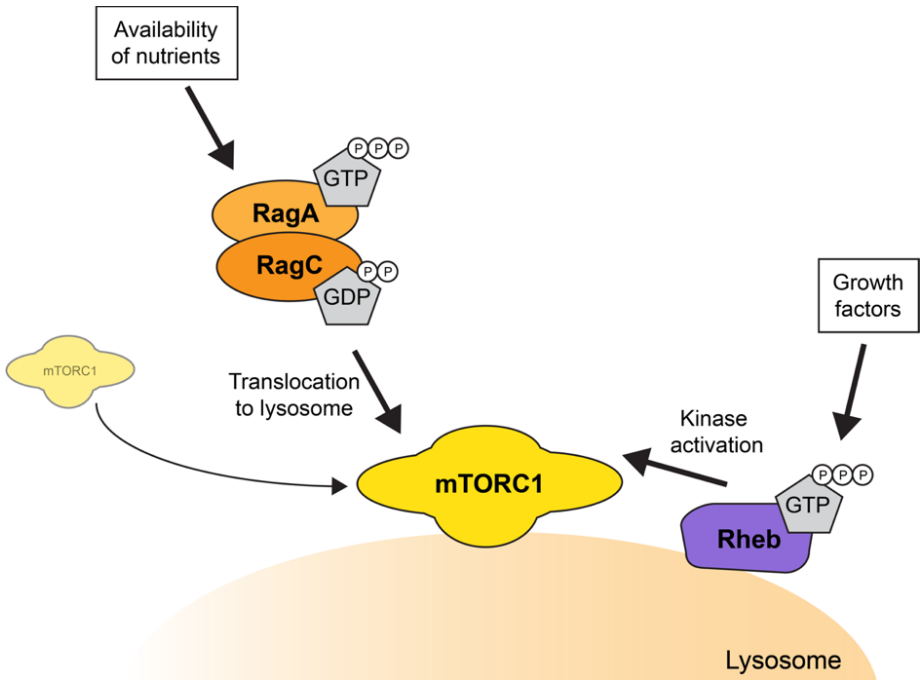

Figure 1-4. Activation of mTORC1 is dependent on detection of both amino acids and growth factors.
The Rag GTPases, heterodimers that are tethered to the lysosomal membrane by the Ragulator complex, are converted to their active states upon detection of amino acids by upstream nutrient sensors. The activated Rags are able to bind Raptor, a component of mTORC1, thus recruiting mTORC1 to the lysosomal membrane. The small GTPase Rheb is located at the lysosome and, when active, is then able to activate mTORC1.

The complex nutrient sensing mechanisms upstream of mTORC1 have only recently been described, and our knowledge is growing as additional components are discovered (**Figure 1-5**). In the several years since these initial discoveries, more than 25 proteins with roles in nutrient detection have been identified (Sabatini, 2017). Cells thus devote a significant amount of work toward nutrient regulation, emphasizing its crucial role. The "Ragulator" complex was one of the first mechanisms describing how nutrients, specifically amino acids, regulate mTORC1 activity upstream of the Rag GTPases (Sancak et al., 2010). The Ragulator complex consists of five LAMTOR subunits (late endosomal/lysosomal adaptor and MAPK and mTOR activator/regulator) that provide a scaffold to recruit mTOR (and MAPK) to the lysosome. Specifically, the LAMTOR2/3 heterodimer associates with the Rag GTPases to tether them to the lysosome and additionally serves as a guanine-exchange factor (GEF) for RagA, a function will be discussed in more detail below (Bar-Peled et al., 2012; Zhang et al., 2014). Ragulator also interacts with the vacuolar H^+-ATPase (v-ATPase) and SLC38A9, both lysosomal membrane proteins that positively regulate mTORC1. SLC38A9 is an amino-acid transporter that senses arginine within the lysosomal lumen and relays arginine sufficiency to mTORC1 (Wang et al., 2015; Wyant et al., 2017). Specifics of how the v-ATPase functions in the pathway are still unknown.

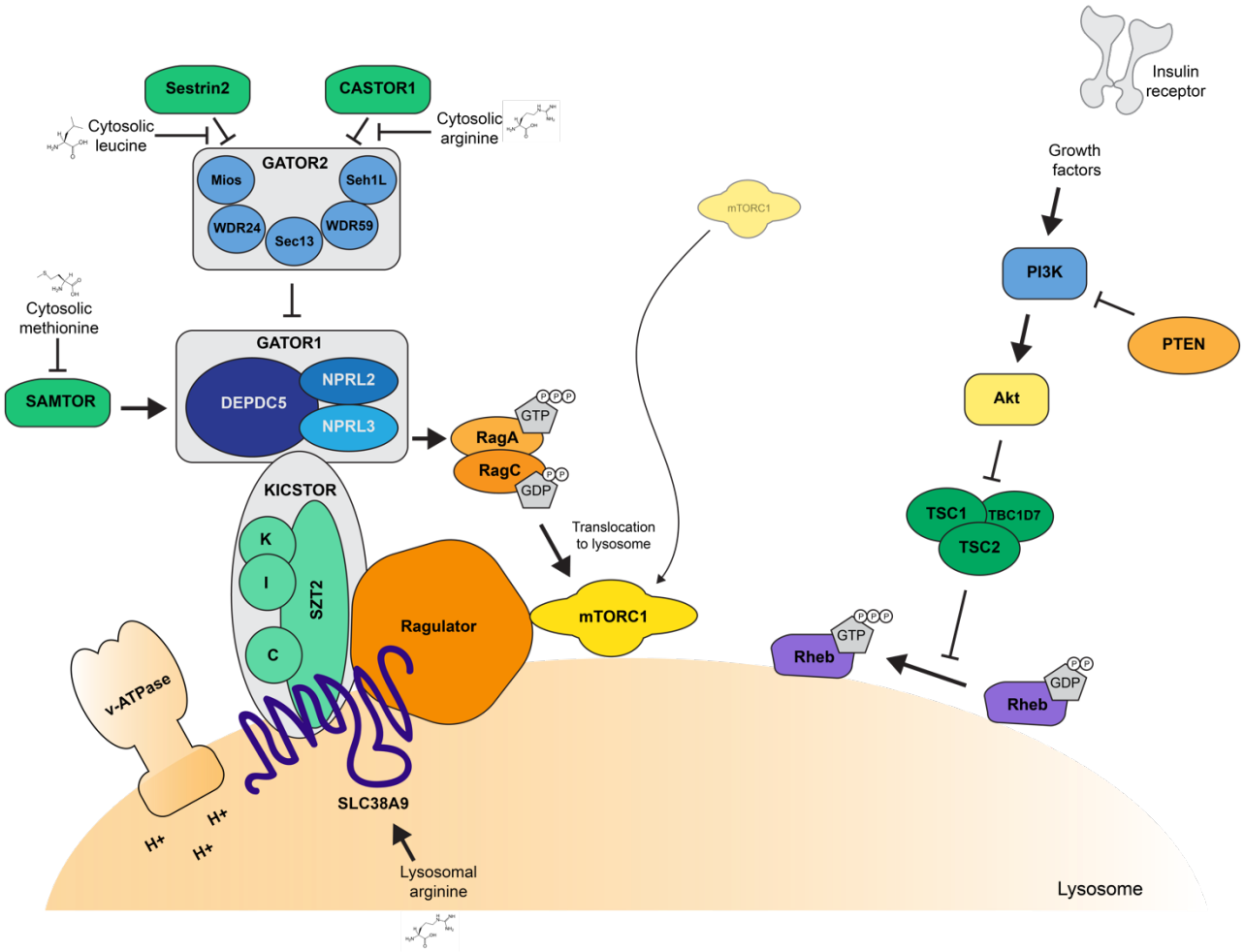

Figure 1-5. Upstream regulators of mTORC1.
mTORC1 senses both intra-lysosomal and cytoplasmic amino acids through a variety of upstream mediators. CASTOR1, Sestrin2, and SAMTOR sense cytosolic amino acids and regulate mTORC1 through GATOR1, while SLC38A9 senses lysosomal arginine.

Identification and function of the GATOR1 complex

Several complexes upstream of the Rag GTPases have since been identified, participating in a multi-armed nutrient sensing pathway. GATOR1 (GAP activity toward Rags) is a heterotrimeric protein complex that negatively regulates mTORC1 (Bar-Peled et al., 2013). GATOR1 consists of three proteins: disheveled, Egl-10, and pleckstrin domain-containing protein 5 (DEPDC5), nitrogen permease regulator-like-2 (NPRL2), and nitrogen permease regulator-like-3 (NPRL3). The complex is involved in attenuation of mTORC1 signaling under conditions of amino acid deprivation (Bar-Peled et al., 2013). A second complex, GATOR2, consists of distinct protein components and lies upstream of GATOR1, functioning as a positive regulator of mTORC1. GATOR2 receives inputs from CASTOR1 and Sestrin2, which communicate cytosolic arginine and leucine sufficiency, respectively (Chantranupong et al., 2016; Chantranupong et al.,

2014). When these amino acids are present in the cell, inhibition of GATOR2 is relieved; GATOR2 then inhibits GATOR1, allowing for lysosomal translocation of mTORC1 by the Rags. Cytosolic methionine is sensed by SAMTOR, which potentiates GATOR1 function in the absence of the methionine metabolite S-adenosylmethionine (Gu et al., 2017).

When amino acids are not available, GATOR1 attenuates mTORC1 signaling by preventing its translocation to the lysosome. This is accomplished by its GTPase-activating protein (GAP) activity toward the Rag guanosine triphosphatases (GTPases). Small G proteins like the Rag GTPases are important in cell signaling and exist in at least two states, an inactive GDP-bound state and an active GTP-bound state. G proteins have an intrinsic rate of hydrolysis of the phosphate bond that attaches GTP to GDP, but this rate is quite slow. GTPase activating proteins (GAPs) speed up the rate of hydrolysis of GTP (**Figure 1-6**). Their counterparts, guanine exchange factor proteins (GEFs) enhance G protein signaling by stimulating GTP binding to G proteins. Inactive G proteins are constantly replenished with active G proteins as cellular GEFs act upon them. The Ragulator serves as the GEF for RagA/B during nutrient replete conditions.

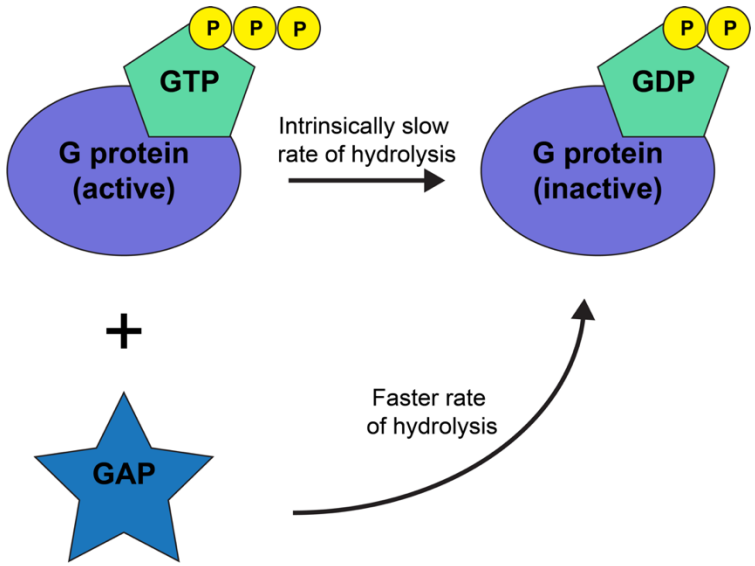

Figure 1-6. GTPase-activating proteins (GAPs) increase the rate of GTP hydrolysis by G proteins.
The Rag GTPase proteins form a heterodimer that regulates the localization of mTORC1 in response to nutrient cues. When amino acids are plentiful, the Rag GTPases interact with Raptor, a component of mTORC1, to localize mTORC1 to the lysosomal membrane (Sancak et al., 2008). However, cells with constitutively active Rag proteins are still sensitive to oxidative stress, mitochondrial inhibition, energy deprivation, and insulin deprivation. This suggests that they cannot override these other inputs that mTORC1 monitors and reinforces the concept of the coincidence detector (Sancak et al., 2008).

When nutrients are plentiful, the heterodimer exists in the active configuration of RagA-GTP/RagC-GDP. This configuration recruits mTORC1 to the lysosome, where it is activated by Rheb. In the nutrient-deprived state, the complex exists as RagA-GDP/RagC-GTP and does not favor association with, and thus recruitment of, mTORC1. GAPs have high specificity for the G proteins they target, accomplished by a combination of site-specific protein expression, location specific scaffold proteins that facilitate G protein-GAP interactions, and particular motifs of GAP proteins that make recognition of certain G proteins more favorable (Xie and Palmer, 2007). Accordingly, each set of Rag proteins (Rag A/B and Rag C/D) has a specific GAP. GATOR1 is the GAP for RagA/B, and the FLCN-FNIP complex (folliculin-FLCN-interacting protein) is the GAP for RagC/D (Petit et al., 2013; Tsun et al., 2013). Interestingly, recruitment of FLCN-FNIP to the lysosome is dependent on GATOR1 (Meng and Ferguson, 2018).

GAPs are thought to facilitate GTP hydrolysis by several mechanisms. They are thought to structurally influence the configuration of G proteins such that the phosphate bond becomes more accessible for nucleophilic attack by water (Rudack et al., 2012). This is canonically accomplished through the use of an arginine finger or asparagine thumb, which can orient GTP appropriately for hydrolysis (Daumke et al., 2004; Fidyk and Cerione, 2002). Originally, because DEPDC5 has a DEP domain, which is associated with G protein signaling, DEPDC5 was proposed to be responsible for the GAP activity of the complex (Consonni et al., 2014). However, a well-conserved arginine residue on NPRL2 (Arg78) was found to be responsible for catalyzing GTP hydrolysis by RagA (Shen et al., 2019). A separate loop on NPRL2 seems to be important for orienting the catalytic pocket to position the Arg78 residue correctly, but this loop is not ultimately necessary for the interaction between NPRL2 and RagA (Shen et al., 2019). Instead, DEPDC5 functions as a scaffolding protein, interacting with both NPRL2 and RagA to allow the NPRL2-NPRL3 heterodimer to access the Rag heterodimer (**Figure 1-7**). The structure of the GATOR1 complex and its interactions with the Rag GTPases was solved in 2018 and identified specific interaction domains within DEPDC5 (Shen et al., 2018). The SABA domain (previously known as the DUF3608 domain) of DEPDC5 mediates redundant interactions with NPRL2 in the form of three loops, while the SHEN domain contains a 'critical strip' for interaction with the nucleotide binding domain (NBD) of RagA, which, when mutated, severely disrupts the DEPDC5-RagA interaction (Shen et al., 2018).

DEPDC5 is thus key for several critical interactions in the regulation of mTORC1. Without the DEPDC5-NPRL2 interaction, GATOR1 fails to inhibit mTORC1 under nutrient-deprived conditions (Shen et al., 2018). Mutations in the

SABA domain of DEPDC5 have the potential to impact this interaction with NPRL2/NPRL3 and thus diminish the effectiveness of the GAP activity of GATOR1. Indeed, a DEPDC5 mutant replicating a patient variant with a single amino acid deletion in the SABA domain was found to interact less readily with NPRL2 and NPRL3 in *in vitro* co-immunoprecipitation assays (van Kranenburg et al., 2015). However, in the same study, interaction of NPRL2 and NPRL3 with another DEPDC5 variant with an amino acid substitution in the SABA domain was not affected, suggesting that certain mutations may be more pathogenic than others. Mutations in the GATOR1 components have been identified throughout their entire protein sequences and do not appear to cluster in any specific regions or functional domains (Baldassari et al., 2016).

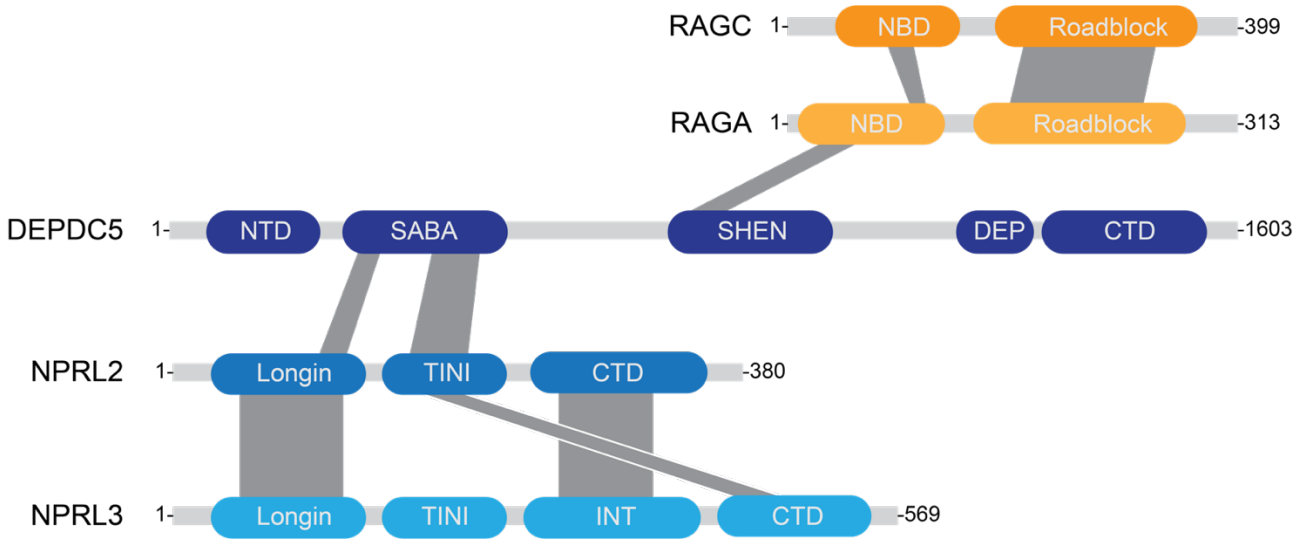

Figure 1-7. DEPDC5 serves as a scaffold to facilitate interaction of NPRL2 and NPRL3 with the Rag GTPases.

Mutations in *DEPDC5* as a Cause of Epilepsy

Mutations in GATOR1, a negative regulator of mTOR, are a significant cause of familial and sporadic focal epilepsies, which as a group account for about 60% of all epilepsies (Gupta et al., 2017). Linkage studies first mapped familial focal epilepsies to a region of chromosome 22q12, a region to which the *DEPDC5* locus was ultimately mapped (Berkovic et al., 2004; Klein et al., 2012; Morales-Corraliza et al., 2010) (**Figure 1-8**). Mutations in *DEPDC5* were initially identified in families with non-lesional autosomal dominant focal epilepsies, specifically in cases of familial focal epilepsy with variable foci (FFEVF) and autosomal dominant nocturnal frontal lobe epilepsy (ADNFLE) (Dibbens et al., 2013; Ishida et

al., 2013). Soon after, Scheffer et al. (2014) reported both lesional and non-lesional epilepsies in a single family with a germline *DEPDC5* mutation. *DEPDC5* mutations were subsequently found in focal epilepsy with auditory features, in epileptic spasms, and in sporadic focal epilepsies, establishing *DEPDC5* mutations as one of the most frequent causes of genetic focal epilepsies (Bisulli et al., 2016; Carvill et al., 2015; Tsai et al., 2017).

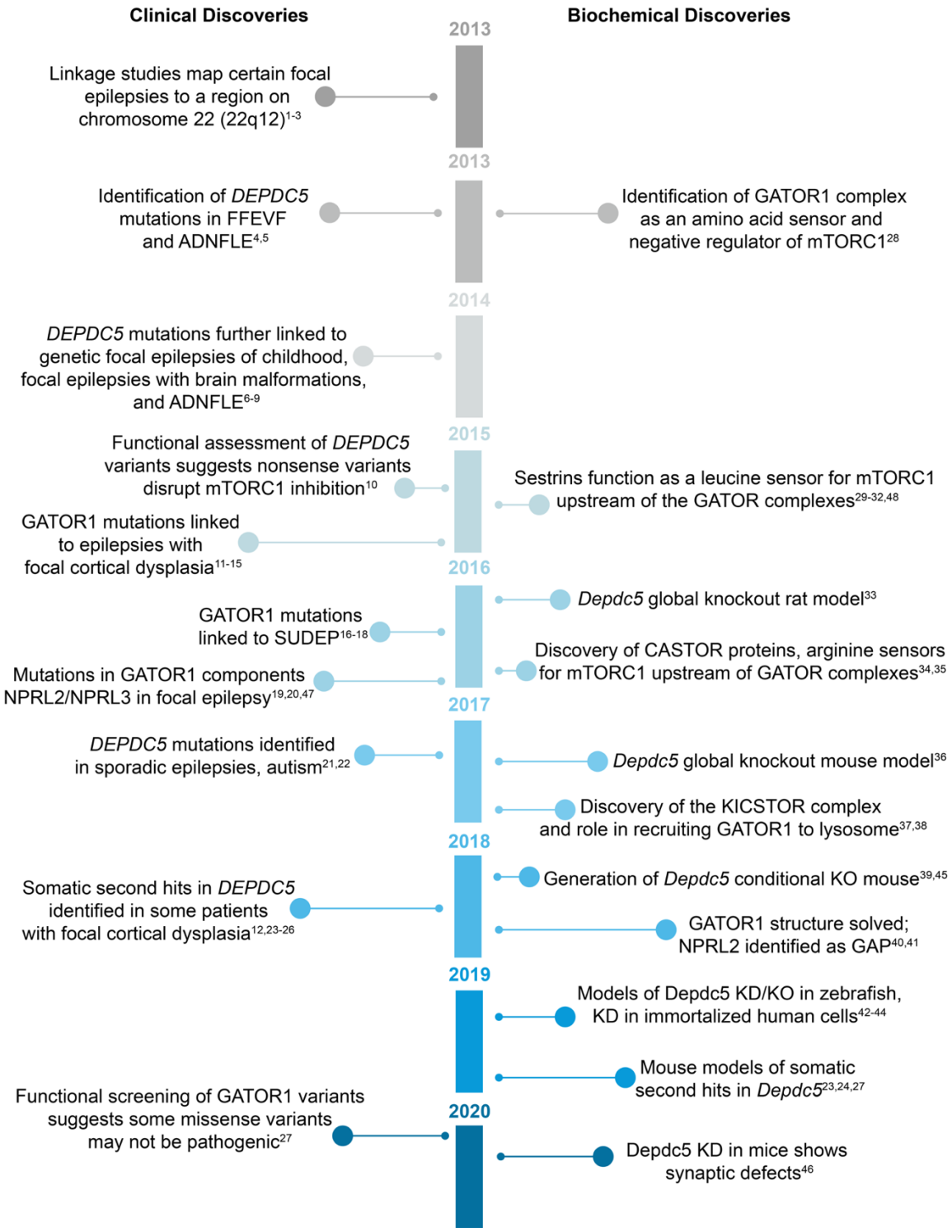

Figure 1-8. Timeline of clinical and biochemical discoveries related to the GATOR1 complex, its function as a regulator of mTORC1, and its link to epilepsy.

FFEVF: familial focal epilepsy with variable foci, ADNFLE: autosomal dominant nocturnal frontal lobe epilepsy, KO: knockout, KD: knockdown.

References: 1. Berkovic et al. (2004) 2. Morales-Corraliza et al. (2010) 3. Klein et al. (2012) 4. Dibbens et al. (2013) 5. Ishida et al. (2013) 6. Lal et al. (2014) 7. Scheffer et al. (2014) 8. Picard et al. (2014) 9. Martin et al. (2014) 10. van Kranenburg et al. (2015) 11. D'Gama et al. (2015) 12. Baulac et al. (2015) 13. Scerri et al. (2015) 14. Sim et al. (2016) 15. Weckhuysen et al. (2016) 16. Nascimento et al. (2015) 17. Bagnall et al. (2016) 18. Bagnall et al. (2017) 19. Ricos et al. (2016) 20. Korenke et al. (2016) 21. Tsai et al. (2017) 22. Burger et al. (2017) 23. Ribierre et al. (2018b) 24. Hu et al. (2018) 25. Lee et al. (2019) 26. Baldassari et al. (2019b) 27. Dawson et al. (2020) 28. Bar-Peled et al. (2013) 29. Parmigiani et al. (2014) 30. Kim et al. (2015) 31. Wolfson et al. (2016) 32. Saxton et al. (2016) 33. Marsan et al. (2016) 34. Chantranupong et al. (2016) 35. Gai et al. (2016) 36. Hughes et al. (2017) 37. Wolfson et al. (2017) 38. Peng et al. (2017) 39. Yuskaitis et al. (2018) 40. Shen et al. (2018) 41. Shen et al. (2019) 42. de Calbiac et al. (2018) 43. Swaminathan et al. (2018) 44. Iffland et al. (2018) 45. Yuskaitis et al. (2019) 46. De Fusco et al. (2020) 47. Baldassari et al. (2019a) 48. Chantranupong et al. (2014)

Mutations in *NPRL2* and *NPRL3*, the other two components of the GATOR1 complex, were subsequently identified in a variety of lesional and non-lesional focal epilepsies (Korenke et al., 2016; Ricos et al., 2016; Sim et al., 2016; Weckhuysen et al., 2016). Importantly, two definite cases of SUDEP were identified in a family with a *DEPDC5* mutation and two probable cases of SUDEP were identified in individuals with mutations in *NPRL2* or *NPRL3* (Nascimento et al., 2015). In an analysis of 61 SUDEP cases, 10% (6/61) of cases were found to have *DEPDC5* mutations, and *DEPDC5* was identified as one of the top 30 SUDEP risk genes in a genome-wide screen (Bagnall et al., 2016; Bagnall et al., 2017). These studies suggest that GATOR1 mutations may confer an increased risk of SUDEP, but more evidence is needed to show a definitive link. An *Nprl3* knockout mouse was found to have profound cardiac abnormalities, suggesting a possible mechanism for SUDEP, which may be related to cardiac arrhythmias (Kowalczyk et al., 2012). As such, it is possible that GATOR1 mutations may have effects that reach beyond the CNS, however this has not been further established to date. *DEPDC5* mutations have also been found in a variety of neoplastic processes such as glioblastoma, lung cancer, breast cancer, serous ovarian tumors, gastrointestinal stromal tumors, and hepatitis C virus-induced hepatocellular carcinoma (Bar-Peled et al., 2013; Miki et al., 2011; Pang et al., 2019; van Kranenburg et al., 2015). However, unlike patients with tuberous sclerosis complex, patients with epilepsy due to GATOR1 mutations do not seem to have an increased susceptibility for benign or malignant neoplasms.

To date, GATOR1 mutations have been identified in upwards of 10% of familial focal epilepsies and up to 1% of sporadic focal epilepsies (Baldassari et al., 2016; Ricos et al., 2016). While mutations occur in all three GATOR1 complex members, the majority of mutations occur in *DEPDC5* (*NPRL2* – 6%, *NPRL3* – 11%, *DEPDC5* – 83%) (Baldassari et al., 2019a). Two-thirds of epilepsy-related *DEPDC5* mutations are nonsense or frameshift mutations leading to premature termination codons, resulting in a truncated transcript predicted to undergo degradation through nonsense-mediated decay. Several groups have shown that *DEPDC5* transcripts undergo nonsense-mediated mRNA decay, indicating that haploinsufficiency may be deleterious (Carvill et al.; Ishida et al., 2013; Picard et al., 2014). Ishida *et al.* found that under standard conditions, the mutant transcript (Arg239*) was not detected in mRNA sequencing, but after inhibition of NMD with emetine, the mutant allele was detected (Ishida 2013).

DEPDC5 mutations causing focal epilepsy have a low penetrance with a high phenotypic variability (Dibbens et al., 2013; Ishida et al., 2013; Scheffer et al., 2014). For example, in seven families with FFEVF, Dibbens *et al.* found the penetrance of *DEPDC5* mutations to be 66% (69/105). Some individuals harboring a *DEPDC5* mutation are unaffected while affected individuals have variable ages of onset, epilepsy severity, locations of epileptogenic focus, and comorbid conditions such as autism spectrum disorders, intellectual disability, and psychiatric disorders (Baldassari et al., 2019a; Dibbens et al., 2013; Ricos et al., 2016; Scheffer et al., 2014). The explanation for this high variability is unknown but may be due to other genetic, epigenetic, or environmental influences.

A potential explanation that has been accumulating evidence is the two-hit hypothesis, originally posited by Dr. Alfred Knudson in 1971 (reviewed in Hino and Kobayashi (2017)). The two-hit hypothesis explains the recessive nature of many tumorigenic gene mutations: loss of one copy of a gene is hypothesized to be benign, whereas loss of the second copy, via an acquired mutation or other mechanism causing loss of heterozygosity, is pathogenic. In GATOR1-related epilepsies with focal cortical dysplasia (FCD), the two-hit hypothesis has been suggested as a disease mechanism. Indeed, several samples of resected brain tissue from FCD patients with germline *DEPDC5* mutations have been found to have acquired second somatic *DEPDC5* mutations in resected brain tissue, but not present in blood (Baulac et al., 2015; Lee et al., 2019; Ribierre et al., 2018b). In a large cohort of patients with FCD, five patients had germline loss-of-function variants in *DEPDC5*; of these five, one patient had a confirmed somatic second-hit in *DEPDC5* and one patient had a splice site variant potentially resulting in loss of heterozygosity (Baldassari et al., 2019a). Mouse models that recapitulate somatic second hits have been effective in generating FCD-like phenotypes, resulting in animals with dysmorphic neurons and seizures (Dawson et al., 2020; Hu et al., 2018; Ribierre et al., 2018b). However, not all patients with GATOR1 mutations and FCD demonstrate second-hits in *DEPDC5*. Another possible mechanism of dysplasia is acquisition of a second hit in another gene involved in regulation of the mTOR pathway, such as *PTEN* or *TSC1/2*. For example, individuals in one family with a germline *DEPDC5* mutation also inherited mutations in *DEPTOR* and *NF1*, both regulators of mTOR, and developed lesional focal epilepsies (Scerri et al., 2015). Thus, while evidence is accumulating to implicate second hits in *DEPDC5* or related proteins as causative of some cases of focal epilepsy with FCD, many questions remain unanswered. For the 80% of patients with *DEPDC5*-related epilepsy but without FCD, it is unknown if the heterozygous mutation may confer a pathogenic state. As a negative regulator of mTOR, *DEPDC5* haploinsufficiency has the potential to result in hyperactivation of mTOR and secondary consequences.

Role of mTOR in Neurodevelopment and Neurological Disease

mTOR is a critical regulator of energy balance. As the organ with the highest energy utilization in the body, it is not surprising that the brain is adversely impacted by dysregulation of mTOR signaling. The link between epilepsy and dysregulation of mTORC1 is well-established within the clinical and basic scientific literature, with mutations in mTOR pathway genes causing diseases such as tuberous sclerosis complex; hemimegaloencephaly, polyhydramnios, megalencephaly and symptomatic epilepsy (PMSE) syndrome, focal cortical dysplasia, and focal epilepsies (Baulac, 2016; Bi et al., 2016; D'Gama et al., 2015; Lipton and Sahin, 2014). Mutated proteins include TSC1/2, PTEN, STRADA, MTOR, AKT3, PIK3CA, DEPDC5, NPRL2, and NPRL3. The exact mechanisms that result in seizures in each of these diseases are not fully understood, but through a combination of *in vitro* and animal models of mTORC1 overactivation, general principles of how excess mTORC1 activity impacts the brain have become clear (**Figure 1-9**).

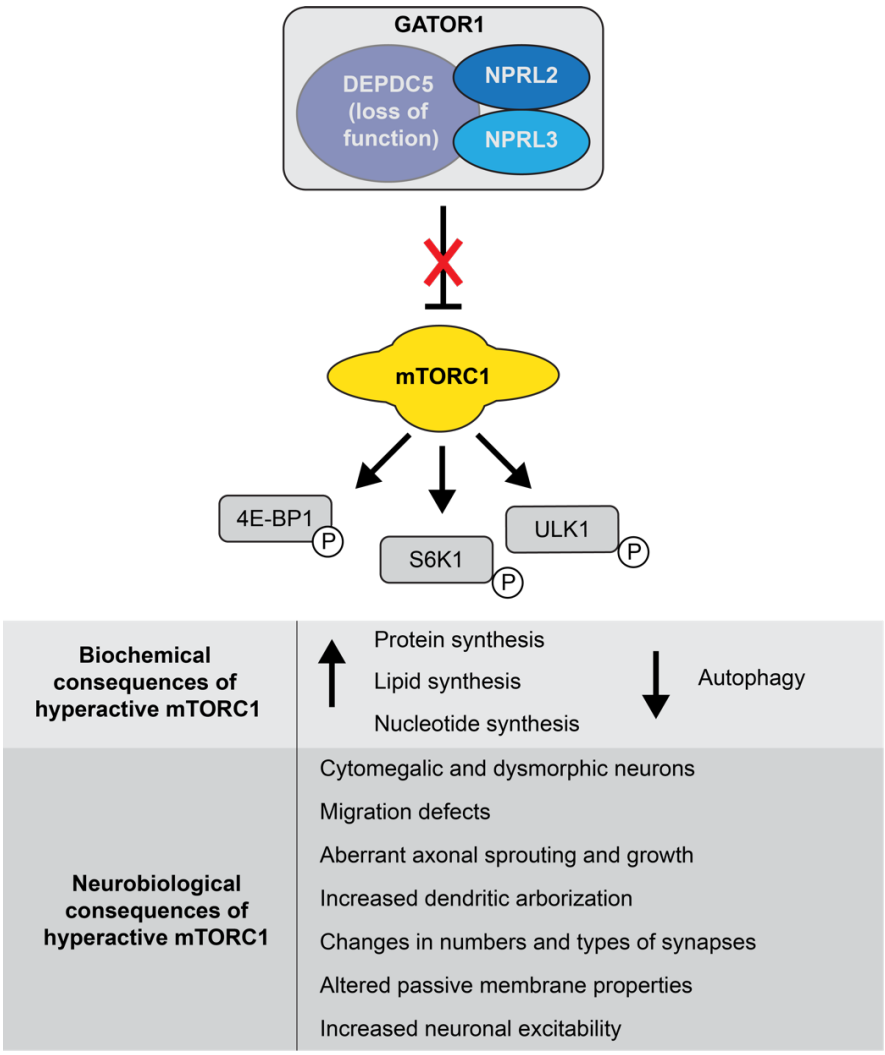

Figure 1-9. Neuronal consequences of hyperactive mTORC1 signaling.
Loss of mTORC1 inhibition, for example as a result of *DEPDC5* loss, can have a range of consequences in neurons leading to a variety of neurological diseases.

Developmental windows of mTOR regulation

mTOR signaling has differing functions depending on the neurodevelopmental stage. Proliferation of neural progenitors is an early critical step during cortical development. Regulation of proliferation and differentiation of progenitors is critical for control of both cortical size and cortical folding (Sun and Hevner, 2014). When constitutively active mTORC1 is overexpressed early in development (driven by the *Emx1* promoter, expression of which begins around E10-11), mice demonstrate marked microcephaly, although with preserved cortical lamination (Kassai et al., 2014). These mice have increased cleaved caspase 3 (CC3) activity in the conditionally-overactivated cells, suggesting that these cells were undergoing cell death during corticogenesis. This resulted in an overall smaller brain, but without overactive-mTORC1 cells in the adult brain.

The same study also expressed overactive-mTORC1 in post-mitotic neurons (under the *CamKII* promoter, expression of which is restricted to post-mitotic neurons in the forebrain, starting in late embryogenesis or the early postnatal period). These mice had a quite different phenotype, with increased cortical thickness, enlarged soma size, and cortical dyslamination, in addition to global growth delay and early death. Strikingly, this is a very similar phenotype to mice with conditional knockout of *Depdc5* (Yuskaitis et al., 2018). When overactive-mTORC1 was expressed beginning 3 weeks postnatally (also under the *CamKII* promoter, but under tamoxifen-inducible control), mice also had increased cortical thickness and enlarged soma sizes but had nearly preserved cortical lamination. Overall, this study suggests that mTORC1 has a temporal role in cortical development: early on, mTORC1 regulates neural stem cell proliferation, followed by neuronal migration, neuronal size, and finally circuit formation (**Table 1-3**). These roles are further reviewed in LiCausi and Hartman (2018).

Interestingly, both mice with constitutive mTORC1 activation in post-mitotic neurons developed seizures; however, mice with constitutively active mTORC1 early in development did not (Kassai et al., 2014). When present, seizures were prevented by treatment with rapamycin. Especially for mice with overactive-mTOR beginning three weeks postnatally, the seizures were likely not due to structural abnormalities alone, because these mice had generally preserved cortical lamination. This suggests that epilepsy can result from mTOR hyperactivation even in the cases of preserved cortical structure. mTOR hyperactivation may drive aberrant synaptic activity and circuit regulation in post-mitotic neurons. This mechanism may explain how some patients with *DEPDC5* mutation, but without evidence of cortical dysplasia, develop seizures. *DEPDC5*-related epilepsy may be due to two separate, but overlapping, mechanisms: one caused by focal cortical dysplasia and one by dysregulated synapse and circuit formation. It is possible that loss of heterozygosity is required for the former mechanism, but that haploinsufficiency may be sufficient to cause the latter. However, more evidence is needed to determine this definitively.

Timing of mTOR overactivation	Microcephaly	Increased cortical thickness	Large neurons	Cortical dyslamination	Seizures
Progenitor cells (~E11)	+	-	-	-	-
Early post-mitotic neurons (~P0)	-	+	+	+	+
Later post-mitotic neurons (~P21)	-	+	+	-	+

Table 1-3. Effects of mTOR hyperactivation at various time points during cortical development.
(Kassai et al., 2014)

mTOR role in dendritic arborization and synaptic regulation

Neurons form large networks of processes in order to communicate with one another. These branched extensions communicate action potentials from one neuron to the next. The network of extensions, called dendrites, extends from neurons much like the branches of a tree and is thus referred to as the dendritic arbor. Dendritic arborization, which is important for proper circuit development, is reliant on the activity of both mTORC1 and mTORC2; inactivation of either results in simplified dendritic arbors (Urbanska et al., 2012). The mTORC1 targets 4E-BP and S6K are both important in dendritic growth, perhaps by regulating local protein translation, which is known to play a role in axon guidance (Cagnetta et al., 2018; Jaworski et al., 2005). Indeed, a constitutively-active mutant of 4E-BP, which prevents mTORC1-driven increased translation, rescued ectopic neurons and dendritic hypertrophy (Lin et al., 2016). Inactivating mTORC1 by knocking out Raptor in neurons resulted in decreased overall total dendritic length (McCabe et al., 2020). Moreover, the number of excitatory synapses were reduced, resulting in an overall decrease in total number of vesicles in the readily-releasable pool and corresponding decrease in mEPSC amplitude (McCabe et al., 2020). Oppositely, overactivating mTORC1 results in increased dendritic complexity, migration defects, and increased mEPSC amplitude (D'Gama et al., 2017; Ribierre et al., 2018b; Sokolov et al., 2018). For example, mice with a biallelic inactivation of *Depdc5* have increased dendritic branching that is present prior to the onset of seizures (Ribierre et al., 2018b). *DEPDC5* knockdown in human neuroblastoma cells caused excessive formation of filopodia, which are precursors of neurites (Iffland et al., 2018). Taken together, these studies suggest that abnormally increased mTORC1 activation may cause hypersynchronous neurons as a result of enhanced neuronal connectivity with early developmental origins.

mTORC1 role in regulation of cell size and neuronal migration

As a key controller of cell size, hyperactive mTORC1 activity also results in cytomegalic neurons (Fingar et al., 2002). In contrast, inactivating mTORC1 in neurons resulted in a 20% decrease in soma size, with corresponding alterations in passive membrane properties, namely increased input resistance and decreased capacitance (McCabe et al., 2020). Alternatively, mTOR-activating overexpression of Rheb or mutations in *Pten* or *Tsc1/2* result in increased neuronal size (Sokolov et al., 2018; Weston et al., 2014). Increased neuronal size is also seen in *in vitro* models of *DEPDC5* knockdown as well as in mouse models with conditional or biallelic knockout of *Depdc5* (Iffland et al., 2018; Ribierre et al., 2018b; Yuskaitis et al., 2018). Neuronal size is important because passive electrical membrane properties, such as capacitance,

are directly related to cell size. Changes in passive and active membrane properties can result in seizure-initiating or seizure-propagating neurons.

Furthermore, somatic MTOR mutations disrupt neuronal ciliogenesis, which is important for migration along radial glial scaffolds. Accordingly, neurons with activating MTOR mutations have impaired migration resulting in cortical dyslamination (Park et al., 2018). One study showed that abnormal activation of mTOR in excitatory neurons resulted in cortical dyslamination and megalencephaly, whereas activation in the inhibitory interneuron lineage results in only subtle defects, demonstrating that mTOR has cell-type specific effects (D'Gama et al., 2017).

As mentioned previously, mutations in GATOR1 components, especially *DEPDC5*, are associated with focal cortical dysplasia (FCD), in which an area of the cortex is malformed during development. The acquisition of a somatic second hit and corresponding mTORC1 overactivation in different stages of cortical development could help explain the incomplete penetrance of the disease as well as its association with FFEVF. The finding that second hits are sometimes, but not always, present in glial cells supports that a second hit may be acquired at different stages during lineage differentiation (D'Gama et al., 2017).

Autophagy in neurons

Autophagy, a catabolic process inhibited by mTORC1, is implicated in a variety of processes such as embryonic development, the adaptive response to starvation, and axonal homeostasis (McMahon et al., 2012). If autophagy is dysregulated, protein aggregates, defective proteins, and/or dysfunctional organelles accumulate within cells and cause oxidative stress (Lakhani et al., 2014). Defects in autophagy have been implicated in many neurologic disease processes, including several pediatric neurodegenerative and neurometabolic diseases, adult neurodegenerative diseases such as Alzheimer's disease and Huntington disease, autism spectrum disorders (ASD), cortical malformations, and epilepsies. This suggests that tight regulation of autophagy is essential for proper nervous system development and function (Ebrahimi-Fakhari et al., 2014; Laplante and Sabatini, 2012). For example, loss of the essential autophagy gene *Atg7* in mice reduced physiologic spine pruning, resulting in ASD-like social deficits (Tang et al., 2014a).

Expression of DEPDC5 and GATOR1 in the brain and during development

The GATOR1 complex is essential for embryonic development, demonstrated by the embryonic lethality of the homozygous null state in *Nprl2, Nprl3,* and *Depdc5* global knockout mouse models (Dutchak et al., 2015; Hughes et al., 2017; Kowalczyk et al., 2012). Expression of GATOR1 complex members was noted in both the human fetal brain and all lobes of the adult human brain (Ricos et al., 2016). In mice, the GATOR1 complex members had similar expression patterns, from approximately E8.5 to E18.5, with peak expression from E12.5-E14.5 (Ricos et al., 2016). Compared to other body areas, expression of *Depdc5* was relatively increased throughout the mouse CNS, including the spinal cord, thalamus, cerebellum, medulla, hippocampus, and cerebrum (Dibbens et al., 2013). Whole-mount RNA *in situ* hybridization of zebrafish at various stages of development similarly showed *Depdc5* expression in the forebrain, midbrain, and hindbrain, as well as in the neural tube and notochord (Swaminathan et al., 2018). Expression of *Depdc5*, *Nprl2* and *Nprl3* is two to three times higher in adult mouse brains than in the developing brain (Dibbens et al., 2013; Ricos et al., 2016). Thus, evidence suggests an important role for the GATOR1 complex in post-mitotic neurons as well as in development

In mice, Depdc5 was found to colocalize with NeuN-positive and GAD67-positive neuronal cell bodies, without significant overlap with MAP2-positive neuronal processes (Dibbens et al., 2013). The same study determined subcellular localization of Depdc5 in mouse and iPSC-derived neurospheres using immunofluorescence, finding expression restricted to the cytosol of neuron, specifically in a perinuclear pattern. The authors concluded that colocalization of DEPDC5 with GFAP in astrocytes was minimal (Dibbens et al., 2013). As mTOR is ubiquitously expressed in eukaryotic cells, it would be difficult to imagine that an essential component of the mTOR pathway, the amino acid sensing arm, including GATOR1, is not expressed in specific cell types without having identified an alternative means for the cell to sense amino acids. In combination with RT-PCR data showing that *Depdc5* is expressed in cultured mouse astrocytes (**Chapter III**), it seems likely that *DEPDC5* is indeed expressed in astrocytes and that the immunofluorescence studies examining Depdc5 and GFAP colocalization had technical limitations.

Impact of GATOR1 loss of function

Loss of GATOR1 function prevents attenuation of mTORC1 during amino acid starvation, leading to constitutive inhibition of autophagy. In cells with shRNA-mediated DEPDC5 knock-down, mTORC1 localizes constitutively to the lysosomal surface regardless of amino acid availability, while overexpression of DEPDC5 is sufficient to block amino acid-induced translocation of mTOR to lysosomal surface (Bar-Peled et al., 2013). *Drosophila* with defective GATOR1 components show increased cell growth and sensitivity to nutrient starvation (Wei et al., 2016). NPRL2/3 mutants fail to activate autophagy in response to low levels of amino acids but can be rescued by overexpressing DEPDC5 (Wei and Lilly, 2014). *Dedpc5*$^{-/-}$ rat embryonic fibroblasts also fail to regulate cell growth appropriately in response to amino acid starvation (Marsan et al., 2016).

Effects in heterozygous animal models

The first two rodent models generated were global *Depdc5* knockouts in a mouse and a rat, using TALEN or CRISPR/Cas9 genomic editing (Hughes et al., 2017; Marsan et al., 2016). These models had many similarities, including embryonic lethality of homozygous null embryos. Homozygous animals died as a result of severe defects including global growth delay and cranial dysmorphology. Vascular defects and edema were noted in the mouse (Hughes et al., 2017). mTORC1 hyperactivation was noted in embryonic brains, embryonic fibroblasts, and mouse neurospheres.

The heterozygous phenotype was originally hypothesized to be most similar to the patient condition, although the field has now identified second-hit mutations in a subset of patients. Heterozygous rodent models showed surprising differences between mice and rats (**Table 1-4**). Heterozygous mice had no noted phenotype of any kind, although another recently published global heterozygous mouse model did note changes (De Fusco et al., 2020). Specifically, Hughes *et al.* did not describe evidence of mTORC1 hyperactivation, cortical dysmorphology, or spontaneous or evoked seizures in their heterozygous mice. Heterozygous rats, however, were noted to have less distinct cortical layering and enlarged cells throughout the cortex, similar to the balloon-like cells and cytomegalic dysmorphic neurons found in different subtypes of FCD (Marsan et al., 2016). While not statistically significant, heterozygous rats tended to have increased p-S6 expression in the cortex as well as increased soma size of pyramidal neurons. Heterozygous rats had some changes in firing properties, although they did not show changes in passive membrane properties. Perhaps surprisingly, neurons were more hyperpolarized with a lower firing rate and were less responsive to excitatory inputs, with a higher minimum current

required to induce firing in the RS-FA neurons. However, the authors did not specifically record from the cytomegalic neurons, which would be hypothesized to be more abnormal. Heterozygous zebrafish showed an approximately 1.5X increase in p-S6 expression, indicating an increase in mTORC1 activation, but showed no other phenotype (Swaminathan et al., 2018).

Importantly, no *Depdc5* heterozygous animal models have displayed seizures, suggesting that haploinsufficiency alone does not cause epilepsy in rodents. However, human patients are heterozygous for *DEPDC5* mutations. This raises several possibilities, including the potential for species-specific differences – perhaps the developing human brain is more sensitive to the gene dosage of DEPDC5 – and the possibility of a second-hit in all patients. Rats may be better models than mice for studying some aspects of neuroscience (Ellenbroek and Youn, 2016). Because heterozygous rats have a phenotype of increased mTORC1 activation in the brain as well as altered neuronal excitability and firing, it is possible that the heterozygous state may be abnormal in humans as well. However, it is not known if the abnormalities seen in the heterozygous state are sufficient to result in functional pathology.

Citation	Model	Increased mTORC1 (by pS6 or S6K1)	Increased soma size	Sensitivity to starvation	Morphology changes	Electrophys. changes	Seizures
Marsan *et al.* (2016)	Rat global knockout	p-S6 trends upward but not significant	Increased soma size	REFs sensitive	Increased neuronal soma size, altered cortical lamination	Altered excitability and firing patterns	None
Hughes *et al.* (2017)	Mouse global knockout	p-S6 trends upward but not significant	No change in soma size	MEFs sensitive	None	N/A	None; no change in PTZ threshold
Yuskaitis *et al.* (2018)	Mouse conditional knockout (Syn1-Cre)	N/A	N/A	N/A	N/A	N/A	None
Swaminathan *et al.* (2018)	Zebrafish global knockout	p-S6 increased by 1.5X	No change in hets or KOs	N/A	None	N/A	N/A
De Fusco *et al.* (2020)	Mouse global heterozygote	p-S6 not increased, but increased number of p-S6+ neurons	No change in soma size	N/A	Increased neurite complexity; more excitatory synapses; no change in synapse structure	No change in mEPSCs or mIPSCs	Decreased threshold to PTZ-induced seizures

Table 1-4. Summary of heterozygous phenotypes seen in published genetic animal models of *Depdc5* loss.
REFs: rat embryonic fibroblasts. MEFs: mouse embryonic fibroblasts.

Conditional animal models

Because heterozygous global knockout rodents did not display consistent phenotypes or epilepsy and because homozygous animals did not survive to birth, conditional knockout models were generated in which *Depdc5* was only deleted in the brain (Yuskaitis et al., 2018). Specifically, the *Syn1*-Cre *Depdc5* conditional knockout model targets excitatory neurons starting at approximately E13-14. These mice survive to adulthood and demonstrate an mTORC1 hyperactivation phenotype in the brain, including enlarged neurons and spontaneous seizures in some mice, the latter of which started after 100 days of life and was prevented with rapamycin (Yuskaitis et al., 2019). While this model is useful to study various aspects of behavior, such as hyperactivity, it may not fully recapitulate the epilepsy phenotype in humans because many patients with *DEPDC5*-related epilepsy have seizure-onset in infancy or childhood (Dibbens et al., 2013; Ishida et al., 2013). A mouse model with a more severe epilepsy phenotype with seizure onset earlier in life would be especially useful for screening various targeted therapeutics, including the mTORC1 inhibitor rapamycin.

Prenatal treatment of rats with rapamycin ameliorated some of the phenotypes seen in the homozygous rat (Marsan et al., 2016). A one-time administration of prenatal rapamycin in pregnant rats increased the proportion of living embryos at E14.5 from 50% to 83% and also appeared to rescue the global growth delay at E21.5, with body length of rapamycin-treated KOs similar to that of WT, although only 31% of KOs were alive at E21.5, suggesting that full rescue was not possible. This one-time rapamycin administration also rescued cytomegalic dysmorphic neurons in heterozygous rats that were analyzed at P11 (Marsan et al., 2016).

Based on the temporal changes in expression levels, it is possible that *DEPDC5* may have different functions during development and during adulthood. If the consequences of *DEPDC5* mutation are cemented during development, we would hypothesize that rapamycin given to adult animals would not rescue the disease phenotype. This would limit its clinical utility because patients with *DEPDC5* mutations and epilepsy are currently identified only after onset of seizures and not during gestation. However, inhibiting mTOR signaling with rapamycin treatment extends survival in zebrafish as long as the treatment is continued, suggesting that increased mTOR signaling in the larvae, not just the developing embryo, is pathogenic (Swaminathan et al., 2018). This suggests that inhibition of mTORC1 may have therapeutic benefits even after completion of cortical development. Moreover, mTORC1 hyperactivation in post-mitotic neurons can induce seizures that can be rescued with rapamycin (Kassai et al., 2014). When taken together with some clinical success

in treating TSC patients with refractory epilepsy with the rapalog everolimus, it is thus reasonable to hypothesize that mTORC1 inhibition with rapamycin may also be effective for *DEPDC5*-related epilepsy (Krueger et al., 2013; Lechuga and Franz, 2019).

Summary and Project Rationale

Mutations in the *DEPDC5* gene cause epilepsy, including forms with and without brain malformations. *DEPDC5* encodes an essential component of the GATOR1 complex, a negative regulator of the mTORC1 pathway (Bar-Peled et al., 2013). As a negative regulator of mTORC1, experimental knockdown of DEPDC5 leads to hyperactive mTORC1 signaling (Bar-Peled et al., 2013; Iffland et al., 2018). Dysregulation of mTORC1 signaling due to *DEPDC5* mutation likely has numerous consequences for brain development and neuronal function, ultimately resulting in epilepsy; however, the underlying mechanisms of how *DEPDC5* mutations result in dysplastic neurons and epilepsies are not clear. In cases of epilepsies with FCD, evidence supports acquisition of a somatic "second hit" resulting in a mutation gradient of biallelic *DEPDC5* (Baldassari et al., 2019b; Baulac et al., 2015; Lee et al., 2019; Ribierre et al., 2018b). Similarly, rodent models with mosaic homozygous brain inactivation of *Depdc5* have a FCD-like phenotype with focal seizures (Dawson et al., 2020; Hu et al., 2018; Ribierre et al., 2018b).

While these studies provide important evidence to explain how a germline loss-of-function mutation can cause focal epilepsies, only about 25% of patients with epilepsy due to *DEPDC5* mutations have reported malformations of cortical development, including FCD (Baldassari et al., 2019a). In *DEPDC5*-related epilepsies without FCD, it is unknown if areas of FCD exist that are not apparent with current imaging sensitivity or whether other mechanisms lead to epilepsy in these cases. Specifically, potential consequences of a heterozygous mutation in *DEPDC5* are not definitively known. When studied in rodent models, consequences of *Depdc5* haploinsufficiency have been variable. No *Depdc5* heterozygous animal models have displayed seizures, suggesting that haploinsufficiency alone does not cause epilepsy in rodents (Hughes et al., 2017; Marsan et al., 2016; Yuskaitis et al., 2018). However, the impact of *DEPDC5* haploinsufficiency has not been characterized in human patient derived cell lines, thus neuronal cultures derived from human induced pluripotent stem cells (iPSCs) provide a promising complementary experimental approach to animal models. As studies in

immortalized human cell lines have been done in the context of homozygous loss or knockdown of *DEPDC5*, it is unclear how heterozygous loss of *DEPDC5* might affect patient-derived stem cells and derivative neurons.

Chapter II investigates the contribution of *DEPDC5* gene dosage to the underlying neuropathology of *DEPDC5*-related epilepsies. We generated induced pluripotent stem cells (iPSCs) from epilepsy patients harboring loss-of-function mutations in *DEPDC5*. Patient iPSCs haploinsufficient for *DEPDC5* demonstrated an increase in phosphorylated ribosomal protein S6 and proliferation rate, consistent with elevated mTORC1 activation. In line with these findings, when iPSCs were differentiated into cortical neurons, we observed increased soma size that was rescued by treatment with rapamycin. These data indicate that *DEPDC5* haploinsufficiency causes increased mTORC1 signaling. Our findings suggest that human pathology differs from mouse models of *DEPDC5*-related epilepsies, which do not show phenotypic differences in heterozygous neurons, and support the need for human-based models to affirm and augment the findings from animal models of *DEPDC5*-related epilepsy.

While human models are essential to determine species-specific effects, generation of epilepsy animal models to define mechanisms of epileptogenesis remain vital for development and testing of novel therapies. **Chapter III** describes the generation of a novel mouse model of *Depdc5* deletion with a severe epilepsy phenotype. We generated a conditional knockout (CKO) mouse with deletion of *Depdc5* in the *Emx1*-expressing embryonic dorsal telencephalic neuroepithelium. *Depdc5*$^{F/F}$*;Emx1*-Cre-CKO mice have a greatly reduced lifespan with terminal seizures, display evidence of mTORC1 hyperactivation in both neurons and astrocytes, and demonstrate dysplastic cortical neurons with an altered response to GABAergic input. These results suggest a potential role for glial cells in *DEPDC5*-related epilepsies and also support that an altered response to inhibitory neuronal inputs may be a feature of *DEPDC5*-related epilepsies. Postnatal treatment with rapamycin prolonged lifespan and prevented seizures, even after its withdrawal. These data not only support a primary role for mTORC1 hyperactivation in epilepsy following homozygous loss of *Depdc5*, but suggest a developmental window for treatment which may have a durable long-term benefit.

CHAPTER II

DEPDC5 HAPLOINSUFFICIENCY DRIVES INCREASED MTORC1 SIGNALING AND ABNORMAL MORPHOLOGY IN HUMAN CORTICAL NEURONS

Abstract

Mutations in the *DEPDC5* gene can cause epilepsy, including forms with and without brain malformations. The mechanism of *DEPDC5*-related epileptogenesis in the absence of a second hit remains unknown. The effect of heterozygous loss of *Depdc5* in animals has been variable. We hypothesized that species-specific effects may exist, rendering the human brain uniquely sensitive to *DEPDC5* haploinsufficiency. The goal of this study was to investigate the contribution of *DEPDC5* gene dosage to the underlying neuropathology of *DEPDC5*-related epilepsies. We generated induced pluripotent stem cells (iPSCs) from epilepsy patients harboring heterozygous loss of function mutations in *DEPDC5*. Patient iPSCs appear to be haploinsufficient for *DEPDC5* with an increase in phosphorylated ribosomal protein S6 and proliferation rate, consistent with elevated mTORC1 activation. In line with these findings, when iPSCs were differentiated into cortical neurons, we observed increased soma size that was rescued with rapamycin treatment. These data indicate that heterozygous *DEPDC5* are haploinsufficient for control of mTORC1 signaling. Our findings suggest that human disease differs from mouse models of *DEPDC5*-related epilepsies, which do not show consistent differences in heterozygous neurons, and support the need for human-based models to affirm and augment the findings from animal models of *DEPDC5*-related epilepsy.

Introduction

As discussed in **Chapter I**, *DEPDC5* encodes an essential component of the GATOR1 complex, a regulator of the Rag GTPases in response to amino acids (Bar-Peled et al., 2013). Thus, as a negative regulator of mTORC1, experimental knockdown of DEPDC5 leads to hyperactive mTORC1 signaling (Bar-Peled et al., 2013; Iffland et al., 2018). In the central nervous system, mTORC1 plays a role in the differentiation of neural stem cells, drives the proliferation of neuroprogenitor cells, and is required for dendrite formation (Li et al., 2018; Lipton and Sahin, 2014; Saxton and Sabatini,

2017). Dysregulation of mTORC1 signaling due to *DEPDC5* mutation likely has numerous consequences for brain development and neuronal function, ultimately resulting in epilepsy.

Despite numerous available antiseizure medications, over one-third of patients with epilepsy are refractory to treatment (Chen et al., 2018). Epilepsies due to pathogenic mutations in *DEPDC5* have even higher rates of drug-resistance, often greater than 50% (Baldassari et al., 2019a; Picard et al., 2014). While initially described in autosomal dominant familial focal epilepsies, *DEPDC5* mutations have also been described in other epilepsy types, including epilepsies with focal cortical dysplasia (FCD) (Baulac et al., 2015; D'Gama et al., 2015; Dibbens et al., 2013; Ishida et al., 2013; Kaur, 2013; Lal et al., 2014; Martin et al., 2014; Scerri et al., 2015; Scheffer, 2014). Notably, FCD is highly associated with medically refractory epilepsy further accentuating the need for improved understanding of disease pathogenesis due to *DEPDC5* mutations (Crino, 2015).

The need for human models of *DEPDC5* mutation

The underlying mechanisms of how *DEPDC5* mutations result in dysplastic neurons and epilepsies are not clear. In cases of epilepsies with FCD, evidence is accumulating to suggest the acquisition of a somatic "second hit" in at least some cases. Indeed, several case reports and a recent cohort study support a model of a mutation gradient of biallelic *DEPDC5* mutation in epilepsies with associated FCD (Baldassari et al., 2019b; Baulac et al., 2015; Lee et al., 2019; Ribierre et al., 2018). Similarly, rodent models with mosaic homozygous brain inactivation of *Depdc5* have a FCD-like phenotype with focal seizures (Hu et al., 2018; Ribierre et al., 2018). While these studies provide important evidence to explain how a germline loss-of-function mutation can cause focal epilepsies, only about 25% of patients with epilepsy due to *DEPDC5* mutations have reported malformations of cortical development, including FCD (Baldassari et al., 2019a). In *DEPDC5*-related epilepsies without FCD, it is unknown if areas of FCD exist that are not apparent with current imaging sensitivity or whether other mechanisms lead to epilepsy in these cases. Specifically, potential consequences of a heterozygous mutation in *DEPDC5* are not definitively known. When studied in rodent models, consequences of *Depdc5* haploinsufficiency have been variable. For example, rats lacking one copy of *Depdc5* demonstrated enlarged neurons with abnormal electrophysiological properties, whereas in mice, no differences in neuronal size or mTORC1 activation were originally reported (Hughes et al., 2017; Marsan et al., 2016). A recently published mouse model did find evidence of increased mTORC1 activation in cortical neurons, but with no corresponding increase in neuronal size (De Fusco et al.,

2020). No *Depdc5* heterozygous animal models have displayed seizures, suggesting that haploinsufficiency alone does not cause epilepsy in rodents (Hughes et al., 2017; Marsan et al., 2016; Yuskaitis et al., 2018). However, the impact of *DEPDC5* haploinsufficiency has not been characterized in human patient-derived cell lines, thus neuronal cultures derived from human induced pluripotent stem cells (iPSCs) provide a promising complementary experimental approach to animal models. As most studies in immortalized human cell lines have been done in the context of homozygous loss or knockdown of *DEPDC5*, it is unclear how heterozygous loss of *DEPDC5* might affect patient-derived stem cells and derivative neurons (Bar-Peled et al., 2013; Iffland et al., 2018).

Induced pluripotent stem cells: value in studying neurological disease

The advent of human embryonic stem cell and induced pluripotent stem cell technology in the past decade makes the study of neurologic diseases in human models more accessible by removing barriers to the accessibility of human neurons. Embryonic stem cells were first isolated in 1981 from the inner cell mass of mouse blastocysts (Evans and Kaufman, 1981). The term "embryonic stem (ES) cell," or ESC, was created to differentiate ESCs from pluripotent cells derived from embryonal carcinoma (EC) cells, which are genetically aneuploid and thus "malignant" equivalents of ES cells (Przyborski et al., 2004). Human blastocyst-derived pluripotent ES lines were first generated in 1998 (Thomson et al., 1998). ESCs are able to differentiate into all three primary germ layers, are stable in culture over long periods of time, and are able to generate a wide range of specific cell types using existing differentiation protocols. However, ethical concerns regarding the derivation of ES cells have limited their wider use.

The discovery of ES cells hastened the determination of master regulators that govern maintenance of pluripotency and self-renewal, both essential properties of stem cells. This culminated in the discovery that previously differentiated cells could be reprogrammed ("induced") back to a stem-cell-like state by introducing four transcription factors. Takahashi & Yamanaka described these essential factors, Oct3/4, Sox2, c-Myc, and Klf4, in 2006, which they showed were necessary and sufficient to reprogram somatic cells, such as dermal fibroblasts, into a pluripotent state (Takahashi and Yamanaka, 2006). These reprogrammed cells were then termed induced pluripotent stem cells (iPSCs) and circumvented the issue of ES cells because they can be derived from consenting adult volunteers or even patients themselves. Because iPSCs have been reprogrammed to a state of pluripotency, they too have the ability to be differentiated into numerous different cell types. Robust protocols exist and are constantly evolving to generate specific cell types, from dopaminergic neurons to

contracting cardiomyocytes to insulin-producing pancreatic beta cells (Abou-Saleh et al., 2018; Beevers et al., 2013; Shahjalal et al., 2018). iPSCs are especially useful for studying neurologic diseases because they allow researchers to model live human neurons which are otherwise inaccessible for study without invasive measures such as brain biopsy.

Many protocols exist to direct neuronal differentiation from iPSCs. Dual SMAD inhibition through the use of small molecules is a well-established method for differentiating iPSCs into neuroectoderm. SMADs are a group of signal transduction proteins that mediate signaling by the transforming growth factor beta (TGF-β) and bone morphogenic protein (BMP) families of ligands. Interfering with regulatory SMAD (R-SMAD) signaling drives cells toward their intrinsic neuronal fate (**Figure 2-1**). This can be achieved through a combined SMAD blockade through application of LDN-193189, a Noggin analog that inhibits BMP type I receptors ALK2 and ALK3 and prevents phosphorylation of Smad1, 5, and 8, and SB-431542, an inhibitor of Lefty/Activin/TGF-β pathways that blocks the ALK4, ALK5, and ALK7 receptors (Chambers et al., 2009; Shi et al., 2012a). Cells then form neural rosettes and begin to express early dorsal forebrain markers, such as FoxG1. Neurons develop in an ordered fate similar to that found in the cortex, with deeper layer neurons forming first followed by upper layer neurons. Cells express neuron-specific β-III-Tubulin and MAP2 as well as markers of excitatory synapses. Neurons can also be subjected to whole-cell patch-clamp to record electrophysiological properties. Thus, iPSC-derived neurons have similarities to endogenous human neurons and are a useful tool to study the impact of genetic mutations on neuronal structure and function.

This study aims to determine the effects of heterozygous *DEPDC5* mutation on mTOR pathway activation and neuronal size in patient cell lines. To better understand the effects of *DEPDC5* haploinsufficiency in humans, we generated iPSCs and neurons from epilepsy patients with inactivating mutations in *DEPDC5*. We found that heterozygous mutations in *DEPDC5* allow increased mTORC1 signaling activity in iPSCs and derivative neurons. Corresponding changes in neuronal size were responsive to chronic treatment with rapamycin. These results reveal a potential role for *DEPDC5* haploinsufficiency in contributing to neuronal dysfunction by driving increased mTORC1 signaling.

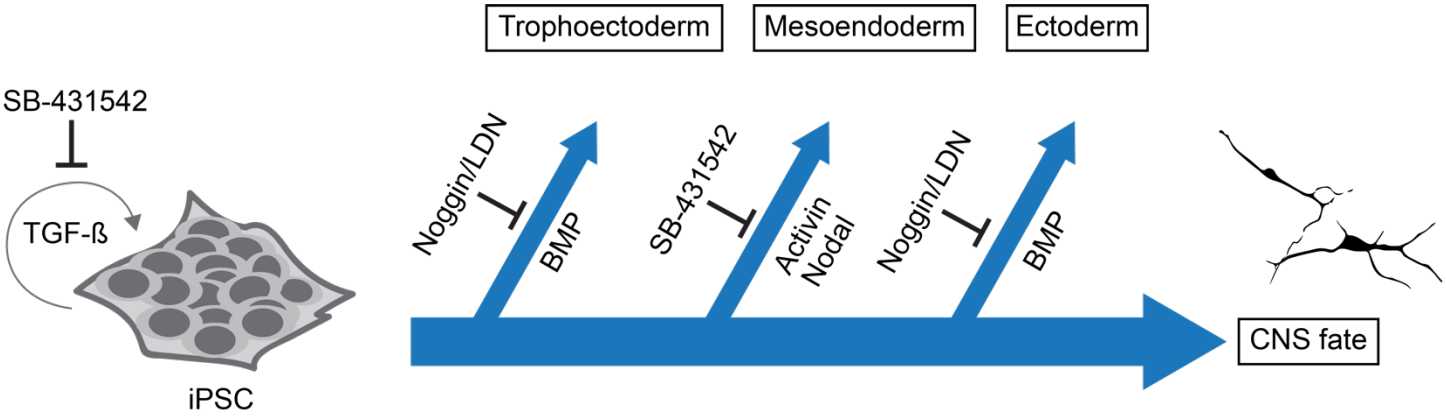

Figure 2-1. Dual SMAD inhibition drives differentiation of pluripotent cells toward a neuronal fate.
SB-431542 and the Noggin analog LDN-193189 synergistically drive cells toward a neuronal fate by suppressing other cell fates. Adapted from Chambers et al. (2009)

Results

Generation of iPSCs from epilepsy patients with *DEPDC5* mutations.

To determine the consequences of *DEPDC5* haploinsufficiency in patient-derived neurons, we generated iPSC lines from three patients (Pt1, Pt2, and Pt3) with epilepsy and *DEPDC5* loss of function mutations. The patient lines were generated from individuals with epilepsy and family histories suggestive of autosomal dominant nocturnal frontal lobe epilepsy (ADNFLE) syndrome (**Figure 2-2**).

Genetic testing of Pt1 revealed a pathogenic *DEPDC5* mutation (c.2620C>T, p.Arg874X) occurring in the SHEN domain (Figure 2-3A) (D'Gama et al., 2017; Lal et al., 2014; Shen et al., 2018). This patient was a 16-year-old otherwise healthy woman with a history of seizures beginning at 10 years of age. Family history was suggestive of an autosomal dominant nocturnal frontal lobe epilepsy (ADNFLE) syndrome, thus a genetic epilepsy panel was sent, leading to identification of the Arg874X mutation in DEPDC5. In Pt2 and Pt3, who were first-degree relatives, targeted genomic sequencing discovered a 1291 base pair deletion in *DEPDC5*, including exon 2 and portions of the surrounding introns (c.59-493_146+710), resulting in a frameshift truncation (D20Afs*25) (**Figure 2-3A**).

All three patients had normal brain magnetic resonance imaging (MRI) scans (data not shown). Additional patient characteristics are detailed in Table 2-1. Control lines were generated from healthy first-degree relatives or unrelated volunteers (CtrlA, CtrlB) who did not have epilepsy or *DEPDC5* mutations. The mutations in the *DEPDC5* gene in iPSC lines were confirmed by direct DNA sequencing (**Figure 2-3B**).

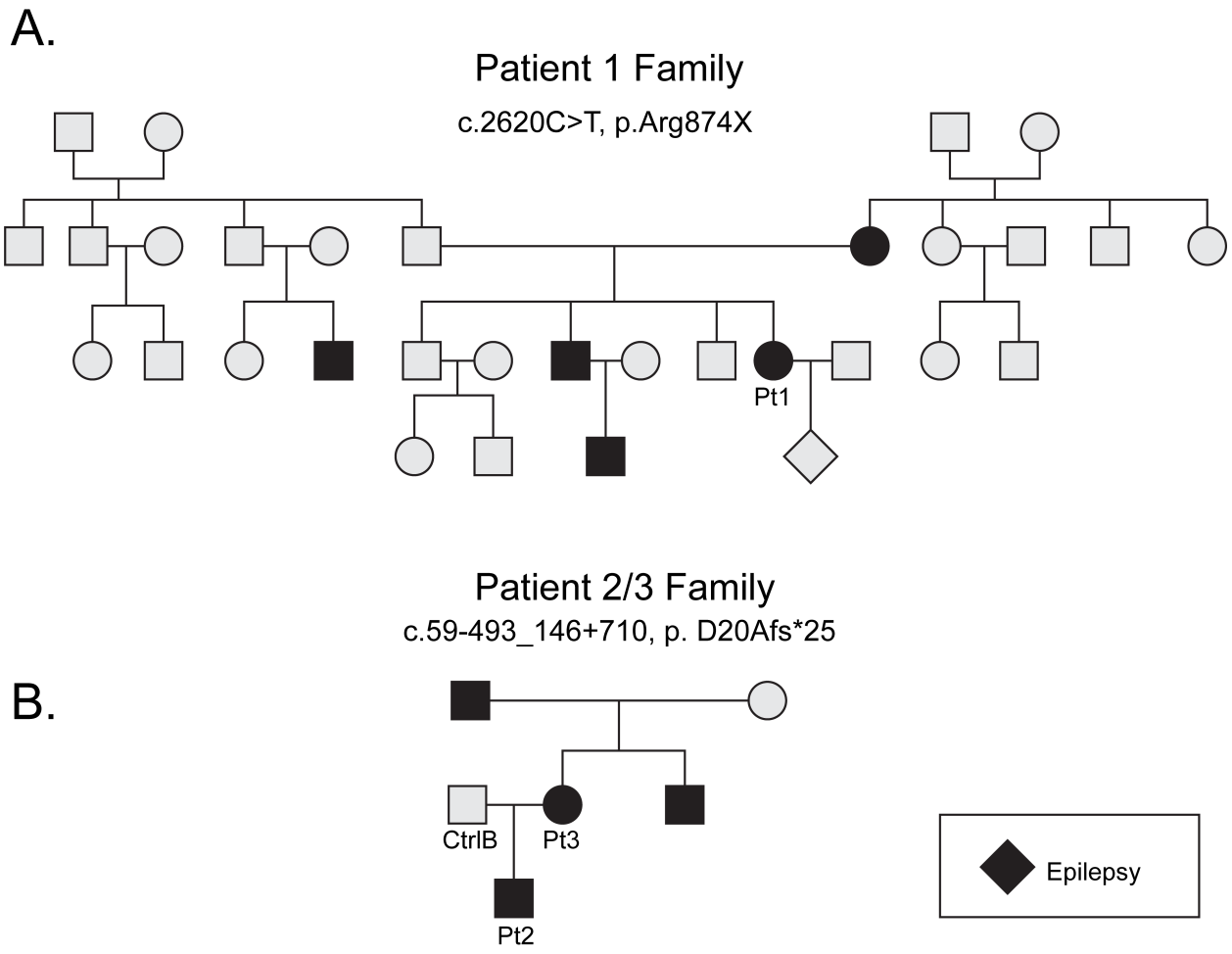

Figure 2-2. Pedigrees of epilepsy patient families suggest an autosomal dominant inheritance pattern.
(A) Pedigree of family of Patient 1. (B) Pedigree of family of Patients 2 and 3 including unaffected relative Control B.

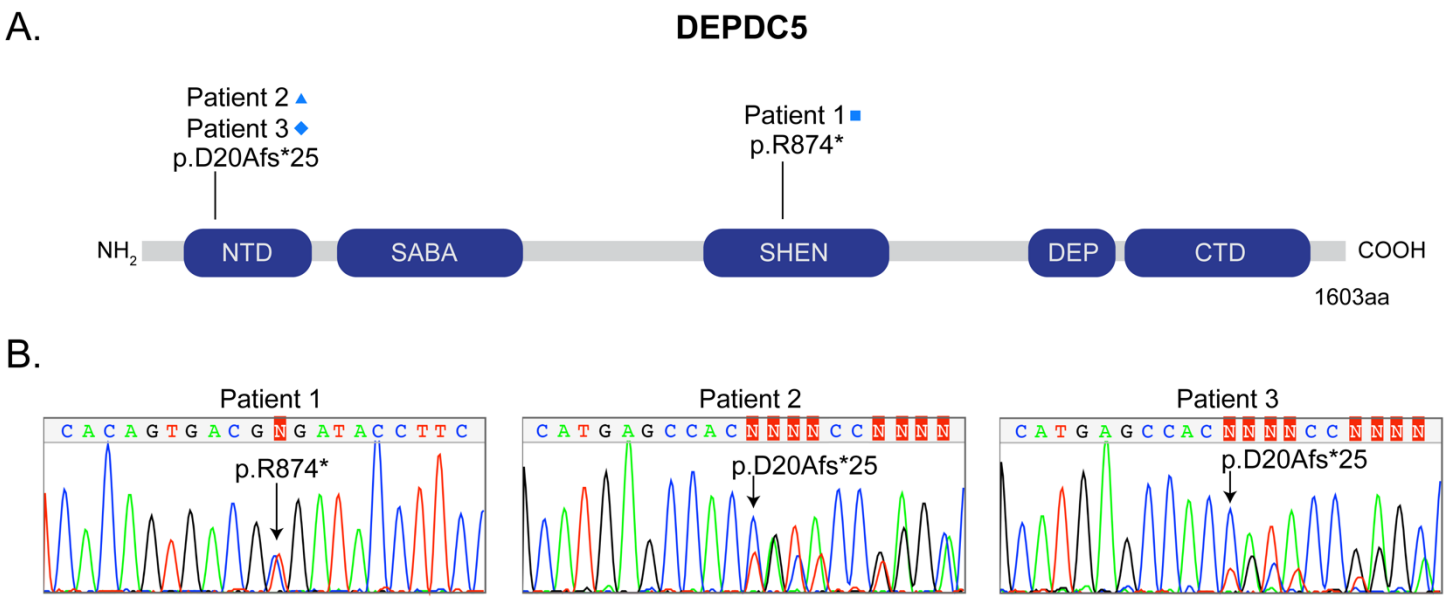

Figure 2-3. Locations of mutation variants in iPSCs generated from patients with epilepsy and *DEPDC5* mutations. (A) Cartoon structure of DEPDC5 protein domains indicating the location of patient mutations. NTD: N-Terminal Domain, SHEN: Steric Hindrance for Enhancement of Nucleotidase-activity, SABA: Structural Axis for Binding Arrangement, DEP: Dishevelled, EGL-10, and Pleckstrin, CTD: C-Terminal Domain. (B) DNA sequencing chromatograms of representative patient-derived iPSC lines demonstrating a single base pair mutation in patient 1 (c.2620C>T; p.R874*) and 1291 bp deletion in patients 2 and 3 (c.59-493_146+710; p.D20Afs*25

Control or patient cell line	Sex	Genotype/ Mutation in *DEPDC5*	Age of onset	Semiology	EEG/MRI findings	Failed medications	Current treatment
Pt1	F	c.2620C>T; p.Arg874X	10 y	Out of sleep; sudden arousal with whole body stiffening	Normal interictal EEG; ictal EEG suggested seizure onset from mesial central region Normal MRI	Topiramate, lamotrigine	Levetiracetam, oxcarbazepine, vagus nerve stimulator
Pt2	M	c.59-493_146+710; p.D20Afs*25	3 y	Most out of sleep, right eye deviation with extremity stiffening	Right frontal seizures/interictal discharges Normal MRI	clobazam	levetiracetam oxcarbazepine lamotrigine
Pt3	F	c.59-493_146+710; p.D20Afs*25	20 y	Exclusively out of sleep	Normal MRI	clobazam	levetiracetam lamotrigine
CtrlA	F	Wild-type					
CtrlB	M	Wild-type					

Table 2-1. Additional characteristics of patients with *DEPDC5* mutations and epilepsy from whom iPSC lines were generated.

Validation of iPSCs

iPSCs colonies had typical morphology (**Figure 2-4A**, **Figure 2-5A**). Newly-generated iPSC lines were validated through trilineage differentiation assays, pluripotency marker immunostaining, and karyotype analysis. For trilineage immunostaining, iPSCs were differentiated as embryoid bodies for ten to fourteen days in DMEM/F12 GlutaMax with 20% knockout serum replacement, 1X non-essential amino acids and 55 μM β-mercaptoethanol, and then probed for lineage-specific markers defining ectoderm (Sox1, β-III-Tubulin), mesoderm (smooth muscle actin, brachyury, and/or desmin), and endoderm (GATA4, Sox17) (**Figure 2-4B**, **Figure 2-5B**). Immunostaining was also performed for pluripotency markers: Oct4, Nanog, TRA-1-60, and SSEA3 (**Figure 2-4C**, **Figure 2-5C**). Karyotype analysis of iPSC clones was performed using G-banding analysis of a metaphase spread; all lines used in experiments had normal karyotypes (Genetic Associates, Inc., Nashville, TN) (**Figure 2-4D**, **Figure 2-5D**). PluriTest analysis (ThermoFisher) demonstrated high pluripotency scores for all iPSC lines (**Figure 2-6)**. Several iPSC lines had borderline novelty scores, indicating the presence of minor potential differences from the 40 validated iPSC lines on which the novelty score is based.

Decreased *DEPDC5* mRNA and NPRL2 protein in *DEPDC5*$^{+/-}$ iPSCs suggests impaired GATOR1 expression

Because of limitations in the specificity of available antibodies directed against DEPDC5, we measured *DEPDC5* mRNA levels to determine if loss of a single copy of *DEPDC5* altered mRNA expression. The majority of *DEPDC5* mutations associated with focal epilepsies cause premature truncations of the transcript, likely leading to nonsense-mediated decay (Baldassari et al., 2016). Evidence of nonsense-mediated decay has been experimentally confirmed for several *DEPDC5* disease variants (Picard et al., 2014). Our patient lines had reduced levels of *DEPDC5* mRNA transcripts, suggesting that these *DEPDC5* truncation mutations similarly caused nonsense-mediated decay (**Figure 2-7A**). Expression of DEPDC5 was not significantly different between the two control lines, although some variability did exist (**Figure 2-7B**). All three patient lines demonstrated significantly reduced levels of *DEPDC5* mRNA compared to controls, although *DEPDC5* mRNA expression varied somewhat between patient 1 and patients 2 and 3 (**Figure 2-7C**).

As noted above, DEPDC5 is a constituent of the GATOR1 complex that also includes nitrogen permease regulator-like 2 and 3 (NPRL2 and NPRL3). Loss of DEPDC5 has been shown to result in decreased levels of NPRL2 in animal models, but not when *DEPDC5* mutants are transfected in human cells (van Kranenburg et al., 2015; Yuskaitis et al., 2019). Given

the role of NPRL2 as the catalytic subunit responsible for the GTPase-activating protein (GAP) function of the GATOR1 complex toward RagA/B, which prevents recruitment of mTORC1 to the lysosome when GDP-bound, we sought to determine the extent to which heterozygous loss of *DEPDC5* altered NPRL2 expression (Shen et al., 2019). Quantitation of NPRL2 expression by immunoblot demonstrated decreased expression in patient iPSC lines with heterozygous *DEPDC5* mutation (**Figure 2-8**), suggesting that DEPDC5 haploinsufficiency affects expression or stabilization of other GATOR1 components.

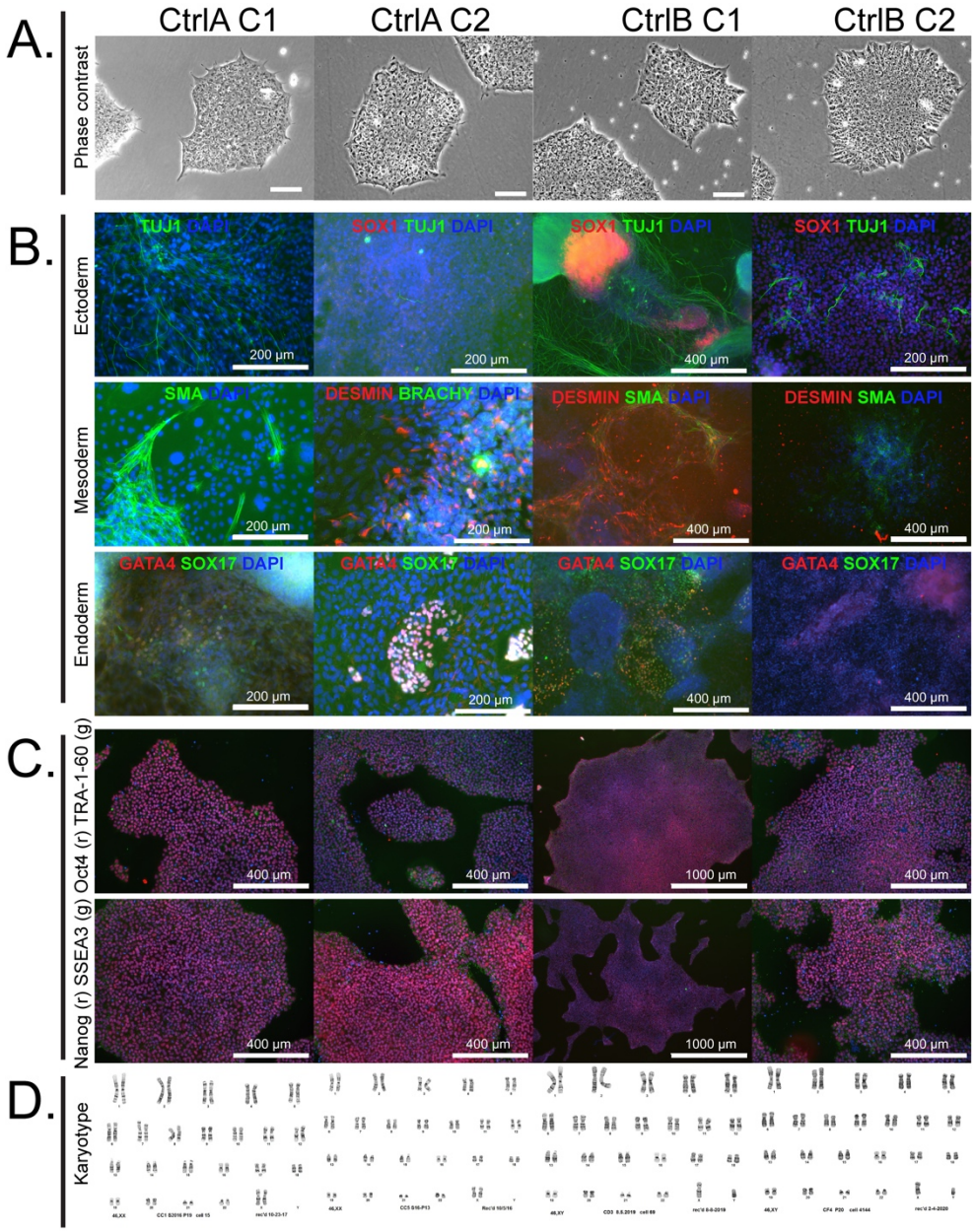

Figure 2-4. Validation of control induced pluripotent stem cell lines.
(A) Representative iPSC colony morphology several days after passage. Scale bars, 100 µm. (B) Embryoid body differentiation from the indicated cell line and clone with immunostaining for markers defining ectoderm (ß-III-Tubulin [green] and/or SOX1 [red]), mesoderm (smooth muscle actin [green], desmin [red], and/or brachyury [green]), and endoderm (GATA4 [red] and/or SOX17 [green]), with DAPI nuclear stain (blue). Scale bars are either 200 or 400 µm and are indicated on each image. (C) Images of iPSC colonies from the indicated cell line and clone stained for pluripotency markers OCT4 (red) and TRA-1-60 (green) (top row) or NANOG (red) and SSEA3 (green) (bottom row), with DAPI nuclear stain (blue). Scale bars are either 400 µm or 1000 µm and are indicated on each image. (D) Karyotype analysis of individual control and patient line clones.

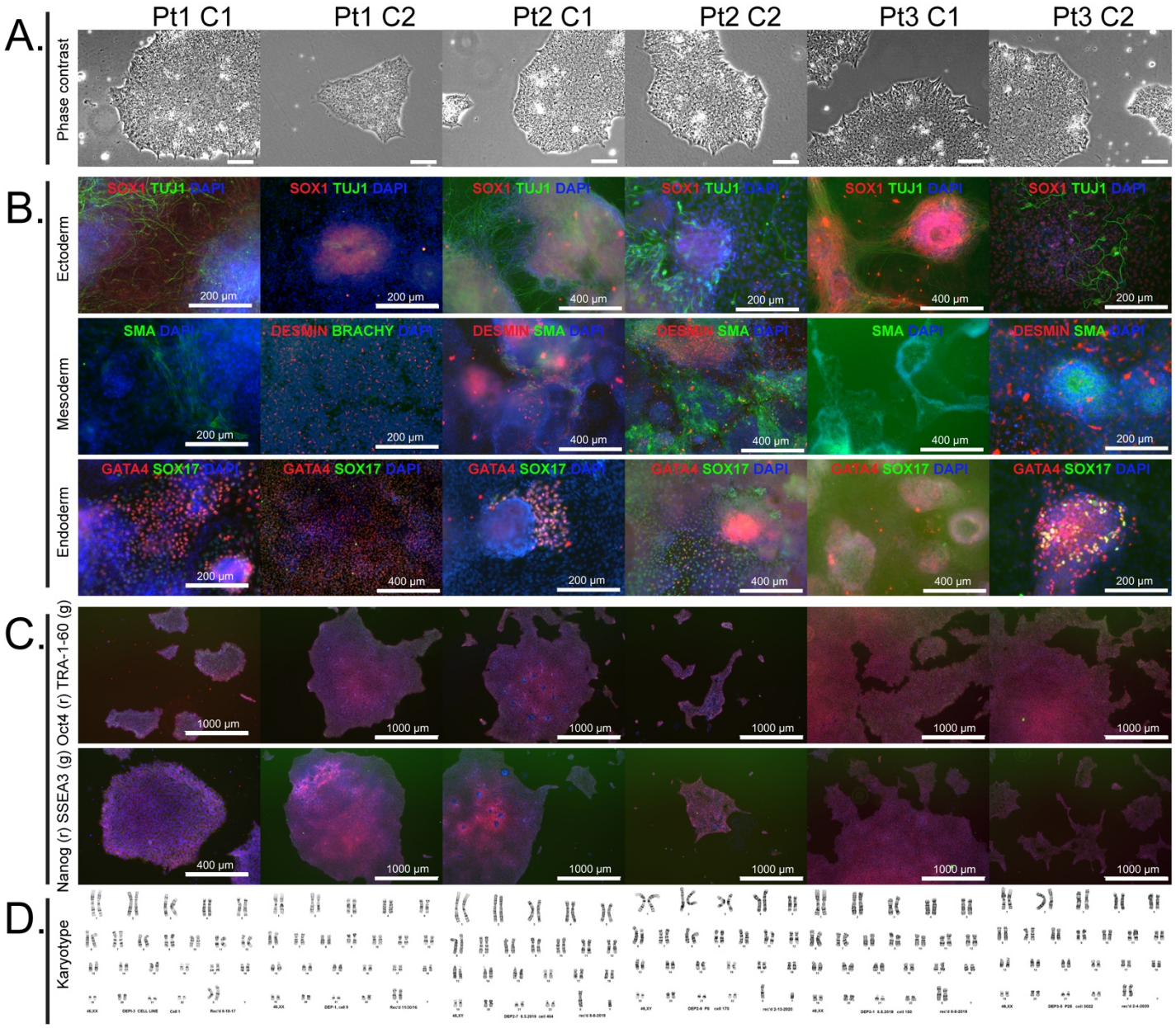

Figure 2-5. Validation of patient-derived induced pluripotent stem cell lines.
(A) Representative iPSC colony morphology several days after passage. Scale bars, 100 µm. (B) Embryoid body differentiation from the indicated cell line and clone with immunostaining for markers defining ectoderm (ß-III-Tubulin [green] and/or SOX1 [red]), mesoderm (smooth muscle actin [green], desmin [red], and/or brachyury [green]), and endoderm (GATA4 [red] and/or SOX17 [green]), with DAPI nuclear stain (blue). Scale bars are either 200 or 400 µm and are indicated on each image. (C) Images of iPSC colonies from the indicated cell line and clone stained for pluripotency markers OCT4 (red) and TRA-1-60 (green) (top row) or NANOG (red) and SSEA3 (green) (bottom row), with DAPI nuclear stain (blue). Scale bars are either 400 µm or 1000 µm and are indicated on each image. (D) Karyotype analysis of individual control and patient line clones.

A.

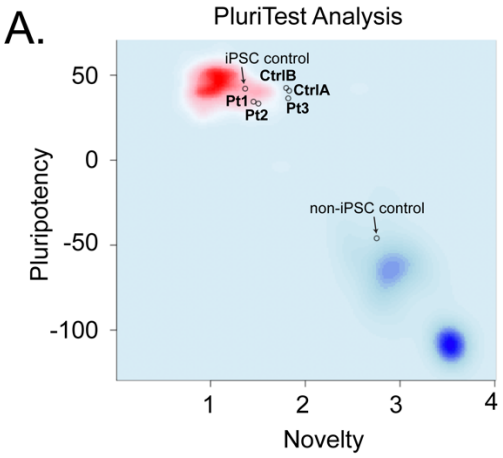

B.

Sample	Sample ID	PluriTest Result	PluriCor	NovelCor
CtrlA C2	CC5 P38	borderline	40.85902	1.829056
CtrlB C1	CD3 P23	borderline	42.47015	1.798372
Pt1 C2	DEP1-29 P30	pass	34.41492	1.453055
Pt2 C1	DEP2-7 P20	pass	33.29757	1.504634
Pt3 C1	DEP3-1 P28	borderline	36.38677	1.819879
	Gibco iPSC	pass	42.0662	1.365211
	HeLa Non_iPSC	fail	-45.9662	2.753088

Figure 2-6. PluriTest results indicate passing pluripotency scores in all lines yet borderline novelty scores in three lines.
(A) PluriTest analysis indicating high pluripotency scores for all iPSC lines and borderline novelty scores for three lines (CtrlA, CtrlB, Pt3), indicating a slightly different molecular signature than the 41 iPSC lines that make up the reference database. Red shaded area indicates expression data from known pluripotent samples, while blue shaded area denotes distribution of non-pluripotent samples. (B) Table showing pluripotency scores (PluriCor, empirical threshold: 20) and novelty scores (NovelCor, empirical threshold: 1.67) for the various iPSC lines tested in addition to a verified iPSC control (Gibco iPSC) and a non-iPSC control (HeLa cells).

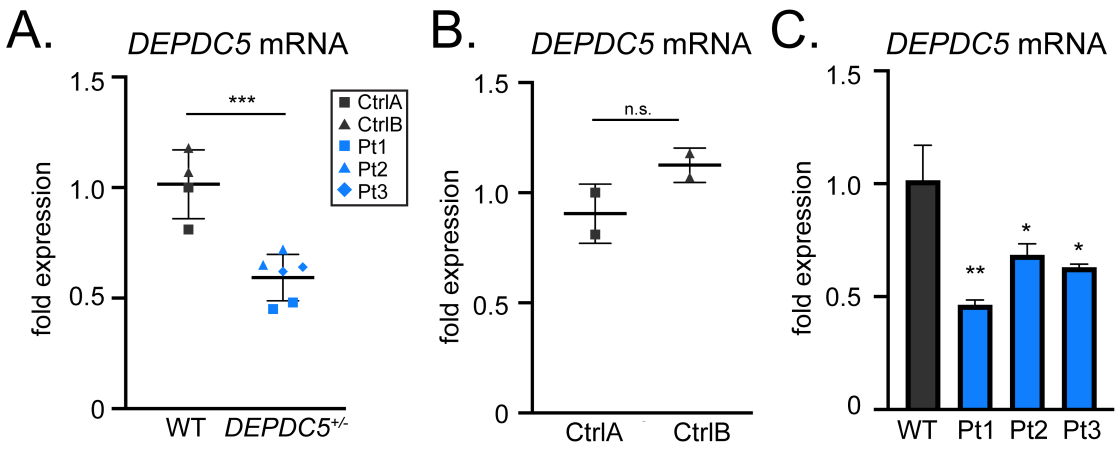

Figure 2-7. iPSCs generated from epilepsy patients with *DEPDC5* mutations demonstrate decreased *DEPDC5* mRNA expression.

(A) mRNA expression in patient-derived cell lines heterozygous for *DEPDC5* mutations. Experiments represent the average of three technical replicates, n=2 controls and n=3 patients, two clones each. Unpaired t-test, p=.0009. Bars represent mean ± SD. (B) *DEPDC5* mRNA expression in control A and control B, n=2 clones, t test, p=.1829. (C) *DEPDC5* mRNA expression in individual *DEPDC5*$^{+/-}$ patient lines compared to control. n=2 clones for each cell line, one-way ANOVA with Dunnett's multiple comparisons; WT vs. Pt1, p=.0034; WT vs. Pt2, p=.0372; WT vs. Pt3, p=.0193.

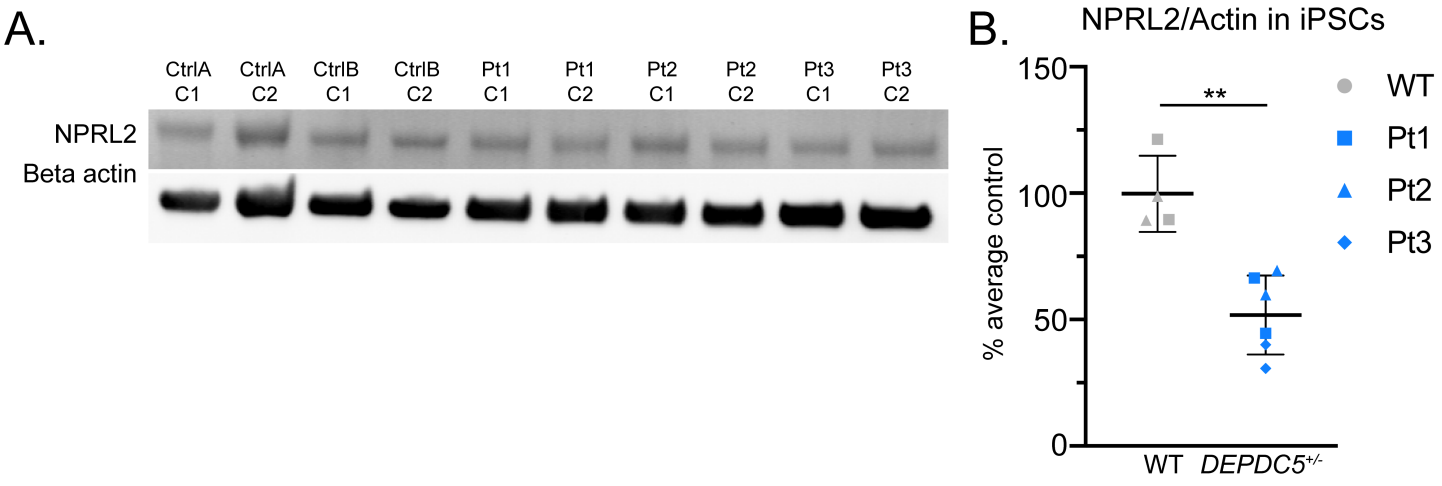

Figure 2-8. NPRL2 expression is decreased in *DEPDC5*$^{+/-}$ patient iPSCs.
(A) Protein immunoblots from control and patient iPSCs probed for NPRL2. Blots were cropped to show the relevant bands. (B) Quantitation of NPRL2/Actin ratio. Groups were compared using unpaired t-test, p=.0052.

Increased activation of mTORC1 signaling in iPSCs from patients with *DEPDC5*-related epilepsy

Knockdown of DEPDC5 has been associated with increased mTORC1 signaling activation, demonstrated by elevated phosphorylation of ribosomal protein S6 (Iffland et al., 2018). Studies examining heterozygous mutations in *TSC1* and *TSC2*, which are also upstream regulators of mTORC1, have reported variable results regarding dysregulation of mTOR signaling in iPSCs (Armstrong et al., 2017; Blair et al., 2018; Li et al., 2017; Winden et al., 2019). We hypothesized that haploinsufficiency of *DEPDC5* caused by heterozygous inactivating mutations (*DEPDC5*$^{+/-}$) would allow increased mTORC1 activity in patient-derived iPSCs. We first evaluated the phosphoprotein signal of ribosomal S6 (Ser240/244), a downstream target of mTORC1, by immunofluorescence. *DEPDC5*$^{+/-}$ iPSCs demonstrated a uniformly increased p-S6 (S240/244) signal intensity when compared to control iPSCs (**Figure 2-9A**), suggesting mTORC1 elevation. To further characterize mTOR signaling pathway activation in iPSCs, we measured phosphorylation of downstream targets of mTOR signaling, including ribosomal S6 (p-S6, mTORC1), 4E-BP1 (p-4E-BP1, mTORC1), and Akt (p-AKT, mTORC2), using protein immunoblotting (**Figure 2-9B**). *DEPDC5*$^{+/-}$ iPSCs showed significantly increased ratios of p-S6 (S240/244)/total S6 and p-4E-BP1 (T37/46)/total 4E-BP1 compared to controls, indicating hyperactive mTORC1 signaling (**Figure 2-9C-D**). p-AKT(S473)/total Akt ratio was variable between cell lines (**Figure 2-9E**).

Given the effects of mTORC1 activation on cellular proliferation, we assessed the growth rate of control and *DEPDC5*$^{+/-}$ iPSCs as a functional metric. We used cell counting assays to calculate population doubling time and found that heterozygous mutant *DEPDC5* iPSCs had a more rapid doubling time compared to wild-type iPSCs, indicating a faster rate of growth (**Figure 2-10A**). Treatment with rapamycin attenuated the growth rate (**Figure 2-10B**). These data further support increased mTORC1 activation in iPSCs with heterozygous *DEPDC5* mutations.

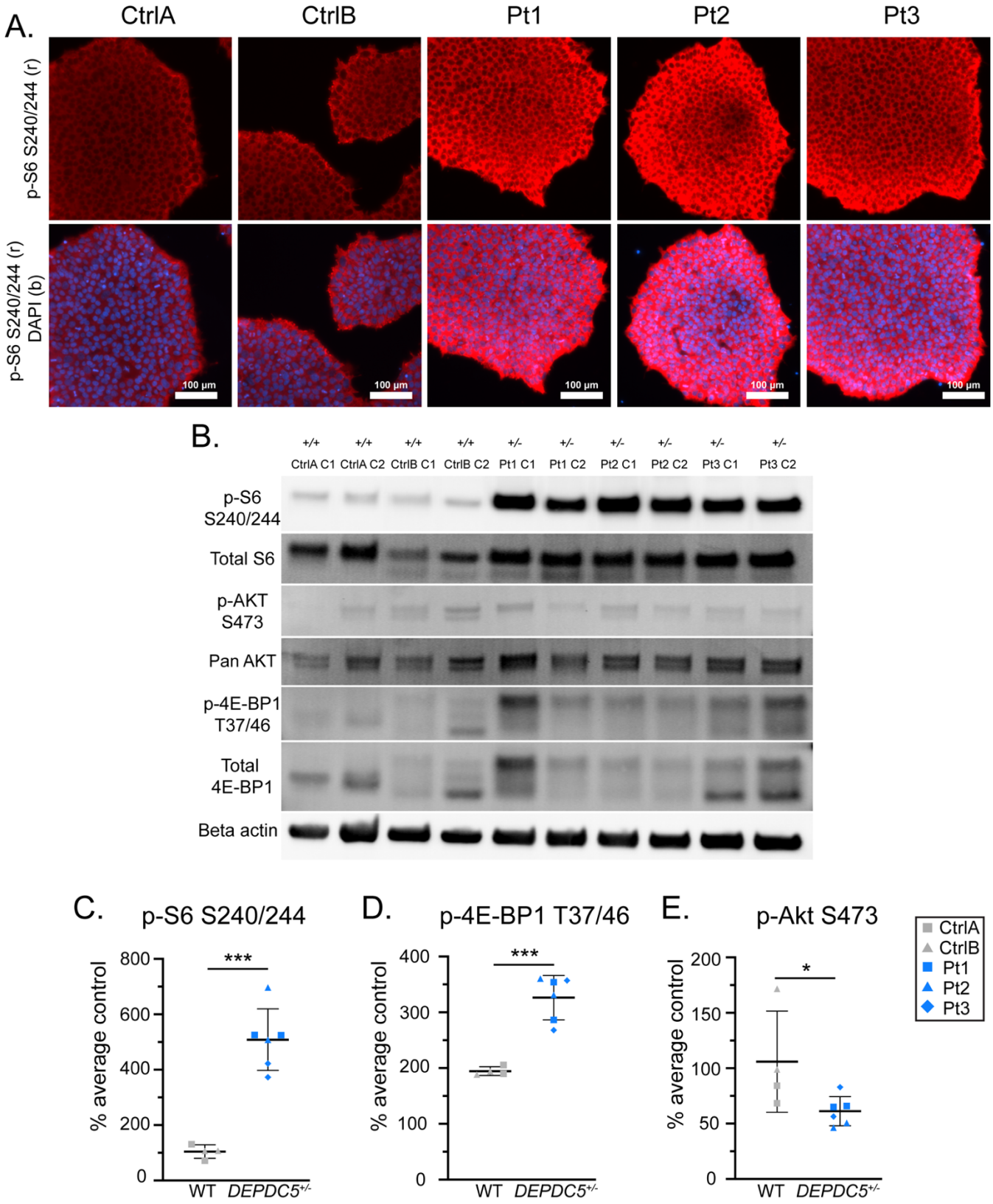

Figure 2-9. Elevated mTORC1 signaling in *DEPDC5*$^{+/-}$ patient iPSCs.
(A) Immunofluorescence images demonstrating p-S6 Ser240/244 (red) expression in control and *DEPDC5*$^{+/-}$ patient iPSCs with DAPI nuclear staining (blue). Scale bar = 100 µm. (B) Representative immunoblot of protein lysates from n=2 control and n=3 *DEPDC5*$^{+/-}$ patient iPSC lines (2 clones per line) evaluating mTOR signaling. Blots were cropped to show the relevant bands. Dots represent the average of 2-3 experimental replicates from different passages. Different symbols indicate different individuals, with each dot representing a unique clone. (C) Quantification of immunoblot results for p-S6 (Ser240/244) in iPSCs, p=.0001. (D) Quantification of immunoblot results for p-4E-BP1 (Thr37/46) in iPSCs, p=.0002. (E) Quantification of immunoblot results for p-AKT (Ser473) in iPSCs, p=.0494.

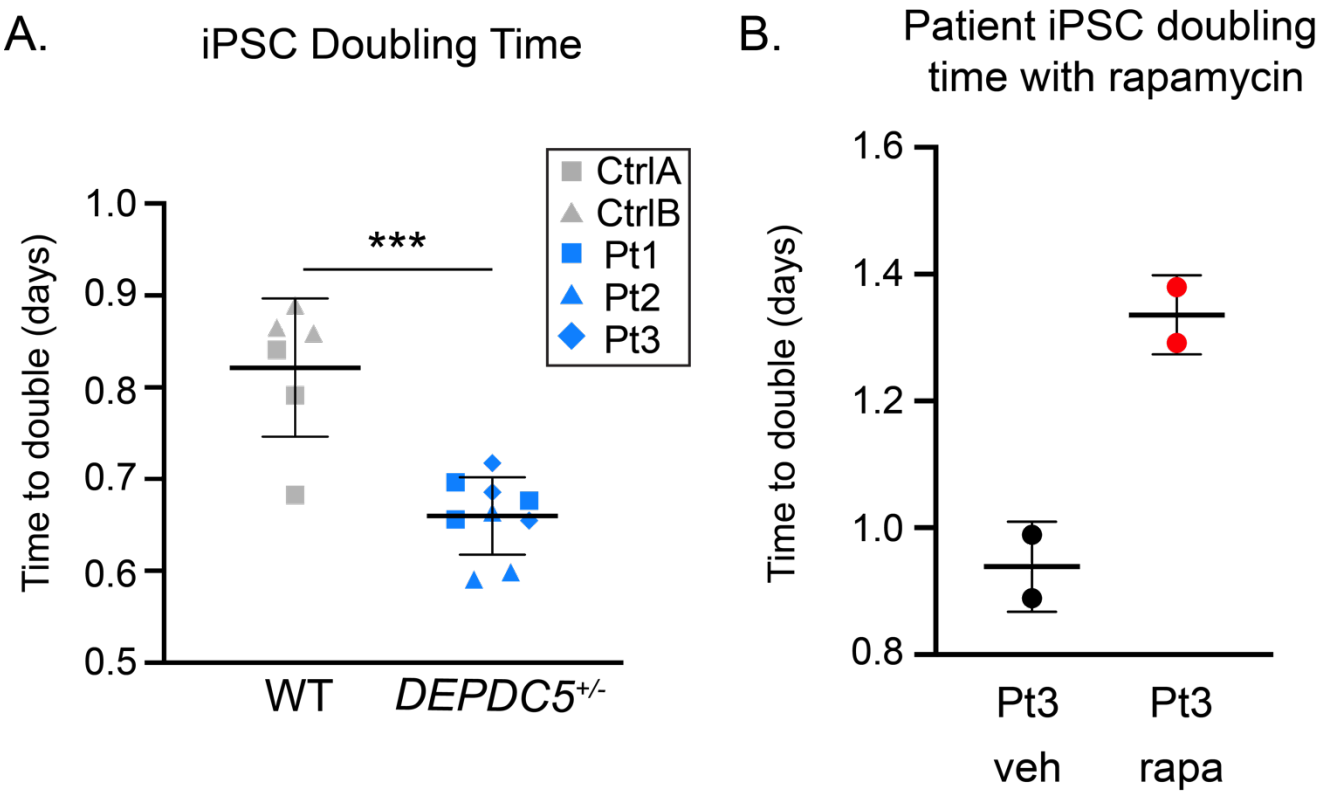

Figure 2-10. *DEPDC5*$^{+/-}$ patient iPSCs demonstate a more rapid doubling time that is slowed with rapamycin. (A) iPSC population doubling time during the logarithmic growth phase. n=3 experimental replicates per each cell line, each dot represents one replicate. Unpaired t-test, p=.0001. One-way ANOVA with Dunnett's multiple comparisons was used to compare individual patient lines to WT, with WT vs. Pt1, p=.0102; WT vs. Pt2, p=.0009; WT vs. Pt3, p=.0155. (B) iPSC population doubling time for patient iPSCs grown in vehicle (40% DMSO in PBS, diluted 1:2000) or rapamycin (10 nM). n=2 experimental replicates, t test, p=.027. Bars on all graphs represent mean ± SD.

Dynamics of mTOR signaling activity in response to rapamycin and nutrient-stimulation differ in *DEPDC5*-mutant cells.

To further characterize the phosphorylation events downstream of mTORC1 and mTORC2, cultured iPSCs were analyzed by flow cytometry (**Figure 2-11**). Based on immunofluorescent staining results, we hypothesized that we may see two populations of control iPSCs, comprising both low and high p-S6 (S240/244) intensity, as opposed to a single population of high p-S6 signal in *DEPDC5*$^{+/-}$ iPSCs. In contrast to the immunoblot results, no significant differences in phosphorylation status of the known mTORC1 targets p-S6 (S240/244) or p-4E-BP1 (T37/46), mTORC2 target p-AKT (S473), or p-S6 (S235/236) were detected in baseline conditions, although DEPDC5+/- iPSCs had a trend toward reduced p-AKT and significant variation existed in p-4E-BP1 (**Figure 2-12, A-D**). Following 24 hours of rapamycin treatment (20 nM), attenuation of the rapamycin-sensitive p-S6 signal occurred in patient and control lines, while there was no change in p-4E-BP1. However, *DEPDC5*$^{+/-}$ iPSCs demonstrated increased p-AKT (S473) signal following rapamycin treatment compared to controls, which did not show changes in p-AKT after rapamycin.

We hypothesized that due to its function as a nutrient sensor, *DEPDC5* haploinsufficiency may cause an altered response to nutrient stimulation. We repeated the flow cytometry experiments in iPSCs, adding a brief 10-minute nutrient stimulus with fresh stem cell media prior to fixation. This timepoint was selected because translocation of mTORC1 to the lysosome peaks minutes after addition of amino acids, with a slight delay in phosphorylation of canonical mTORC1 targets (Manifava et al., 2016). We confirmed that these temporal dynamics were applicable in iPSCs, which display recovered phosphorylation of p-S6 10 minutes after refeeding (**Figure 2-13**). Again, no significant differences in the phosphorylation status of chosen targets were detected in vehicle-treated conditions even after nutrient stimulation (**Figure 2-12, E-H**). However, *DEPDC5*$^{+/-}$ iPSCs demonstrated divergent responses following rapamycin treatment when compared to controls. While attenuation of the rapamycin-sensitive p-S6 (S240/244) signal was still evident, *DEPDC5*$^{+/-}$ iPSCs had higher p-S6 (S240/244) and p-4E-BP1 signal compared to controls after nutrient stimulation in rapamycin-treated conditions. Control iPSCs did not show significant changes in either p-AKT or p-4E-BP1.

Biaxial plots were generated to determine the relationship between p-S6 (S240/244) and p-4E-BP1 signals (**Figure 2-14A**). The population of cells high for both p-4E-BP1 and p-S6 decreased following rapamycin treatment in both controls and patient-derived lines (**Figure 2-14B**). However, the population of cells high in p-4E-BP1 but low for p-S6 increased in *DEPDC5*$^{+/-}$ lines following rapamycin treatment (**Figure 2-14C**). This population of cells thus had

attenuation in S6 phosphorylation in response to rapamycin but hyperphosphorylation of 4E-BP1. Biaxial plots were also generated to determine if 4E-BP1 phosphorylation correlated with Akt phosphorylation (**Figure 2-14D**). Cells with high p-4E-BP1 signal in *DEPDC5*$^{+/-}$ lines following rapamycin treatment were generally also high for p-AKT, with *DEPDC5*$^{+/-}$ lines having a greater percentage of high p-4E-BP1/high p-AKT cells than controls (**Figure 2-14E**). These data indicate that while the p-S6 signal in *DEPDC5*$^{+/-}$ iPSCs can be attenuated with rapamycin, *DEPDC5*$^{+/-}$ lines differ from controls in mTOR signaling pathway activation patterns even after rapamycin treatment, including increased p-AKT (S473) and altered temporal dynamics of the nutrient response.

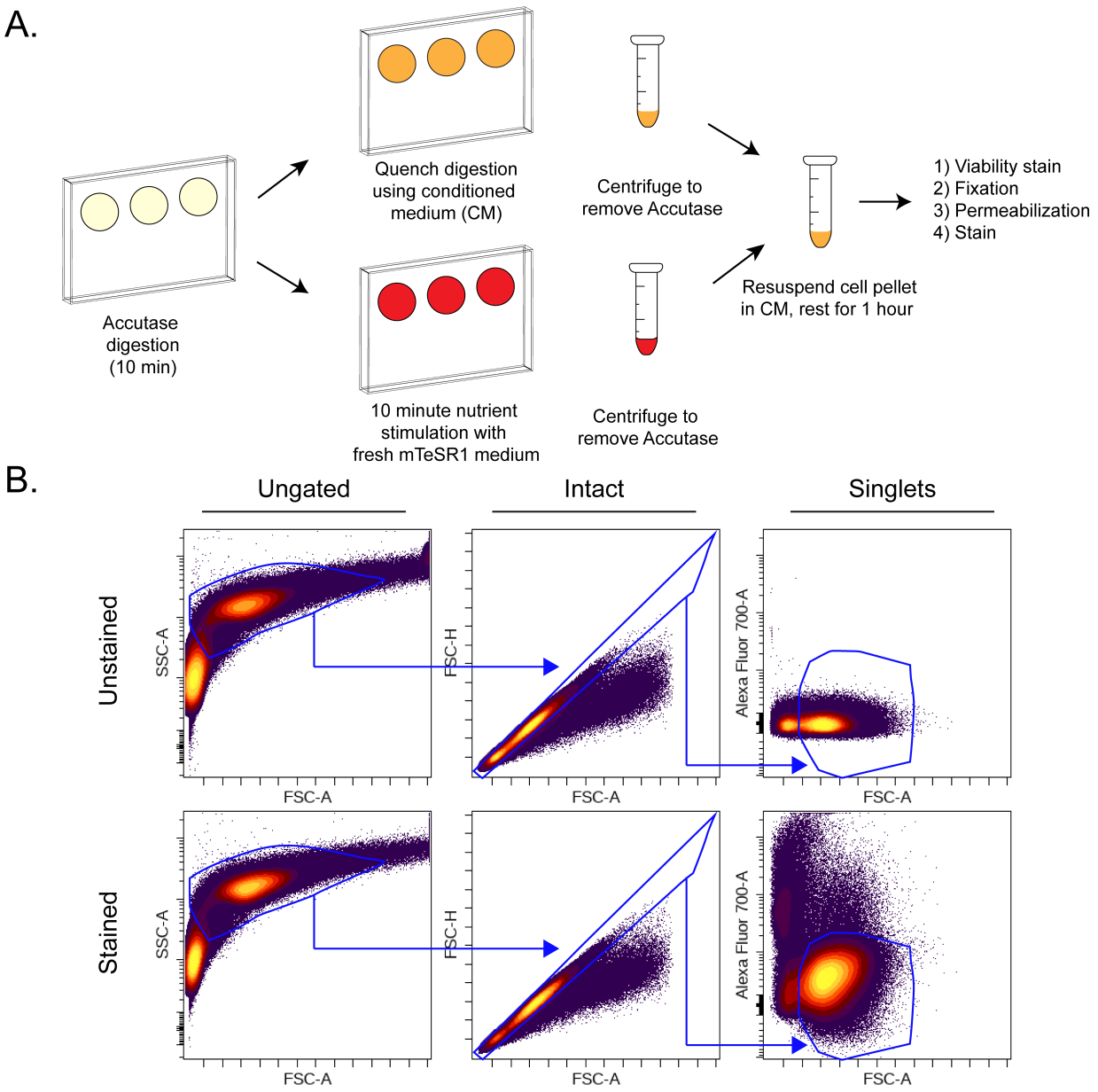

Figure 2-11. Experimental and gating strategy for flow cytometry studies.
(A) Experimental design for nutrient stimulation experiments. Cells were digested with Accutase for 10 minutes to dissociate to single cells. Digestion of each well of cells was either quenched with its own conditioned mTeSR1 medium (after 24h of culture) or fresh mTeSR1 medium. Cells were pelleted and resuspended in additional conditioned medium taken from the original well, rested, stained for viability, fixed, permeabilized, and stained for target proteins. (B) Gating strategy for identifying viable single cells.

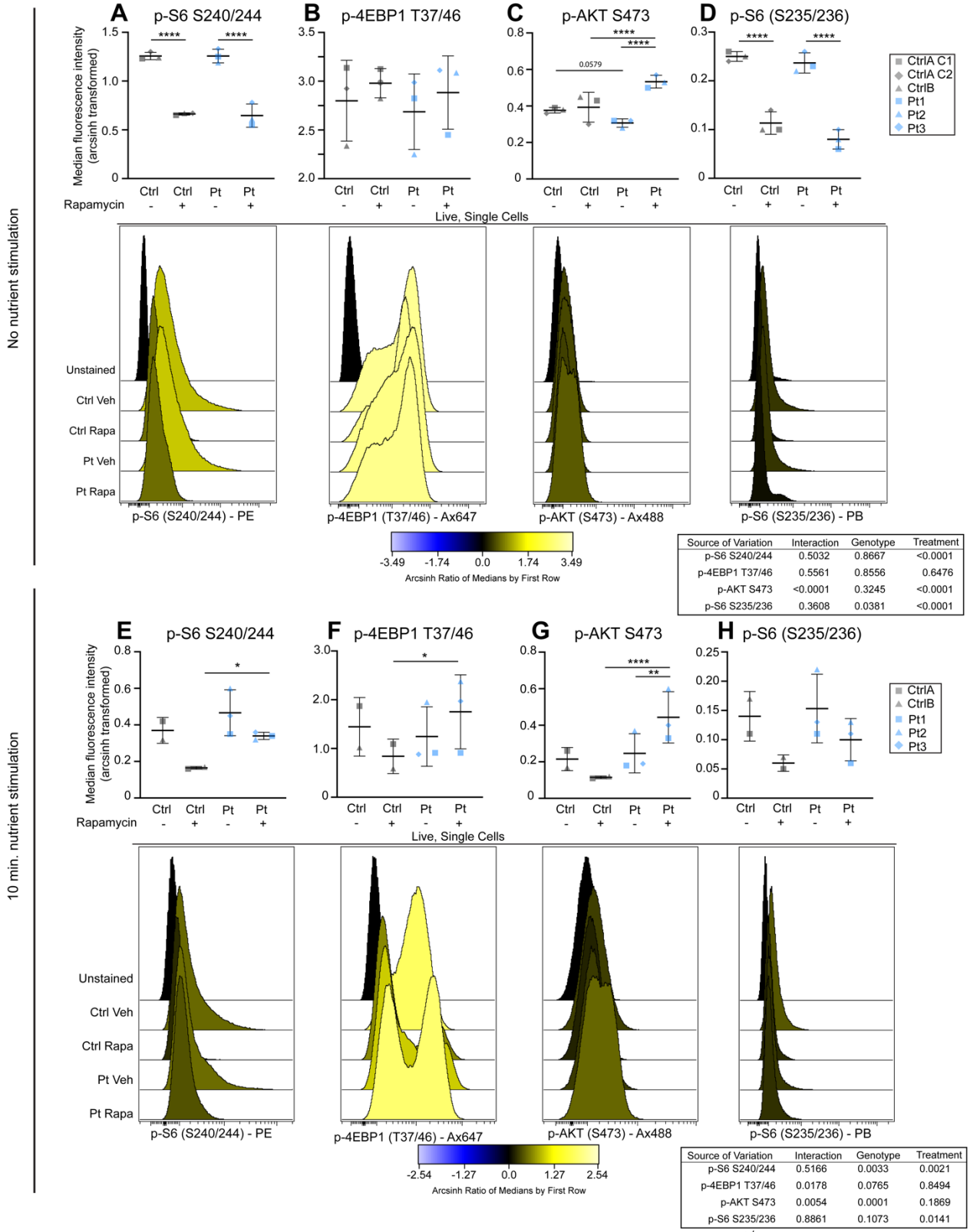

Source of Variation	Interaction	Genotype	Treatment
p-S6 S240/244	0.5032	0.8667	<0.0001
p-4EBP1 T37/46	0.5561	0.8556	0.6476
p-AKT S473	<0.0001	0.3245	<0.0001
p-S6 S235/236	0.3608	0.0381	<0.0001

Source of Variation	Interaction	Genotype	Treatment
p-S6 S240/244	0.5166	0.0033	0.0021
p-4EBP1 T37/46	0.0178	0.0765	0.8494
p-AKT S473	0.0054	0.0001	0.1869
p-S6 S235/236	0.8861	0.1073	0.0141

Figure 2-12. Divergent responses to rapamycin and nutrient stimulation in *DEPDC5*$^{+/-}$ iPSCs.
Graphs and representative histograms of median fluorescence intensity, relative to unstained samples, of phosphorylated proteins measured by flow cytometry. (A-D) No nutrient stimulation. (E-H) After 10-minute nutrient stimulation with fresh stem cell medium (mTeSR1). Scale indicates transformed arcsinh scale comparing intensity to unstained cells for each line. A difference of 0.4 on the arcsinh scale represents an approximately twofold difference in total phosphorylated epitope levels per cell. Each dot represents the median of three experimental replicates from a single individual. Histograms represent the median of control or *DEPDC5*$^{+/-}$ lines. Groups were compared using two-way ANOVA with Tukey's multiple comparisons, with significant differences indicated by *p<.05, **p<.01, ***p<.001, ****p<.0001. All bars represent mean ± SD.

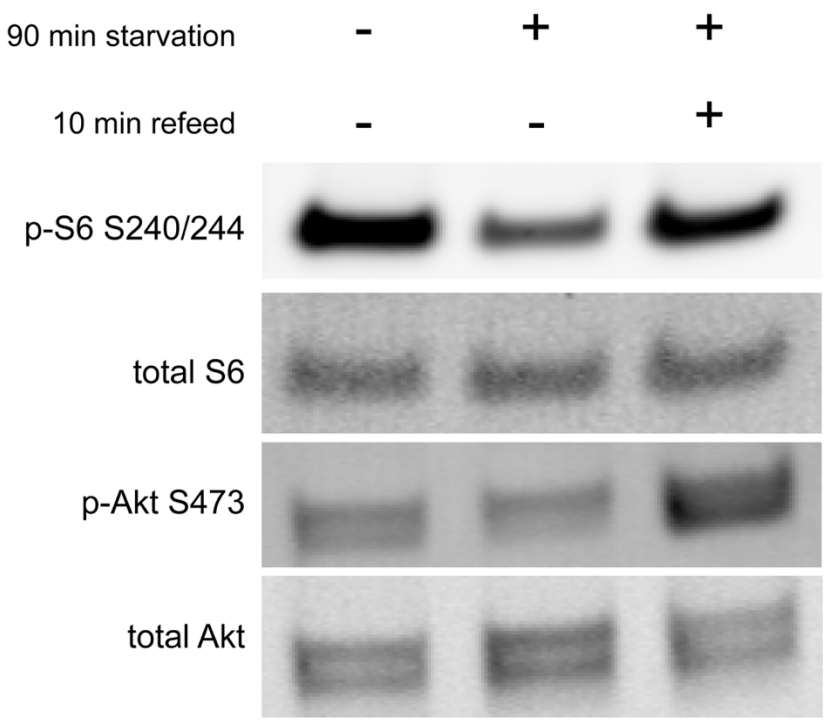

Figure 2-13. Temporal response of iPSCs to refeeding after nutrient starvation.
90-minute starvation followed by refeeding indicates that iPSCs have temporal dynamics similar to those described by (Manifava et al.), with phosphorylation of mTORC1 downstream target p-S6 evident within 10 minutes following refeeding.

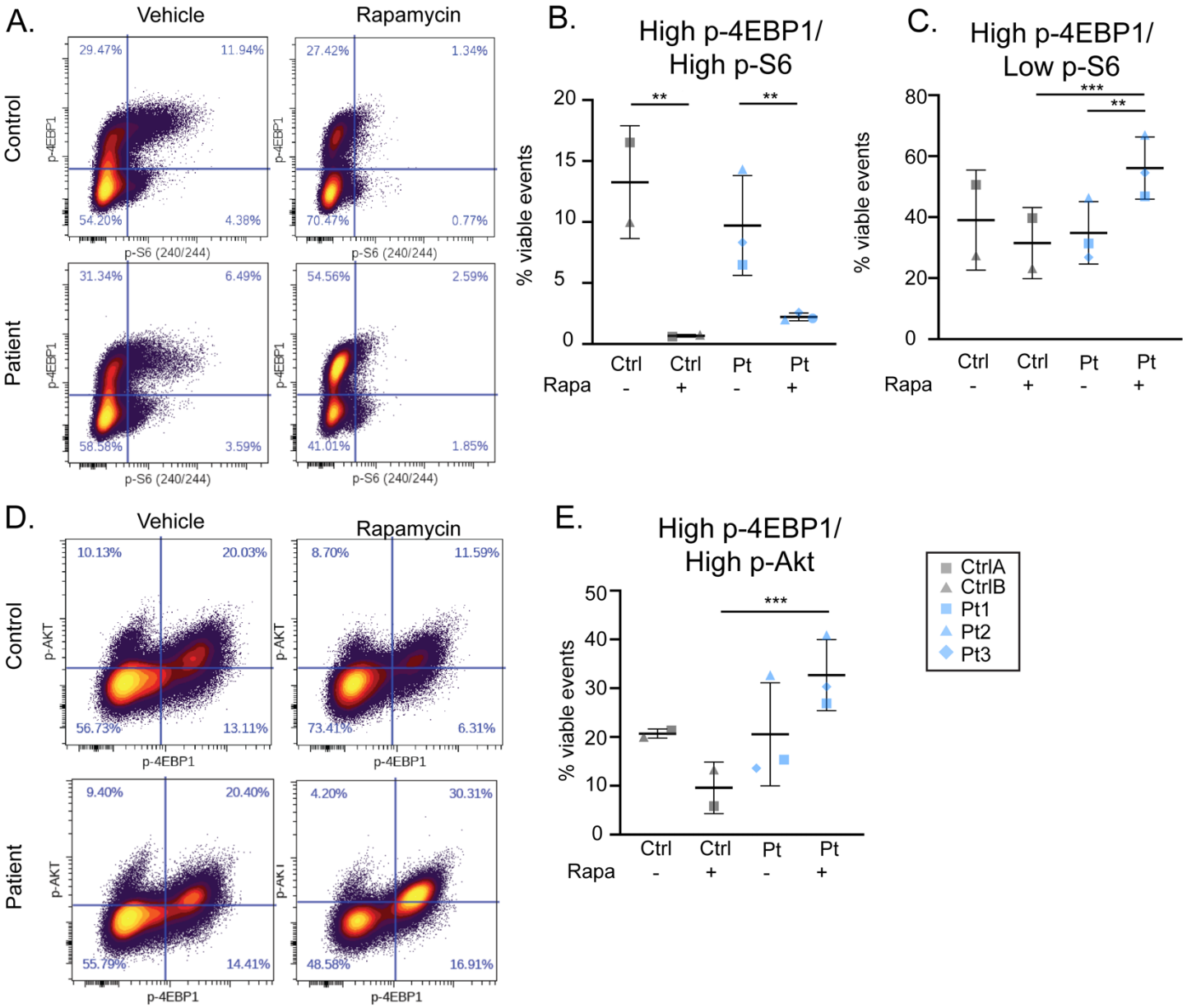

Figure 2-14. Biaxial plots demonstrate mTOR pathway changes following rapamycin treatment specific to *DEPDC5*$^{+/-}$ iPSCs.

(A) Biaxial plots of p-4E-BP1 vs. p-S6 generated using a quad gate strategy. (B) Percentage of cells with high expression of both p-4E-BP1 and p-S6, before and after 24h of treatment with 20 nM rapamycin. (C) Percentage of cells with high expression of p-4E-BP1 but low expression of p-S6, before and after 24h of treatment with 20 nM rapamycin. (D) Biaxial plots of p-4E-BP1(T37/46) vs. p-AKT (S473) created using a quad gate strategy. (E) Percentage of cells with high expression of both p-4E-BP1 and p-AKT, before and after 24h of treatment with 20 nM rapamycin. Groups were compared using two-way ANOVA with Tukey's multiple comparisons, with significant differences compared to control indicated by *p<.05, **p<.01, ***p<.001, ****p<.0001. All bars represent mean ± SD.

Therapeutic potential of drugs promoting readthrough of premature termination codons

While rapamycin is a potent mTORC1 inhibitor, long-term use may have unwanted side effects, particularly metabolic changes such as insulin resistance (Salmon, 2015). The development of alternative therapeutic strategies with fewer long-term side effects represents a possible solution. For example, forced pharmacologic readthrough of premature termination codons (PTCs) in order to stabilize mRNA and generate a full protein represents an alternative therapeutic strategy for patients with truncating nonsense mutations in *DEPDC5,* which represent the majority (Baldassari et al., 2019a). Indeed, this type of therapy is currently approved for treatment of Duchenne muscular dystrophy, has been studied in cystic fibrosis (although without clear efficacy), and has been successful in *in vitro* models of congenital blindness and frontotemporal dementia (Kuang et al., 2020; Landfeldt et al., 2019; Shahi et al., 2019; Zainal Abidin et al., 2017). *DEPDC5*$^{+/-}$ iPSCs from Patient1, which have a nonsense mutation (R874X) causing a PTC midway through the protein sequence, were treated with the translational readthrough-inducing drug PTC124 at a concentration of 50 μm for 24 hours. Following treatment, iPSCs had reduced levels of p-S6 (S240/244), suggesting potential recovery of *DEPDC5* expression (**Figure 2-15**). Further experiments assessing DEPDC5 protein levels will be needed to confirm that this effect is indeed due to mRNA stabilization and recovery of protein expression.

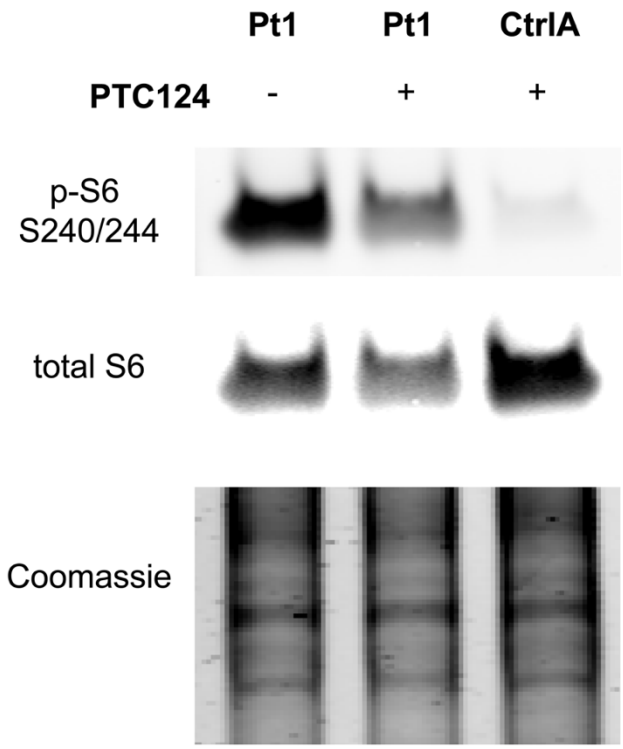

Figure 2-15. Forced pharmacologic readthrough of a premature translation codon attenuates mTORC1 activity in *DEPDC5*$^{+/-}$ iPSCs with R874X mutation.
iPSCs with a truncating mutation in *DEPDC5* (Pt1) were treated with PTC124 or vehicle for 24 hours prior to harvest. The p-S6/total S6 ratio decreased by one-third, from 20.05 in the vehicle-treated condition to 13.24 in the PTC124-treated condition, although the ratio was still elevated compared to CtrlA (0.9325).

Derivation of neuroprogenitor cells and neurons from induced pluripotent stem cells

To investigate the hypothesis that *DEPDC5* haploinsufficiency alters cell morphology and mTOR activation in human neural progenitor cells (NPCs), two control lines and three patient lines were used for neuronal differentiation experiments. iPSCs were differentiated toward a cortical neuronal fate by dual-SMAD inhibition based on modifications of the differentiation protocol initially described by Shi et al. (**Figure 2-16A**) (Shi et al., 2012b). iPSCs subjected to this differentiation protocol undergo a series of morphological changes (**Figure 2-16B**), first going through a neuroepithelial sheet stage, a neural rosette stage, then forming post-mitotic neurons in a developmentally appropriate layer-specific manner. By day 16, nearly 100% of cells of both genotypes are dually positive for Pax6 and Nestin expression (**Figure 2-17A**). Both control and *DEPDC5*$^{+/-}$ patient neurons generated greater than 80% neurons at day 60 (data not shown), based on β-III-Tubulin-positive cells analyzed by flow cytometry. We did not quantify neuronal proportions for each differentiation and instead relied on immunostaining to identify neuroprogenitor cells and neurons. Neurons generated by this protocol develop excitatory synapses, demonstrated by colocalization of Synapsin1 and PSD95 (**Figure 2-17B**), and display electrical activity (Shi et al., 2012b).

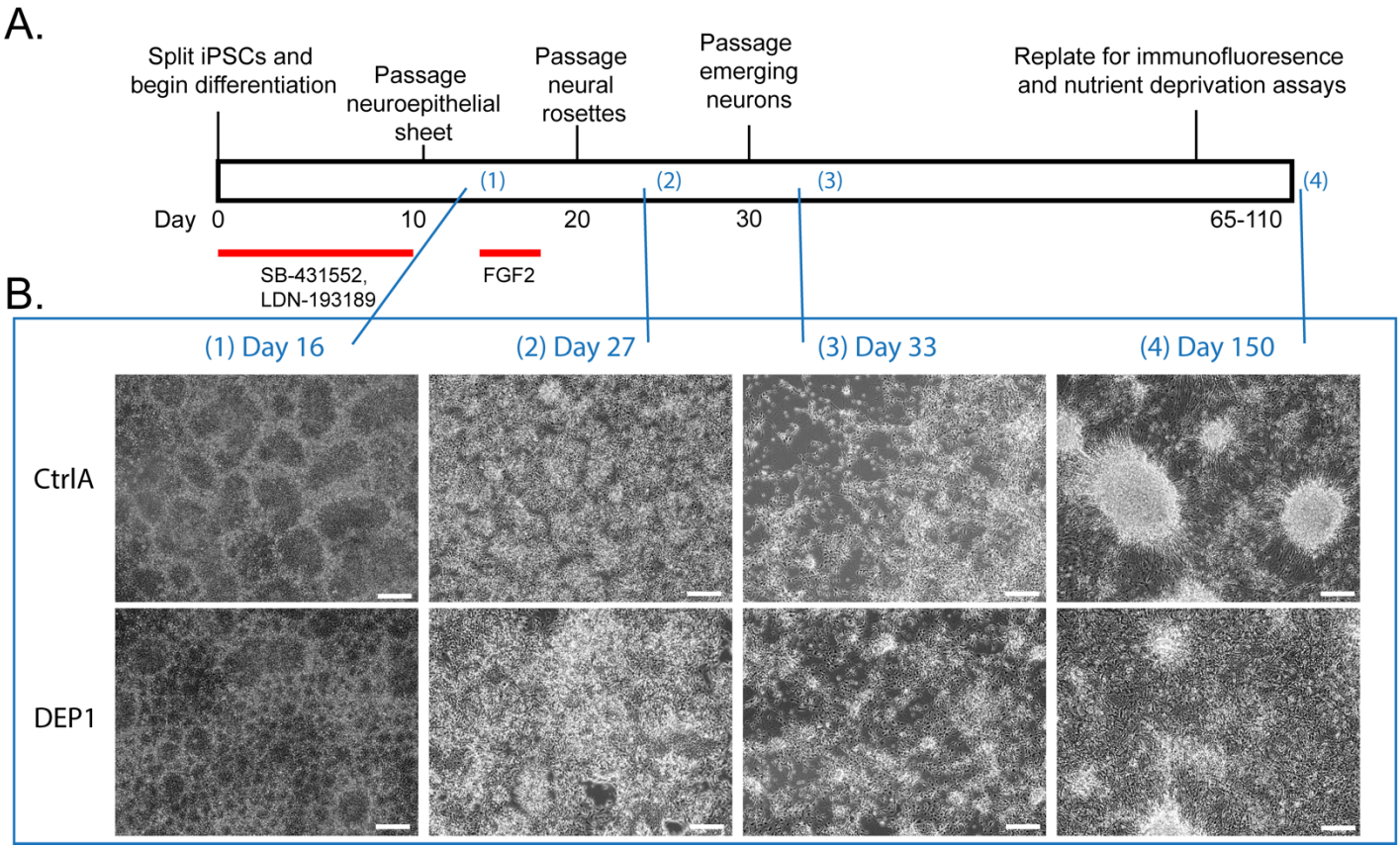

Figure 2-16. Differentiation of cortical neurons from iPSCs.
(A) Cortical neuronal differentiation protocol modified from (Shi et al.). Dual SMAD inhibition with SB-431542 and Noggin analog LDN-193189 is induced for ten days to drive cells toward a neuroprogenitor cell fate. A brief pulse of FGF2 is applied from days 16-18 to promote expansion of neural stem cells. Neurons begin to emerge around day 30, with deep-layer neurons emerging prior to upper-layer neurons. Numbers in blue represent timepoints corresponding to images shown in (B). (B) Representative brightfield images demonstrating morphology of control and DEPDC5+/- cell lines undergoing neuronal differentiation. Scale bar, 200 µm.

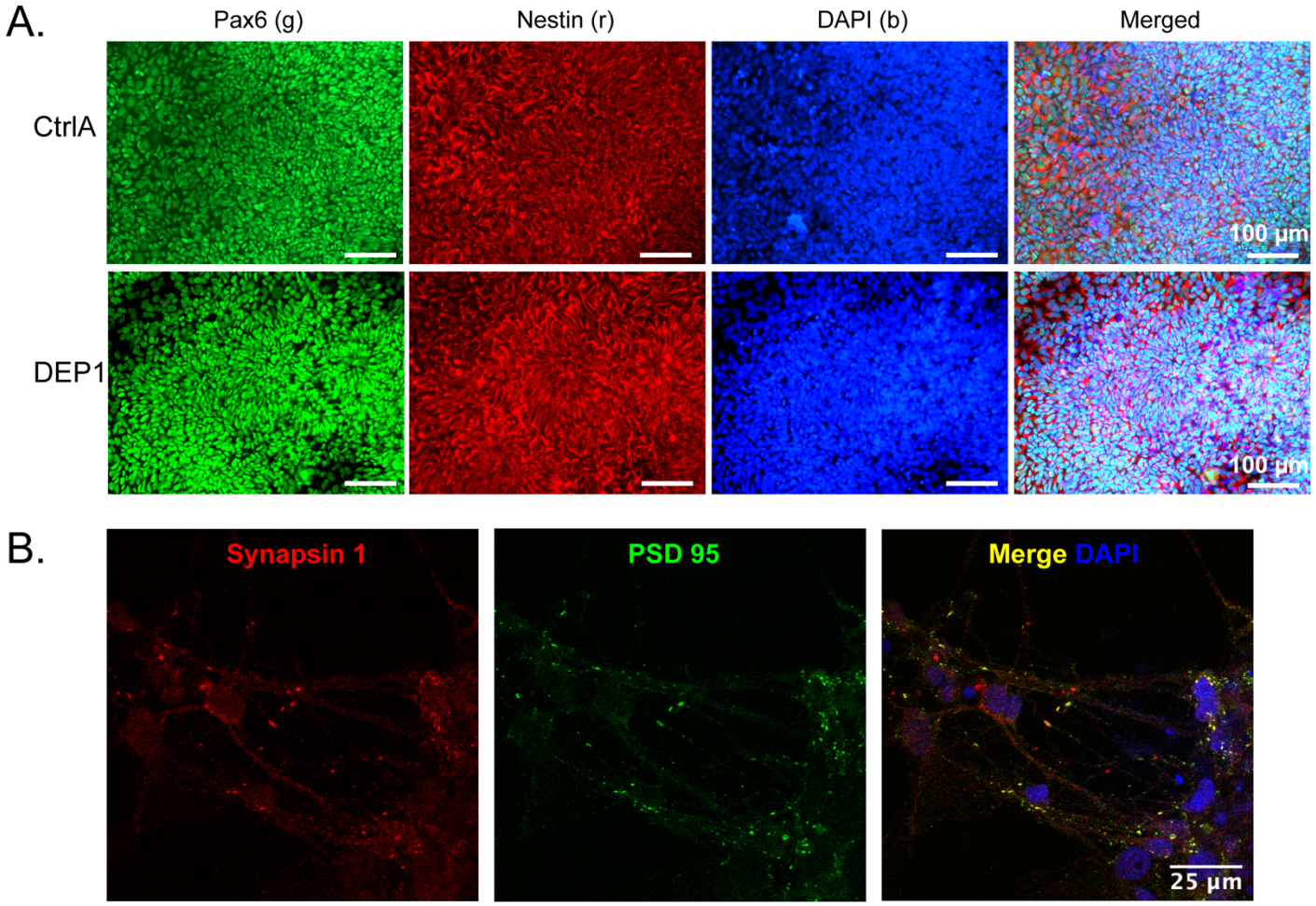

Figure 2-17. Immunofluorescent images of neuroprogenitor cells and physical synapses.
(A) Representative immunofluorescence images taken at day 16, showing control and DEPDC5+/- neuroprogenitor cells beginning to form rosettes. Nearly 100% of cells in both genotypes are positive for both Nestin and Pax6 expression. PAX6 (green), NESTIN (red), DAPI (blue). Scale bar, 100 µm. (B) Immunofluorescence for excitatory synapse proteins Synapsin1 (red), PSD95 (green), and DAPI nuclear stain (blue). Overlap of presynaptic Synapsin1 and postsynaptic PSD95 indicates a physical synapse. Scale bar, 25 µm.

Cytomegaly and increased mTORC1 activation in *DEPDC5*-mutant neuroprogenitor cells.

To determine if haploinsufficiency alters development of neuroprogenitor cells, we examined NPCs for cell size changes and differences in mTORC1 signaling (**Figure 2-18A**). NPCs were defined as Pax6+/Nestin+ cells prior to the formation of neural rosettes and were sparsely plated in order to identify individual cell borders. NPC soma size was measured by filamentous actin staining. The two control lines did not have significantly different NPC soma sizes from one another (unpaired t-test, p=.1521), however we found that *DEPDC5*$^{+/-}$ NPCs had larger soma areas than control cells (**Figure 2-18B-C**). *DEPDC5*$^{+/-}$ NPCs also had higher intensity of mTORC1 target p-S6 (S240/244) expression (**Figure 2-18D**). Larger soma sizes and increased phospho-S6 intensity were consistently seen in all patient lines. These data indicate that *DEPDC5* haploinsufficiency results in increased mTORC1 signaling and cell size during early neurodevelopment.

Cytomegaly in *DEPDC5*$^{+/-}$ neurons is ameliorated by mTORC1 inhibition with rapamycin

To determine if the cell size phenotype persisted as neurons developed, we examined early neurons following the rosette stage (**Figure 2-19A**). Soma size of immature neurons was measured using neuron-specific microtubule-associated protein (MAP2), a protein expressed first in neural precursor cells with subsequent increased expression upon neuronal maturation (Dehmelt and Halpain, 2005). We found that cells at this stage are smaller than NPCs, though immature neurons haploinsufficient for *DEPDC5* continued to demonstrate a larger cell size than control neurons (**Figure 2-19B).**

To confirm that the changes in neuronal size were due to increased mTORC1 activity, rapamycin or vehicle was added to culture media on day 1 of differentiation and continued until cells were fixed for analysis at day 21. Rapamycin was sufficient to attenuate p-S6 (S240/244) intensity in *DEPDC5* haploinsufficient neurons and decrease soma size to a level comparable to controls (**Figure 2-19C-E**). The size of control neurons was not significantly altered by treatment with rapamycin. Immunoblot analyses confirmed a decrease in p-S6 (S240/244) following rapamycin treatment (**Figure 2-19F**). Altogether, these data indicate that the increase in neuronal soma size upon heterozygous *DEPDC5* mutation can be prevented with inhibition of mTORC1. However, the addition of long-term rapamycin did impair the percentage of cells that survived the neuronal differentiation in both control and *DEPDC5*$^{+/-}$ cell lines.

Cytomegaly persists in post-mitotic neurons heterozygous for *DEPDC5* mutation

Since each *DEPDC5*$^{+/-}$ patient line displayed both increased mTORC1 signaling and increased cell size in NPCs and immature neurons, we selected one set of patient clones (Pt1) for the evaluation of mature neuronal morphology. To address cell autonomous phenotypes and limit possible confounding effects of glia, we focused on post-mitotic neurons (after day 65 of differentiation) prior to the emergence of significant glial populations (Shi et al., 2012). Both control and *DEPDC5*$^{+/-}$ lines formed β-tubulin-III+/MAP2+ neurons with well-defined neuronal processes (**Figure 2-20A-B,** data not shown). The increase in soma size first seen in NPCs persisted in post-mitotic neurons with *DEPDC5* heterozygous mutant neurons demonstrating significantly larger MAP2-positive soma sizes than control neurons (**Figure 2-20C**). These findings support that *DEPDC5* haploinsufficiency results in dysregulated and increased mTORC1 activity throughout neuronal development.

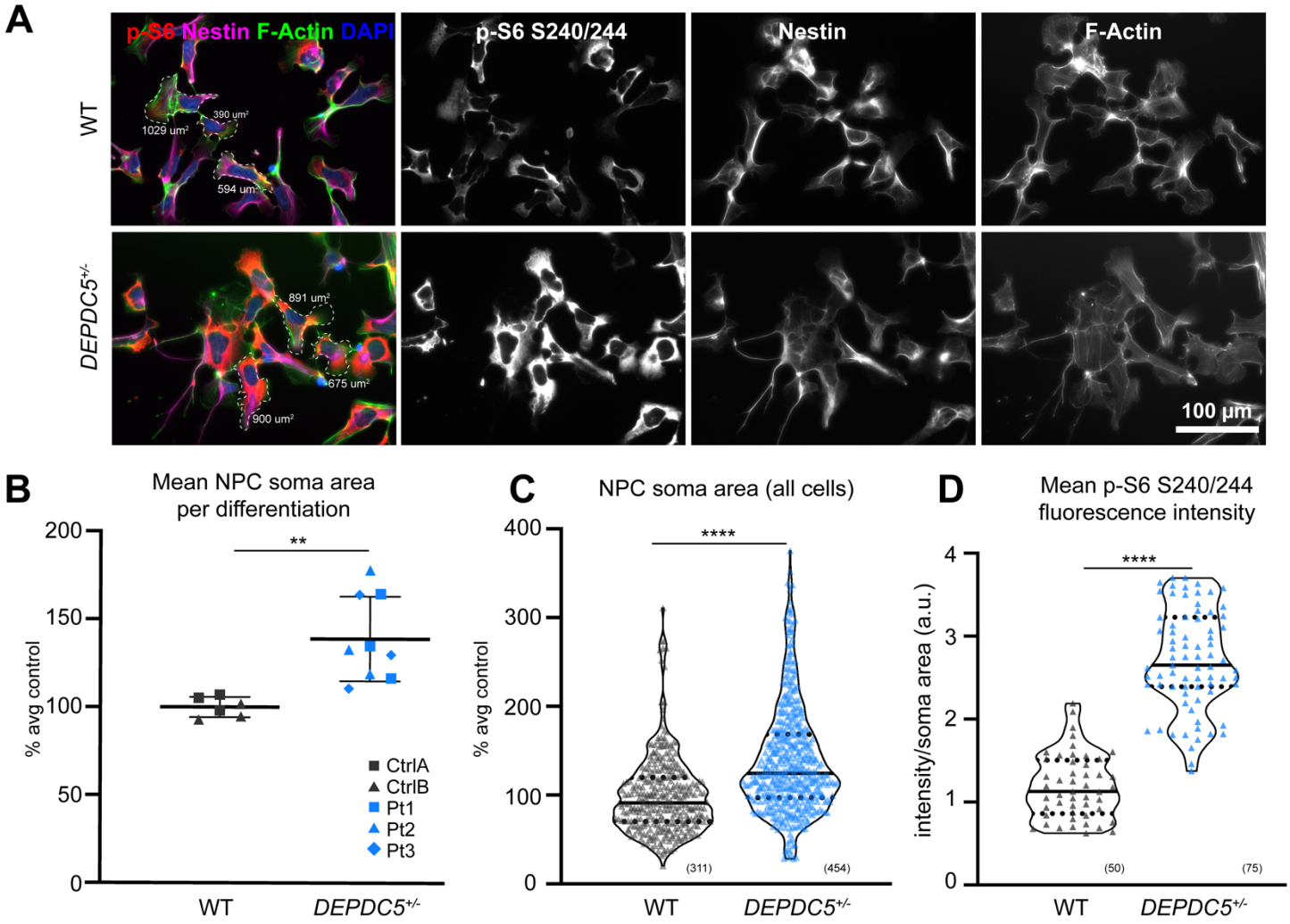

Figure 2-18. *DEPDC5*$^{+/-}$ patient neuroprogenitor cells (NPCs) are cytomegalic with increased mTORC1 signaling. (A) Representative images of control and *DEPDC5*$^{+/-}$ patient NPCs (differentiation day 10) showing expression of p-S6 S240/244 (red), nestin (neuroprogenitor cells, magenta), F-actin (cytoskeleton, green), and DAPI (nuclei, blue). Representative cell size measurements identified with dashed border. (B) Plot of mean soma area in control (grey) or *DEPDC5*$^{+/-}$ patient (blue) neuroprogenitor cells. These plots represent data from two control clones and three patient clones, each with 3 separate differentiations. Each dot indicates an average of 50 cells counted per differentiation. Unpaired t-test, p=.002. (C) Violin plots of F-actin+ soma size of patient and control NPCs. Plots represent data from 311 control or 454 *DEPDC5*$^{+/-}$ cells pooled from 3 separate differentiation experiments. Mann-Whitney test, p<.0001. (D) Violin plot of p-S6 S240/244 fluorescence intensity divided by soma area in *DEPDC5*$^{+/-}$ and control NPCs. Data is pooled from three separate wells of one differentiation, 25 cells per line. Mann-Whitney test, p<.0001. For violin plots, solid line represents mean value and dotted lines represent 25th and 75th percentiles.

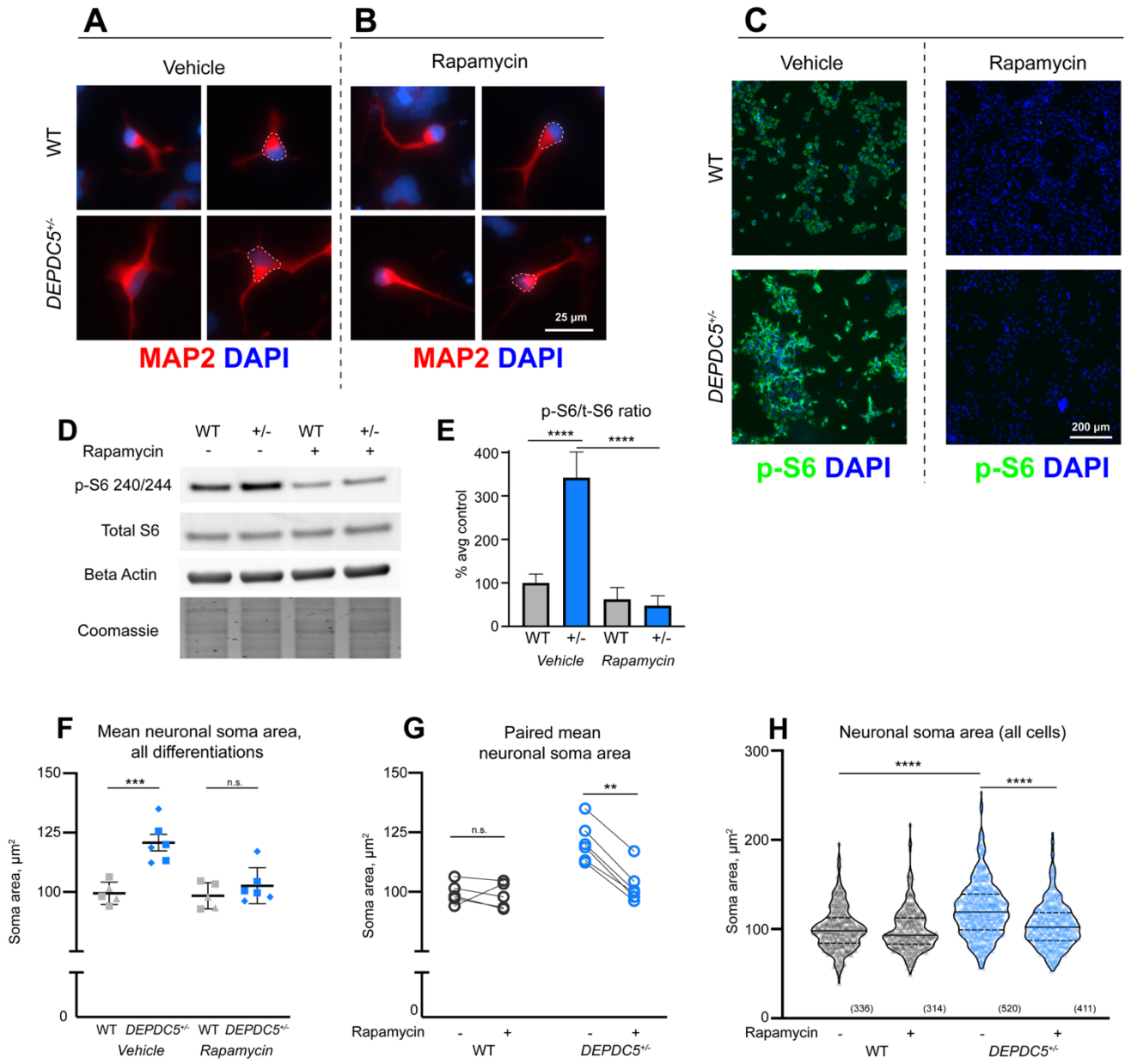

Figure 2-19. Cytomegalic *DEPDC5*$^{+/-}$ neurons are sensitive to mTORC1 inhibition.
(A, B) Neuronal cell size of MAP2+ (red) neurons following vehicle (A) or rapamycin (B) treatment, with DAPI nuclear staining (blue). (C) Chronic treatment with 20 nM rapamycin throughout neuronal differentiation attenuates p-S6 S240/244 (green) expression in *DEPDC5*$^{+/-}$ and control neurons. (D) Representative protein immunoblots of lysates from control and *DEPDC5*$^{+/-}$ patient neurons. Blots were cropped to show the relevant bands. (E) Quantification of p-S6 S240/244 to total S6 ratio with and without rapamycin treatment. Data represent two control lines and one *DEPDC5*$^{+/-}$ line from two separate differentiations. Bars indicate mean ± SD. Groups were compared using two-way ANOVA with Sidak's multiple comparisons, p<.0001. (F) Plot of mean neuronal soma size of control (gray) and *DEPDC5*$^{+/-}$ (blue) early neurons with or without chronic treatment with 20 nM rapamycin. These plots represent data from two control clones and two patient clones, each with 2-3 separate differentiations. Each dot indicates an average of 50 cells counted per differentiation. Groups were compared using two-way ANOVA with Sidak's multiple comparisons, p=.0001. (G) Paired plots of mean neuronal soma size. Each pair of points represents the mean soma size of a single differentiation with or without rapamycin. Groups were compared using paired t-tests: WT veh vs. rapa, p=.7157; *DEPDC5*$^{+/-}$ veh vs. rapa, p<.0001. (H) Violin plots of control (gray) and *DEPDC5*$^{+/-}$ (blue) early neuronal soma size; plots represent data from 336 WT-veh, 314 WT-rapa, 520 *DEPDC5*$^{+/-}$-veh, and 411 *DEPDC5*$^{+/-}$-rapa cells pooled from 2-3 separate differentiation experiments. Solid line represents mean value and dotted lines represent 25th and 75th percentiles. Groups were compared using two-way ANOVA with Sidak's multiple comparisons. See Figure S6 for soma areas of each cell line and uncropped immunoblots.

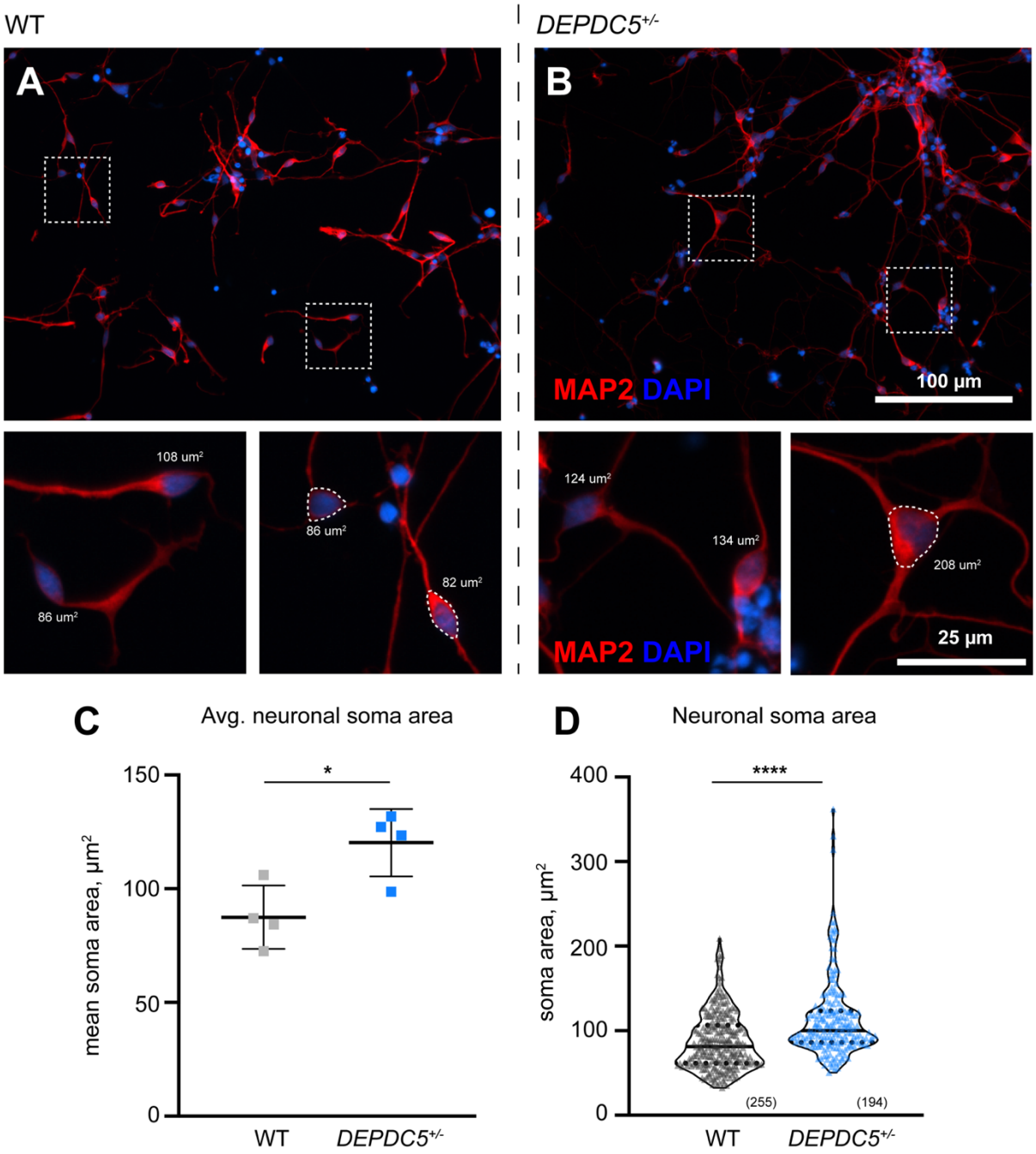

Figure 2-20. Post-mitotic neurons haploinsufficient for *DEPDC5* continue to display larger cell size.
(A-B) Neuronal soma size of post-mitotic neurons identified with immunocytochemistry for MAP2 (red) in control (A) and *DEPDC5*$^{+/-}$ patient (B) neurons, with DAPI nuclear staining (blue). Representative cell size measurements identified with dashed border. (C) Mean neuronal soma size of patient and control neurons. Each dot represents the mean soma size of a separate differentiation; 1-3 differentiations per clone; n=2 clones per genotype; at least 25 cells per differentiation were counted. Unpaired t-test, p=.0179. Bars represent mean ± SD. (D) Violin plots of neuronal soma size of wild-type and *DEPDC5*$^{+/-}$ patient neurons. Plots represent data from 255 control or 194 *DEPDC5*$^{+/-}$ cells pooled from separate differentiation experiments. Mann-Whitney test, p<.0001. Solid line represents mean value and dotted lines represent 25th and 75th percentiles.

Post-mitotic neurons have elevated mTORC1 activity that persists after amino acid deprivation

To confirm that elevated mTORC1 signaling persisted in mature neurons, we performed protein immunoblots to evaluate markers of mTOR pathway activation (**Figure 2-21A**). Similar to the findings in NPC and immature neurons, S6 phosphorylation (S240/244) was elevated in older *DEPDC5*$^{+/-}$ neurons. Statistically significant differences in p-4E-BP1 or p-AKT were not detected (**Figure 2-21B-D**).

Because the GATOR1 complex functions as part of the nutrient-sensing arm of the mTOR signaling pathway, we hypothesized that *DEPDC5*$^{+/-}$ neurons may have an impaired response to nutrient starvation, a response which would ordinarily suppress mTOR activity (Bar-Peled et al., 2013; Wolfson and Sabatini, 2017). GATOR1 knockdown has previously been shown to result in an inappropriate persistence of mTORC1 activation in response to amino acid deprivation in transformed human cell lines and in homozygous, but not heterozygous, *Depdc5*-mutant rodent embryonic fibroblasts (Hughes et al., 2017; Iffland et al., 2018; Marsan et al., 2016). In patient neurons, one hour of amino acid deprivation resulted in decreased S6 phosphorylation in all lines, but p-S6 expression trended toward persistent elevation in *DEPDC5*$^{+/-}$ neurons versus controls. By two hours of amino acid deprivation, p-S6 expression was further reduced in all lines (**Figure 2-22**).

As in iPSCs, quantitation of NPRL2 expression by immunoblot demonstrated decreased expression in patient neurons heterozygous for *DEPDC5* mutation (**Figure 2-21E**). Furthermore, while control neurons showed a significant elevation in NPRL2 after one hour of starvation, *DEPDC5* heterozygous mutant lines did not show a similar increase in NPRL2. The level of NPRL2 expression is especially relevant during times of nutrient deprivation because mTORC1 signaling is thought to be suppressed by the GATOR1 complex to allow autophagy initiation.

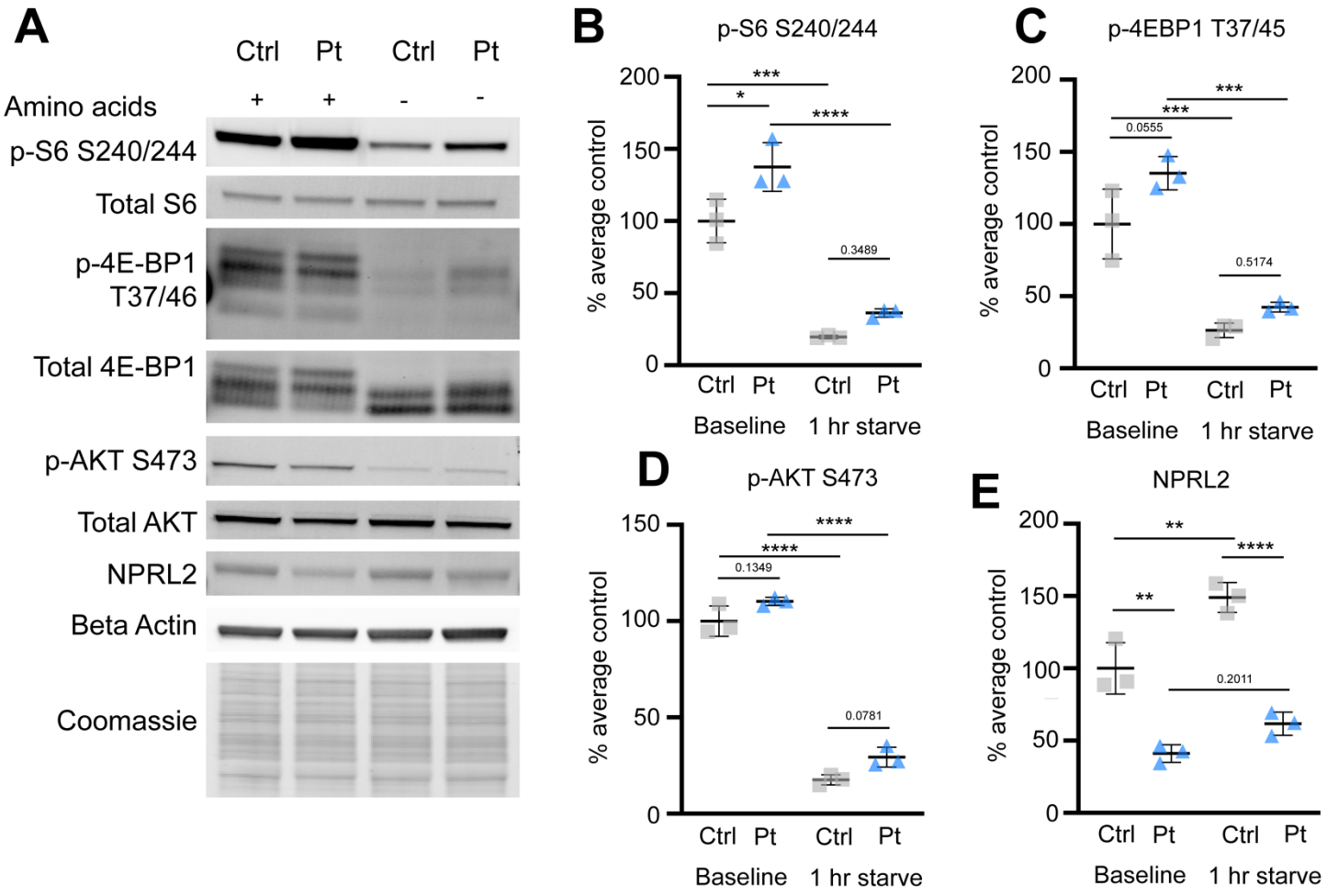

Figure 2-21. *DEPDC5*$^{+/-}$ neurons have elevated mTORC1 activity at baseline but remain sensitive to starvation. (A) Representative protein immunoblots of lysates from control and *DEPDC5*$^{+/-}$ patient neurons probed for markers of mTOR signaling and NPRL2. Western blots were cropped to show the relevant bands. (B) Quantification of immunoblot results for p-S6 (Ser240/244). (D) Quantification of immunoblot results for p-4E-BP1 (Thr37/46). (E) Quantification of immunoblot results for p-AKT (Ser473). (E) Quantification of NPRL2. Groups were compared using two-way ANOVA with Tukey's multiple comparisons, *p<0.05, **p<0.01, ***p<0.001, ****p<0.0001. Each dot represents a biological replicate.

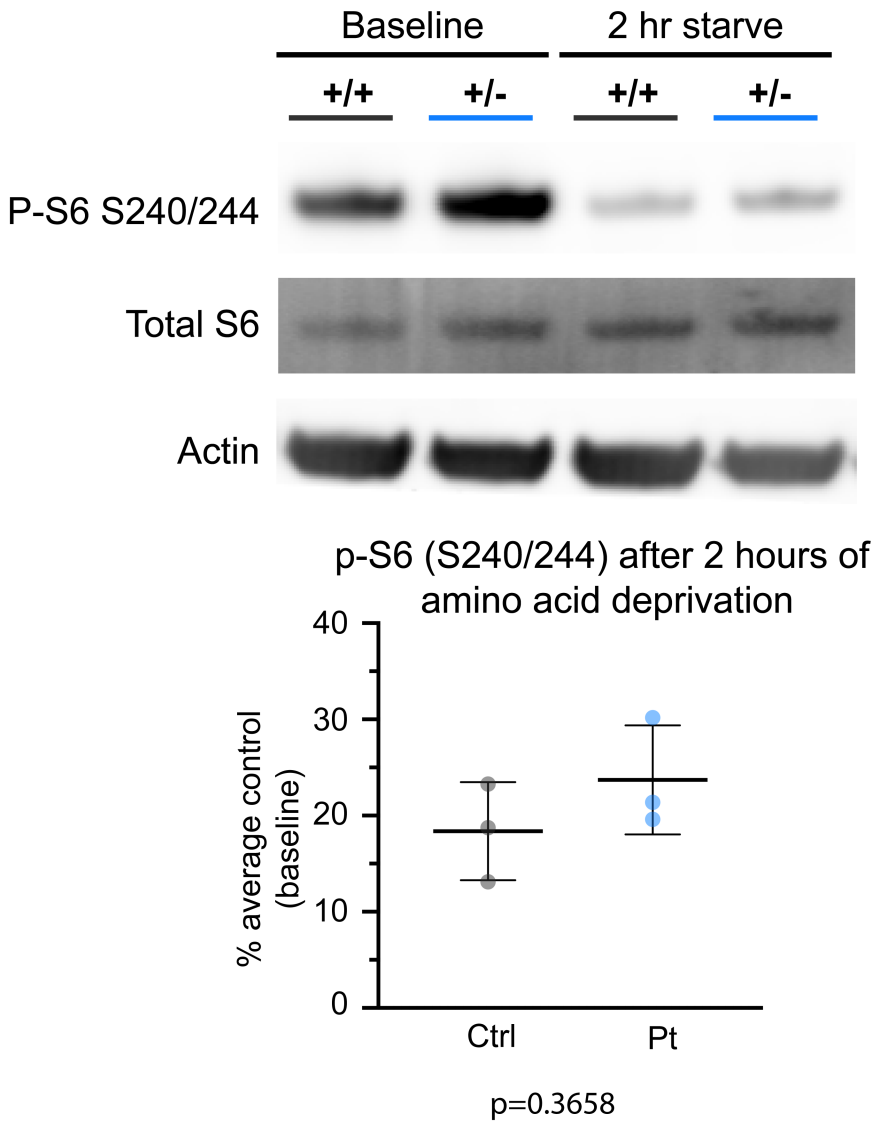

Figure 2-22. P-S6 (S240/244) in *DEPDC5*$^{+/-}$ neurons is further decreased after two hours of nutrient starvation. Protein immunoblots and quantitation of lysates from control and patient neurons probed for p-S6 (S240/244) at baseline and after 2 hours of nutrient deprivation. Western blots were cropped to show the relevant bands.

Discussion

Mutations in the component proteins of the GATOR1 complex (DEPDC5, NPRL2, and NPRL3) are increasingly appreciated as causes of focal epilepsies. In epilepsies with focal cortical dysplasia (FCD), accumulating evidence suggests that acquisition of a second-hit drives pathogenesis. For these epilepsies and for the majority of *DEPDC5*-related epilepsies without FCD, it is not known whether other mechanisms may lead to or contribute to epilepsy. Specifically, the consequences of a heterozygous mutation in *DEPDC5* have not been characterized in a human model. To better understand the effects of *DEPDC5* haploinsufficiency in humans, we generated iPSCs and neurons from epilepsy patients with inactivating mutations in *DEPDC5* but without evidence of FCD. We found that heterozygous mutations in *DEPDC5* allow increased mTORC1 signaling activity in iPSCs and derivative neurons. Corresponding increases in neuronal size were responsive to chronic treatment with rapamycin. These results reveal a potential role for *DEPDC5* haploinsufficiency in contributing to neuronal dysfunction by driving increased mTORC1 signaling.

A major finding of our study is the presence of an mTORC1-hyperactivation phenotype in cells heterozygous for *DEPDC5*. We analyzed mTORC1 activation using a variety of methods, finding increased phosphorylation of the mTORC1 targets S6 (S240/244) and 4E-BP1 (T37/46) in $DEPDC5^{+/-}$ patient lines with immunofluorescence and immunoblot. $DEPDC5^{+/-}$ patient iPSC lines had a faster rate of cell growth consistent with increased mTORC1 activity. $DEPDC5^{+/-}$ iPSCs also showed decreased p-AKT (S473), which is consistent with the well-described compensatory feedback in mTORC2 activity (reviewed in Rozengurt et al. (2014)). However, significant variation in p-AKT existed between control iPSC lines by immunoblot. We also analyzed mTOR activation in iPSCs by flow cytometry. Due to the differing modes of sample preparation for flow cytometry and immunoblotting, differing modes of signaling may be detected. By both techniques, we observed a trend toward decreased p-AKT in $DEPDC5^{+/-}$ iPSCs, while phosphorylation of S6 and 4E-BP1 at baseline diverged between the two methods. Collectively, these approaches support increased mTORC1 activation in $DEPDC5^{+/-}$ iPSCs. Future studies may further examine whether the changes observed via immunoblot are due to subpopulations of cells with high mTORC1 activation or an overall increase in mTORC1 activation in all cells.

DEPDC5$^{+/-}$ iPSCs treated with 24 hours of rapamycin and analyzed by flow cytometry also demonstrated differences in mTOR signaling pathway activation compared to controls, especially in response to brief nutrient stimulation. Rapamycin inhibition of mTORC1 has been shown to trigger a negative feedback loop through mTORC2 that results in activation of Akt signaling after drug exposure times greater than one hour (Shi et al., 2005; Wan et al., 2007). *DEPDC5*$^{+/-}$ lines appeared more susceptible to this negative feedback and had significantly increased p-AKT (S473) after rapamycin treatment, both with and without nutrient stimulus. While baseline p-S6 (S240/244) was not significantly different when analyzed by flow cytometry, *DEPDC5*$^{+/-}$ iPSCs demonstrated higher levels of p-S6 and p-4E-BP1 (T37/46) than controls in the rapamycin with nutrient stimulation condition, suggesting that *DEPDC5*$^{+/-}$ iPSCs may be able to more quickly recruit mTORC1 after a stimulus. Additional studies focusing on the temporal dynamics of mTOR signaling in response to amino acids and other nutrient stimuli may reveal further differences in patients with *DEPDC5* mutations.

The finding of increased mTORC1 activation and resultant increased soma size in neurons heterozygous for *DEPDC5* mutations was surprising given that no heterozygous phenotype has been observed in two existing *Depdc5* mouse models (Hughes et al., 2017; Yuskaitis et al., 2018). Interestingly, increased neuronal size was noted in a heterozygous rat model, suggesting that species-specific differences may influence the effects of the heterozygous state (Marsan et al., 2016). In contrast to the early mouse models, a recent study demonstrated an increased number of p-S6 (S240/244)-positive cortical neurons along with an increase in excitatory synaptic puncta in mice heterozygous for *Depdc5* (De Fusco et al., 2020). Thus, even within the same species, the effects of *Depdc5* haploinsufficiency may vary depending on a combination of as-of-yet undetermined factors. However, all heterozygous models seem to retain sensitivity to strict nutrient-starvation, including our iPSC-derived neurons. It thus seems likely that not all mTORC1 functions are affected by *DEPDC5* heterozygosity. Even though they remained sensitive to extreme nutrient starvation, *DEPDC5*$^{+/-}$ neurons had elevated mTORC1 activity at baseline, which is likely responsible for driving the increased cell size. As multiple new modulators of GATOR1 and GATOR2, and thus mTORC1, have been discovered and described in the past few years, perhaps additional unknown upstream or downstream regulators play a role in modulating aspects of mTORC1 signaling in response to nutrient availability (Chantranupong et al., 2016; Gu et al., 2017; Wolfson et al., 2016).

Our findings of mTORC1-dependent cell size differences in neuroprogenitor cells (NPCs) and neurons suggest possible mechanisms by which heterozygous *DEPDC5* mutation may contribute to the pathogenesis of epilepsy. The persistence of

cytomegaly in *DEPDC5*$^{+/-}$ neurons may have functional significance with respect to epilepsy. As a result of the larger soma size, heterozygous neurons are likely to have an increased membrane capacitance and may respond differently than wild-type neurons to action potentials and aberrant electrical activity. While we describe a model of *DEPDC5* haploinsufficiency resulting in abnormal cell signaling, growth, and morphology, evidence is accumulating to support the requirement of a "second hit" for the development of FCD. Our data presented here do not address how a second mutation would impact specific neurons or the surrounding heterozygous neuronal population, but our model does provide a framework for further studies using co-culture models and detailed electrophysiologic analysis.

iPSC technology offers a unique opportunity to study DEPDC5 haploinsufficiency in human neurons, however our model does have some caveats. One is the potential for genetic variability in unaffected control lines. To control for this, one of our control lines (Control B) was generated from the healthy parent of one of the epilepsy patients (Patient 2) used to generate our iPSC lines. The control lines used in the study were both significantly different from patient lines, with attenuated mTORC1 activation and resultant smaller cell size; however, a larger set of unaffected samples would be useful to further control for the inherent genetic variability present in unrelated individuals. Additionally, for future studies, using CRISPR-Cas9 to create matched sets of isogenic control, heterozygous, and homozygous cell lines represents an ideal strategy to definitively isolate the effects of *DEPDC5* gene dosage. Due to lack of availability of a specific DEPDC5 antibody, we were limited in our evaluation of DEPDC5 protein expression and instead evaluated mRNA levels as a proxy to assess for functionally relevant changes resulting from *DEPDC5* mutations. Furthermore, the results of the rapamycin rescue experiment support that the increased neuronal size is dependent on mTORC1 activation, but translating these results to patient care requires caution. While treatment of cells with rapamycin throughout the entire differentiation rescued the cytomegalic phenotype, it also impaired the survival of cells throughout the neuronal differentiation process, both in control and *DEPDC5*$^{+/-}$ patient cell lines. Because of this and the possibility of other effects of long-term rapamycin treatment (reviewed in Tran and Zupanc, 2015), prolonged rapamycin treatment during neurodevelopment is unlikely to be clinically feasible. Future experiments exploring the potential efficacy of targeted treatment windows of mTORC1 suppression to modulate the disease phenotype will be valuable.

Future studies focused specifically on the evaluation of changes in the electrical activity of human neurons with *DEPDC5* mutations will be essential. Studies that combine neurons with both heterozygous and homozygous *DEPDC5* mutations as

well as glia will further provide invaluable information on network effects and the contributions of heterozygous mutant neurons to epilepsy. As such, determination of the contributions of different central nervous system cell types and their interactions remains vital. Non-cell-autonomous interactions between various cell types may contribute to disease, as has recently been demonstrated in cultures of variably *TSC*-mutant neurons and oligodendrocytes (Nadadhur et al., 2019). Mixed neuronal and glial cultures, ideally in three-dimensional cerebral organoids or "brain-on-a-chip" culture systems, will be particularly relevant to such studies.

In summary, we differentiated neurons from iPSCs generated from three patients with epilepsy due to loss-of-function mutations in *DEPDC5* in order to determine if *DEPDC5* haploinsufficiency contributes to epilepsy pathology in a human disease model. We found that loss-of-function of one allele of *DEPDC5* is sufficient to cause increased mTORC1 signaling in iPSCs and neurons as well as development of cytomegalic neuroprogenitor cells and neurons. These results suggest that germline haploinsufficiency may play a role in the pathogenesis of epilepsy with *DEPDC5* mutation. Our findings suggest that human disease may differ from rodent models, which do not consistently show differences in heterozygous *Depdc5*-mutant neurons. These findings support the need for human-based models to expand and verify discoveries in animal models of *DEPDC5* mutations and epilepsy.

Methods

Generation and validation of iPSCs from epilepsy patients with *DEPDC5* mutations.

After obtaining informed consent from patients or their legal guardians under Vanderbilt Institutional Review Board protocol #080369, fibroblasts were isolated by 3 mm skin punch biopsies from patients and control donors with no history of epilepsy. Fibroblasts from the biopsies were cultured in DMEM with 10% FBS and 1% penicillin-streptomycin. iPSCs were generated from fibroblasts as previously described, either via transduction with non-integrating Sendai virus-based reprogramming vectors or via electroporation with episomal vectors(Armstrong et al., 2017). Sendai reprogramming was performed using the CytoTune iPS 2.0 Sendai Kit (ThermoFisher) in feeder-free conditions according to the manufacturer's instructions. After one week, nascent stem cells were passed to Matrigel and grown in mTeSR1 media (Corning; StemCell Technologies). iPSCs were confirmed to be Sendai vector-free after 5-10 passages using RT-PCR. Fibroblasts were also reprogrammed by transfection of cells using the Neon system (Invitrogen) with plasmids expressing

KLF4, SOX2, OCT4, L-MYC and LIN28 (Addgene #27076, 27077, 27078, 27080) according to previously published protocols (Okita et al., 2011). Cells were switched to TeSR-E7 media (StemCell Technologies) 48 h post-transfection. After three weeks, defined iPSC-like colonies emerged and were manually picked and transferred to plates coated with a 1:25 dilution of Matrigel (Corning/BD Sciences 354277) in DMEM/F12 (ThermoFisher 11320033) and maintained in feeder-free conditions with daily media changes with mTeSR1 (StemCell Technologies 85850). iPSCs were passaged once per week for maintenance using ReLeSR (StemCell Technologies 05873) at a ratio of 1:25. All experiments were performed within 50 passages of the original iPSC generation.

New iPSC lines were validated through trilineage differentiation assays, pluripotency marker immunostaining, and karyotype analysis. For trilineage immunostaining, iPSCs were differentiated as embryoid bodies for ten to fourteen days in DMEM/F12 GlutaMax with 20% knockout serum replacement, 1X non-essential amino acids and 55 μM β-mercaptoethanol, and then probed for lineage markers defining ectoderm (Sox1, β-III-Tubulin), mesoderm (smooth muscle actin, brachyury, and/or desmin), and endoderm (GATA4, Sox17). Immunostaining was performed for pluripotency markers Oct4, Nanog, TRA-1-60, and SSEA3. Karyotype analysis of iPSC clones was performed using standard techniques; all lines used in experiments had normal karyotypes (Genetic Associates, Inc., Nashville, TN). PluriTest analysis was performed by ThermoFisher. *DEPDC5* gene mutations in iPSC lines were confirmed by direct DNA sequencing. Genomic DNA was extracted via DNeasy Blood & Tissue Kit (Qiagen) according to the manufacturer's protocol. DNA extracts were amplified by PCR using Phusion Flash (F-548S) and the resultant PCR products sequenced via Sanger sequencing (GenHunter). Sequencing primers are listed below in **Table 2-2**.

Primer	**Sequence**	**Tm**
Pt1 sequencing (F)	GGCAGAACGTTCCACAAAGT	64.1
Pt1 sequencing (R)	TGCAAAATAAAGGGCAGGTC	
Pt2/3 sequencing (F)	CCTGATGGGGTTGTGAGGAA	61.9
Pt2/3 sequencing (R)	GGAAACAGTGAATTGCCCAGT	

Table 2-2. *DEPDC5* sequencing primers.

mRNA quantification.

Total RNA was extracted from iPSCs and neurons using the RNeasy kit (Qiagen #74134) and QIAShredder columns (Qiagen #79654) according to the manufacturer's instructions. DNA digestion was performed using either on-column DNA digestion (Qiagen #79254) or gDNA wipeout buffer (Qiagen #205311). cDNA was synthesized using random primers with the SuperScript VILO cDNA synthesis kit (Invitrogen #11754) or Quantitect Reverse Transcription kit (Qiagen #205311). Real-time PCR was then performed with Taqman assays (ThermoFisher) using a CFX96 Touch (Bio-Rad). Primers with overlapping exon-exon boundaries were selected to prevent amplification of genomic DNA. Reactions were run in quadruplicate and expression data were normalized to the mean of housekeeping gene HPRT1 to control for the variability in expression levels and analyzed using the $2^{-\Delta\Delta CT}$ method (Livak and Schmittgen, 2001). Assays used are listed below in **Table 2-3**.

Gene	Assay ID (ThermoFisher)	Exon boundary
HPRT1	Hs99999909_m1 (FAM-MGB)	6-7
Beta-2 microglobulin	Hs99999907_m1 (FAM-MGB)	2-3
DEPDC5	Hs00206348_m1 (FAM-MGB)	39-40
DEPDC5	Hs00823262_m1	7-8

Table 2-3. Assays used for quantitative RT-PCR.

Immunofluorescence

For immunofluorescence, patient-derived and unaffected control iPSCs, NSCs, and neurons were fixed in 2% (w/v) paraformaldehyde at room temperature for 5 minutes, made by adding 4% PFA directly to cell culture media, then in 4% paraformaldehyde for 15 minutes. Cells were blocked with 5% (w/v) normal goat serum in PBS containing 0.3% (v/v) Triton X-100 for 1 h at room temperature and incubated with primary antibodies overnight at 4 degrees Celsius in PBS containing 1% bovine serum albumin and 0.3% Triton X-100. Cells were then washed three times in PBS and incubated for 1 h at room temperature with anti-rabbit or anti-mouse AlexaFluor 488 or 647 conjugated secondary antibodies at a 1:500 dilution (Life Technologies). F-Actin staining was performed using ActinGreen ReadyProbes reagent (Invitrogen R37110) following the manufacturer's specifications. Cell nuclei were counterstained with Hoescht (1:2000) or 4',6-diamidino-2-phenylindole (DAPI). Antibody dilutions and manufacturers are listed below in **Table 2-4**.

Immunoblotting

Cultured cells were rinsed twice with 1X D-PBS, collected by scraping, and lysed by sonication in RIPA buffer (PBS with 1% NP40, 0.5% Na deoxycholate, 0.1% SDS) containing protease and phosphatase inhibitor cocktails (Sigma), then clarified via centrifugation at 10,000×*g* for 10 min at 4°C. Protein concentrations were calculated using the Bradford method (Bio-Rad). Samples were diluted with 3x loading buffer (0.25 M Tris-HCl, 40% glycerol, 8% SDS, 15% BME, 0.008% bromophenol blue) and separated by electrophoresis on 4–12% Bis-Tris gels, followed by tank transfer to polyvinylidene difluoride membrane (Pall Corp., Pensacola, FL, USA). Membranes were blocked for 1 h at room temperature in Odyssey blocking buffer (LI-COR 927-40000 or 927-0001), then incubated with primary antibody at 4°C overnight in 5% BSA in Tris-buffered saline with 0.1% Tween-20 (TBS-T). Blots were washed with TBS-T and then probed with fluorescent-tagged secondary antibodies diluted in TBS-T with 5% BSA and 0.01% SDS. Fluorescent-conjugated secondary antibodies were visualized using an Odyssey fluorescence scanner set at default intensity, high quality, with 84 uM resolution. After visualization, digitized band densities were quantified using the Odyssey quantification software ImageStudio Lite. The integrated intensities of bands were measured using default settings with the 3-pixel-width border mean average background correction method. Bands that were measured for quantification are indicated by the red boxes in the supplemental material. If possible, phospho-proteins were normalized to total protein. Specifically, p-S6 S240/244 was normalized to total S6 protein, p-AKT S473 was normalized to total Akt, and p-4E-BP1 was normalized to total 4E-BP1. NPRL2 was normalized to beta-actin as an internal reference protein. Following normalization of all samples, data were then compared to % average control. See **Table 2-4** below for antibody dilutions and manufacturers.

Table 2-4. Antibodies used for immunocytochemistry (IF), immunoblot (WB), and flow cytometry (FC).

Antibody	Species	Dilution	Vendor/ Manufacturer	Catalog Number
Anti-DEPDC5	Rabbit	1:100 (WB)	Origene	#AP51242PU-N
Anti-beta-actin	Rabbit	1:2000 (WB)	Cell Signaling Technology	#4967
Anti-beta-actin	Mouse	1:2000 (WB)	Sigma	#A5441
Anti-Phospho-Akt (Ser473)	Rabbit	1:1000 (WB)	Cell Signaling Technology	#4060
Anti-p62	Rabbit	1:1000 (WB)	Cell Signaling Technology	#5114
Anti-Phospho-4E-BP1 (Ser65)	Rabbit	1:500 (WB)	Cell Signaling Technology	#9451

Anti-Phospho-4E-BP1 (Thr37/46)	Rabbit	1:250 (WB)	Cell Signaling Technology	#2855
Anti-4E-BP1 (clone 53H11)	Rabbit	1:500 (WB)	Cell Signaling Technology	#9644
Anti-Pan-Akt (clone 40D4)	Mouse	1:1000 (WB)	Cell Signaling Technology	#2920S
Anti-Phospho-S6 (Ser240/244)	Rabbit	1:1000-1:2000 (WB); 1:800 (IF)	Cell Signaling Technology	#5364
Anti-S6 (clone 54D2)	Mouse	1:500 (WB)	Cell Signaling Technology	#2317S
Anti-LC3	Mouse	1:1000 (WB)	MBL International	#M186-3
Anti-MAP2	Rabbit	1:150 (IF)	Cell Signaling Technology	#4542
Anti-Beta-tubulin III (clones TUJ1 and TU-20)	Mouse	1:250 (IF)	Millipore Sigma	#MAB1637
Anti-Nestin (clone 10C2)	Mouse	1:250 (IF)	Abcam	#ab22035
Anti-Pax6*	Mouse	1:250 (IF); 1:500 (WB)	University of Iowa Developmental Studies Hybridoma Bank	#PAX6
Anti-Oct4	Rabbit	1:250 (IF)	Cell Signaling Technology	#2750S
Anti-TRA-1-60 (clone TRA-1-60)	Mouse	1:250 (IF)	Millipore Sigma	#MAB4360
Anti-Nanog (clone D73G4)	Rabbit	1:250 (IF)	Cell Signaling Technology	#4903S
Anti-SSEA3 (clone MC-631)	Rabbit	1:100 (IF)	Millipore Sigma	#MAB4303
Anti-alpha smooth muscle actin (clone 1A4)	Mouse	1:250 (IF)	Abcam	#ab7817
Anti-Desmin (clone Y66)	Rabbit	1:250 (IF)	Abcam	#ab32362
Anti-VGLUT1	Guinea pig	1:1000 (IF)	Millipore Sigma	#ab5905
Anti-PSD95	Rabbit	1:1000 (WB), 1:250 (IF)	Cell Signaling Technology	#2507S
Anti-GATA4	Rabbit	1:250 (IF)	Abcam	#ab84593
Anti-Sox1	Rabbit	1:250 (IF)	Abcam	#ab22572
Anti-Sox17 (clone OTI3B10)	Mouse	1:100 (IF)	Abcam	#ab84990
Anti-Brachyury (clone D-10)	Mouse	1:250 (IF)	Santa Cruz Biotechnology	#sc-166962
Anti-DEPDC5	Rabbit	1:100 (WB)	ThermoFisher Invitrogen	#PA5-63150
Anti-Phospho-Ulk1 (Ser758)	Rabbit	1:500 (WB)	Abcam	#ab156920
Anti-Phospho-4E-BP1 Thr37/46 conjugated to Ax647 (clone 236B4)	Rabbit	1:100 (FC)	Cell Signaling Technology	#5123S

Anti-Phospho-S6 Ser240/244 conjugated to PE (clone D68F8)	Rabbit	1:800 (FC)	Cell Signaling Technology	#14236S
Anti-Human Akt phospho Ser473 conjugated to Ax488 (clone M89-61)	Mouse	1:100 (FC)	BD Pharmigen	#560404
Anti-Phospho-S6 Ser235/236 conjugated to PB (clone D57.2.2E)	Rabbit	1:100 (FC)	Cell Signaling Technology	#8520S
Secondary antibodies:				
Anti-rabbit 488	Goat	1:500 (IF)	ThermoFisher	#A11034
Anti-rabbit 555	Goat	1:500 (IF)	ThermoFisher	#A21429
Anti-rabbit 647	Goat	1:500 (IF)	ThermoFisher	#A21244
Anti-mouse 488	Goat	1:500 (IF)	ThermoFisher	#A11029
Anti-mouse 647	Goat	1:500 (IF)	ThermoFisher	#A21235
Anti-rabbit 800	Donkey	1:15,000 (WB)	LICOR	926-32213
Anti-mouse 800	Donkey	1:15,000 (WB)	LICOR	926-32212
Anti-rabbit 680	Donkey	1:15,000 (WB)	LICOR	926-68073
Anti-mouse 680	Donkey	1:15,000 (WB)	LICOR	926-68072

*PAX6 was deposited to the DSHB by Kawakami, A. (DSHB Hybridoma Product PAX6)

Doubling time assays.

Cells were seeded in 12-well plates at a concentration of 100,000 cells per well in mTeSR1 and Rock inhibitor. After 24 hours, treatment (10 nM rapamycin or vehicle – 60% PBS/40% DMSO) was applied. Cells were dissociated to single cells using Accutase and counted at 24, 48, 72, 96, 120, and 144 hours. A Nexelcom Cellometer Auto T4 was used for counting. Growth curves were plotted and population doubling time was calculated from the linear portion of the growth curve (days 3-5) using the equation (t2 – t1)/3.32 x (logn2 -logn1).

Flow cytometry – iPSCs.

Cultured iPSCs were collected for flow cytometry experiments using previously described protocols (Rushing et al., 2019). Media was removed from dish and iPSCs were treated with Accutase with ROCK inhibitor Y-27632 for 10 minutes at 37°C, 5% CO2, quenched with either their original conditioned media (mTeSR1) or stimulated with nutrients by the addition of fresh mTeSR1 media for 10 minutes, then triturated into a single-cell suspension. Cells were pelleted at 200 x *g* and resuspended in their original conditioned media (mTeSR1), then rested 75 minutes, with Alexa Fluor 700-SE

dye (A-20010; Life Technologies) added for the last 15 min of incubation to label non-intact cells. Subsequently, the cells were fixed with a final concentration of 1.6% PFA for 20 min at room temperature, washed with 1X PBS, and spun for 5 min at 800 x *g* at room temperature. Supernatant was decanted and cells were resuspended in the void volume using vigorous vortexing. 100% cold methanol was added to permeabilize cells. Cells were stored in methanol at −80°C until staining. After fixation and permeabilization, intracellular staining was conducted for 1 hr at room temperature using directly-labeled primary antibodies in PBS/1% bovine serum albumin. All antibody clones and dilutions are listed in **Table 2-4**. Following staining, cells were run on a BD LSR II 5-laser cytometer. Single fluorophore–labeled beads and unstained cell lines were used as compensation and sizing controls. For signal quantification, the arcsinh transformed median fluorescence intensity of per-cell phosphoprotein of stained samples was compared to unstained samples from the same experiment. The inverse hyperbolic sine (arcsinh) with a cofactor was used to measure signaling intensity in samples as previously described (Irish et al., 2010). The arcsinh median of intensity value × with cofactor c was calculated as $\text{arcsinhc}(x) = \ln(x/c + \sqrt{((x/c)2 + 1)})$. The cofactor (c) is a fluorophore-specific correction for signal variance. All analyses were completed using Cytobank software (Kotecha et al., 2010).

Generation of cortical neural progenitor cells and neurons from iPSCs.

iPSCs were neuralized using a dual-SMAD inhibition protocol described by Shi *et al.* with minor modifications (Shi et al., 2012b). Briefly, iPSCs were plated at a concentration of $1x10^6$ per well in 12-well plates coated with Matrigel. At day 0, the culture medium was changed to neural induction medium (50/50 mix of Neurobasal and DMEM/F12) with small-molecule inhibitors of SMAD (SB-431542, 10 uM; LDN-193189, 100 nM). Once uniform (day 10), the neuroepithelial sheet was passed using dispase. On day 11, the medium was changed to neural maintenance medium without SMAD inhibitors. 20 ng/mL FGF2 was added to the medium for three days (days 16-18) upon the appearance of neural rosettes. Neural rosettes were passed with dispase on day 20. Cells were expanded a final time at day 30 using Accutase and maintained in neuronal maintenance medium.

Neuronal size analysis.

Neuroprogenitor cells were dissociated to single cells at differentiation day 10 using Accutase and plated sparsely in order to distinguish individual cells ($1.5x10^4$ cells/cm^2). After 24 hours, cells were fixed and immunostained with p-S6 S240/244 (mTORC1 target), Nestin (neuroprogenitor cells), and phalloidin to label filamentous actin (F-Actin). F-Actin+

soma area was quantified using ImageJ (NIH, version 1.52i). In a blinded fashion, soma area of >50 cells per experimental group was measured in patient and control lines, with n=3 differentiations per experiment. Overlapping cells with unclear borders were excluded from measurement. Mean area and standard deviation were calculated from each differentiation and results were compared for statistical significance. For p-S6 (S240/244) intensity analysis in NPCs, p-S6+ soma size was measured and the integrated density was divided by soma area to obtain mean p-S6 fluorescence intensity. For early neurons, cells were dissociated and sparsely replated on differentiation day 20 and fixed for immunostaining 24 hours later. Post-mitotic neurons were replated after differentiation day 65 and fixed after 72 hours. For early neurons and post-mitotic neurons, MAP2+ soma area was quantified.

Nutrient starvation assays.

Ten to fourteen days before the experiment, neurons were plated in 6-well plates containing Matrigel at a concentration of 1 million cells per well. Two hours prior to starvation, media was changed to fresh neuronal maintenance media (NMM) containing B27 and N2 supplements. Fresh baseline media (NMM) or nutrient-limited media (NLM, consisting of DMEM lacking amino acids (USBiological D9800-13)) was added at time zero. Cells were harvested and lysed for protein after 1 hour, then analyzed via immunoblot.

Statistical analysis and controls.

We used cell lines from two individual healthy controls and three individual patients with *DEPDC5*-related epilepsy. Multiple clones from each fibroblast line were generated and experiments were performed in multiple clones from each line to ensure reproducibility. Multiple differentiations were performed to control for variability between differentiations. The number of clones and specific clones used for each set of experiments is provided in **Table 2-5**. Data from continuous variables are expressed as mean ± SD. Two-group comparisons were performed using a t test or Mann-Whitney *U* test for non-parametric data. Three-group or greater comparisons were performed using one-way ANOVA with Dunnett's multiple comparisons for experiments with one independent variable or two-way ANOVA for experiments with two independent variables. For two-way ANOVA, Tukey's multiple comparisons was used when comparing all means and Sidak's multiple comparisons was used when a set of means was selected. $p<.05$ was considered statistically significant. GraphPad Prism 8 was used to complete statistical tests.

Table 2-5. Specific iPSC clones used in individual experiments.

	Number of patient clones	Number of control clones	Patient clones	Control clones
Figure 1	4	2	Pt1-C1 (DEP1-3) Pt1-C2 (DEP1-29) Pt2-C2 (DEP2-7) Pt3-C1 (DEP3-1)	CtrlA-C1 (CC1) CtrlA-C2 (CC5)
Figure 2	6	4	Pt1-C1 (DEP1-3) Pt1-C2 (DEP1-29) Pt2-C1 (DEP2-7) Pt2-C2 (DEP2-9) Pt3-C1 (DEP3-1) Pt3-C2 (DEP3-5)	CtrlA-C1 (CC1) CtrlA-C2 (CC5) CtrlB-C1 (CF3) CtrlB-C2 (CF4)
Figure 3, A-D	3	3	Pt1-C2 (DEP1-29) Pt2-C2 (DEP2-7) Pt3-C1 (DEP3-1)	CtrlA-C2 (CC5) CtrlA-C3 (CC3) CtrlB-C2 (CF3)
Figure 3, E-H	3	2	Pt1-C2 (DEP1-29) Pt2-C2 (DEP2-7) Pt3-C1 (DEP3-1)	CtrlA-C2 (CC5) CtrlB-C2 (CF3)
Figure 4	3	2	Pt1-C2 (DEP1-29) Pt2-C2 (DEP2-7) Pt3-C1 (DEP3-1)	CtrlA-C2 (CC5) CtrlB-C2 (CF3)
Figure 5	3	2	Pt1-C2 (DEP1-29) Pt3-C1 (DEP3-1)	CtrlA-C2 (CC5) CtrlB-C2 (CF3)
Figure 6	2	2	Pt1-C1 (DEP1-3) Pt1-C2 (DEP1-29)	CtrlA-C1 (CC1) CtrlA-C2 (CC5)
Figure 7	2	2	Pt1-C1 (DEP1-3) Pt1-C2 (DEP1-29)	CtrlA-C2 (CC5) CtrlB-C1 (CD3)

CHAPTER III

PREVENTION OF PREMATURE DEATH AND SEIZURES IN A DEPDC5 MOUSE EPILEPSY MODEL THROUGH INHIBITION OF MTORC1.

Parts of this chapter were published under the same title in *Human Molecular Genetics* (Klofas, Short, Zhou, and Carson, 2020; doi: 10.1093/hmg/ddaa068).

Abstract

Mutations in *DEP domain containing 5* (*DEPDC5)* are increasingly appreciated as one of the most common causes of inherited focal epilepsy. Epilepsies due to *DEPDC5* mutations are often associated with brain malformations, tend to be drug-resistant, and have been linked to an increased risk of sudden unexplained death in epilepsy (SUDEP). Generation of epilepsy models to define mechanisms of epileptogenesis remains vital for future therapies. Here, we describe a novel mouse model of Depdc5 deficiency with a severe epilepsy phenotype, generated by conditional deletion of *Depdc5* in dorsal telencephalic neuroprogenitor cells. In contrast to control and heterozygous mice, *Depdc5*-*Emx1*-Cre conditional knockout (CKO) mice demonstrated macrocephaly, spontaneous seizures, and premature death. Consistent with increased mTORC1 activation, targeted neurons were enlarged, and both neurons and astrocytes demonstrated increased S6 phosphorylation. Electrophysiologic characterization of miniature inhibitory post-synaptic currents (mIPSCs) in excitatory neurons was consistent with impaired post-synaptic response to GABAergic input, suggesting a potential mechanism for neuronal hyperexcitability. mTORC1 inhibition with rapamycin significantly improved survival of CKO animals and prevented observed seizures, including for up to forty days following rapamycin withdrawal. These data not only support a primary role for mTORC1 hyperactivation in epilepsy following homozygous loss of *Depdc5,* but also suggest a developmental window for treatment which may have a durable benefit for some time even after withdrawal.

Introduction

Mutations in *DEP domain containing 5* (*DEPDC5)* (HGNC#18423; OMIM#614191) are a significant cause of focal epilepsies and brain malformations (Baldassari et al., 2019a; Baulac et al., 2015; Carvill et al., 2015; Dibbens et al., 2013; Ishida et al., 2013; Lal et al., 2014; Picard et al., 2014; Scerri et al., 2015; Scheffer et al., 2014). Patients with epilepsy due to *DEPDC5* mutation are also at increased risk of sudden unexpected death in epilepsy (SUDEP) (Bagnall et al., 2016; Bagnall et al., 2017; Nascimento et al., 2015). The link to SUDEP combined with the drug-resistant nature of *DEPDC5*-related epilepsies underscores the importance of identifying treatment strategies for patients with epilepsies due to *DEPDC5* mutations. Most anti-epileptic drugs act as modulators of various ion channels to attenuate seizure activity. However, *DEPDC5* is unique in that it is one of the few epilepsy-associated genes that does not code for an ion channel or channel modulator, suggesting that new treatment paradigms, such as signaling pathway modulation, may be warranted.

DEPDC5 is one of three members of the GATOR1 complex, along with NPRL2 and NPRL3. The GATOR1 complex acts to inhibit RagA/B-mediated recruitment of mTORC1 to the lysosomal membrane during times of nutrient deprivation, thereby preventing its activation and phosphorylation of downstream targets (Bar-Peled et al., 2013). Dysregulation of mTOR signaling is linked to epilepsy as well as other neurodevelopmental diseases, including malformations of cortical development (D'Gama et al., 2015; D'Gama et al., 2017). Modulation of mTORC1 signaling is used clinically to treat patients with mTORopathies with initial pre-clinical evidence suggesting that mTORC1 modulation may be useful in cases of *DEPDC5*-related epilepsies (Yuskaitis et al., 2019).

To discover and effectively test new epilepsy therapeutics, a pre-clinical *Depdc5*-related epilepsy mouse model is essential. Homozygous germline loss of *Depdc5* is embryonic lethal in mice and rats (Hughes et al., 2017; Marsan et al., 2016). Germline heterozygosity does not result in seizures in mice or rats, though it does lead to mTORC1 hyperactivation in the brain and cytomegalic neurons in rats (Hughes et al., 2017; Marsan et al., 2016). Two models of *in utero* electroporation have been created to generate biallelic inactivation of *Depdc5* in the brains of mice, leading to areas resembling focal cortical dysplasia (Dawson et al., 2020; Ribierre et al., 2018a). These mice demonstrated increased pS6 expression, cytomegalic neurons, and abnormal cortical lamination (Ribierre et al., 2018a). Thirty percent of the Ribierre *et al*. mice demonstrated focal seizures, while the Dawson *et al.* mice had a decreased seizure threshold in response to

pentylenetetrazol (PTZ) but no spontaneous seizures (Dawson et al., 2020; Ribierre et al., 2018a). Thus, while both are novel models for *Depdc5*-related epilepsies with brain malformations, they are somewhat limited in the robustness of their epilepsy phenotypes. Another mouse model with neuron-specific *Depdc5* conditional knockout was generated using Cre recombinase driven by the *Syn1* promoter, beginning at embryonic day 12-13 (Yuskaitis et al., 2018). The *Syn1*-CKO mice that survive until adulthood and have seizures starting after 100 days of life. We hypothesized that an earlier conditional knockout of *Depdc5* in neural progenitors would result in an earlier onset of seizures to allow for therapeutic testing at an earlier age. We based our model generation on a prior mouse model of tuberous sclerosis complex (TSC) generated by our laboratory, in which the *Emx1* promoter was used to drive Cre-recombinase expression beginning at embryonic day 10 (Carson et al., 2012). The *Emx1*-lineage gives rise to excitatory neurons in the cerebral cortex as well as a subset of glial cells, including certain astrocytes and some oligodendrocytes (Gorski et al., 2002; Magri et al., 2011). Like *DEPDC5*-related epilepsies, TSC is also a disease of dysregulated mTOR signaling. In the case of the *Emx1-Tsc1* CKO model, deleting *Tsc1* in embryonic neural progenitor cells resulted in spontaneous seizures beginning at an early age (P13-P20). Thus, to create a mouse model of *DEPDC5*-related epilepsy with a severe epilepsy phenotype in which early therapeutic interventions could be tested, we generated a conditional knockout (CKO) mouse with deletion of *Depdc5* in the *Emx1*-expressing embryonic dorsal telencephalic neuroepithelium. The targeting of glial cells in addition to projection neurons was an additional advantage of the *Emx1*-Cre driver because it allowed us to also investigate the consequences of *Depdc5* loss in this glial subset.

Depdc5-Emx1-Cre-CKO mice have a greatly reduced lifespan with terminal seizures, display evidence of mTORC1 hyperactivation in both neurons and astrocytes, and demonstrate dysplastic cortical neurons with an altered response to GABAergic input. These results suggest that an altered response to inhibitory neuronal inputs may be a feature of *DEPDC5*-related epilepsies and also raise the possibility of a role for glial cells in contributing to disease pathogenesis. Postnatal treatment with rapamycin prolonged lifespan and prevented observed seizures, even for weeks after its withdrawal. We thus present a novel *Depdc5* conditional knockout mouse model with early development of epilepsy and seizure-associated death that will be useful for testing additional therapeutic strategies.

Results

Generation of *Depdc5-Emx1*-Cre CKO transgenic mice

To develop an epileptic *Depdc5* mouse model and determine the consequences of conditional knockout of *Depdc5*, we targeted cortical neuroprogenitor cells using mice expressing *Emx1*-Cre crossed to mice with a floxed alleles of *Depdc5* (**Figure** 3-1Figure 1-1). $Depdc5^{F/FEmx1}$ homozygous conditional knockout mice (henceforth $Depdc5^{Emx1}$ CKO) mice are viable and born at the expected Mendelian ratio (**Table 3-1**).

Table 3-1. $Depdc5^{Emx1}$ mice are born at a Mendelian ratio.

Cre+ F/F	Cre- F/F	Cre+ F/Wt	Cre- F/Wt	Litter size	Sequential Litters
40	31	33	30	7.1 ± 1.6	19

Depdc5-CKO mice have decreased life expectancy with terminal seizures

The very early postnatal development of $Depdc5^{Emx1}$ CKO mice was similar to control and heterozygous mice. After postnatal day (P) day 15 of life, CKO mice lost body weight but continued to demonstrate enlargement of brain size, resulting in a significant increase in both the absolute brain size and in the brain-to-body ratio (**Figure 3-2A**). The gross and relative enlargement of brain size is consistent with that seen in other mouse models with mTORC1 hyperactivation (D'Gama et al., 2017; Kwon et al., 2006; Roy et al., 2015; Zhou et al., 2009a).

Characterization of the natural history of the $Depdc5^{Emx1}$ mouse model demonstrated both clinical seizures and premature death as early as P11 in the CKO mouse. With routine handling, clinical seizures were noted in 25% of CKO mice, leading to a relative risk for seizures of nearly 50% by P25. Typical seizures observed included tonic convulsions, tonic-clonic convulsions and hypermotor seizures with running and jumping (Pinel and Rovner, 1978). With one exception, CKO mice died by P26, with no difference in mortality between male and female mice (p=.6727 by Mantel-Cox Log-rank test) (**Figure 3-2B**). Some CKO mice were noted to lose weight or appear lethargic in the days prior to death, though no gross abnormalities were seen in heart, lung, liver or kidneys upon routine inspection. No seizures were observed in heterozygous or control mice with routine observation. Given that seizures were only observed in the CKO mice, we

sought to determine if the seizure threshold was altered similarly in both the heterozygous and the CKO mice. Following the administration of the GABA antagonist flurothyl, the seizure latency was found to be reduced by greater than 50% in the CKO mice in comparison to both control and heterozygous mice (**Figure 3-2C**). In addition, the character of the seizures in the CKO mice was different from heterozygous mice or controls, with a prolonged ictal course characterized by intermittent jerking before the stereotypical rearing then whole-body convulsing that is typically seen following flurothyl administration. Given the absence of observed seizures, the normal seizure threshold in the heterozygous animals, and the lack of a heterozygous phenotype in a previously published mouse model (Yuskaitis et al., 2018), subsequent studies focused on CKO animals and wild-type littermate controls.

To determine if the premature death in CKO animals was proximally related to seizures and may represent a model of SUDEP, a cohort of mice underwent continuous video monitoring from P18 to P29. At P23, two of three CKO mice demonstrated hypermotor running and jumping events followed immediately by tonic stiffening. Neither animal recovered from the tonic seizure and both died in place, supporting both that the previously observed hypermotor events are seizures and that the premature death in our model is likely a direct consequence of seizures. The remaining CKO from this cohort was the only CKO to survive past 26 days, living until sacrifice at P43.

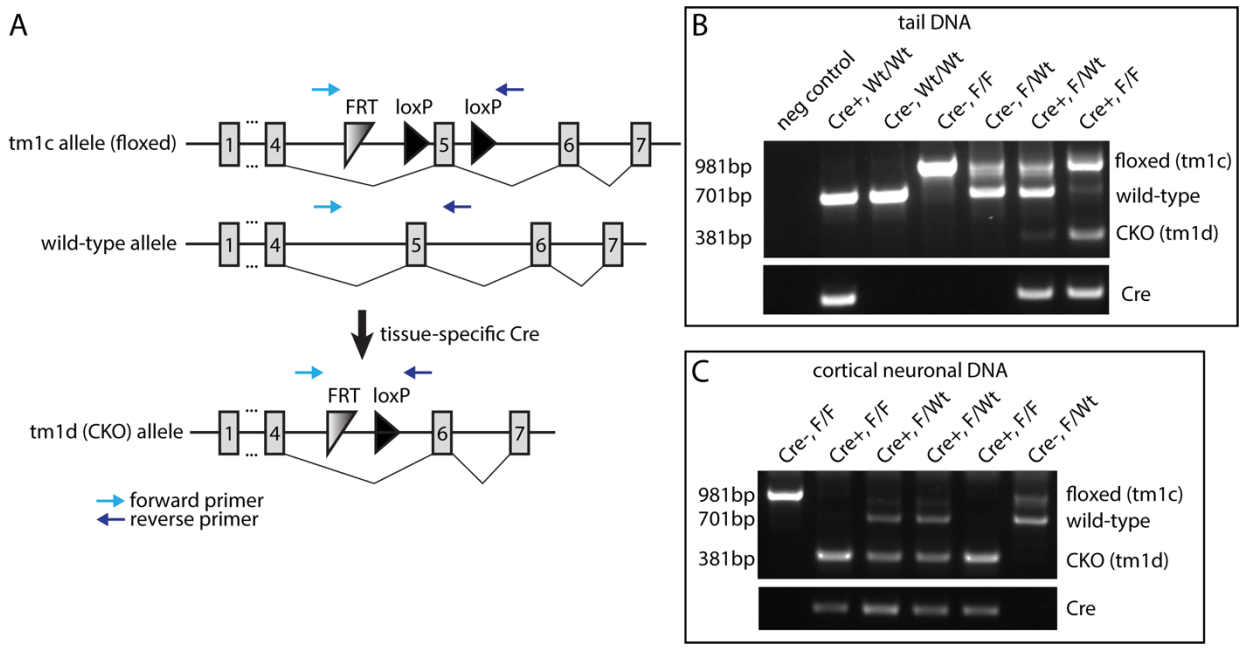

Figure 3-1. Generation of Depdc5F/FEmx1-Cre CKO mice and genotyping strategy.
(A) Schematic demonstrating targeting of the *Depdc5* allele. Genotyping primers are indicated by red arrows. (B-C) Representative genotyping of tail DNA (B) as well as DNA from primary neuronal cultures (C). Wild-type (Wt) mice show a 701 bp band, while conditional mice (F) show a larger 981 bp band due to inclusion of the FRT and LoxP sites. Cre+ mice with a conditional allele show a 381 bp band representing excisional loss of exon 5 and a LoxP site following Cre-mediated recombination. Cre+ mice are identified using primers targeting Cre.

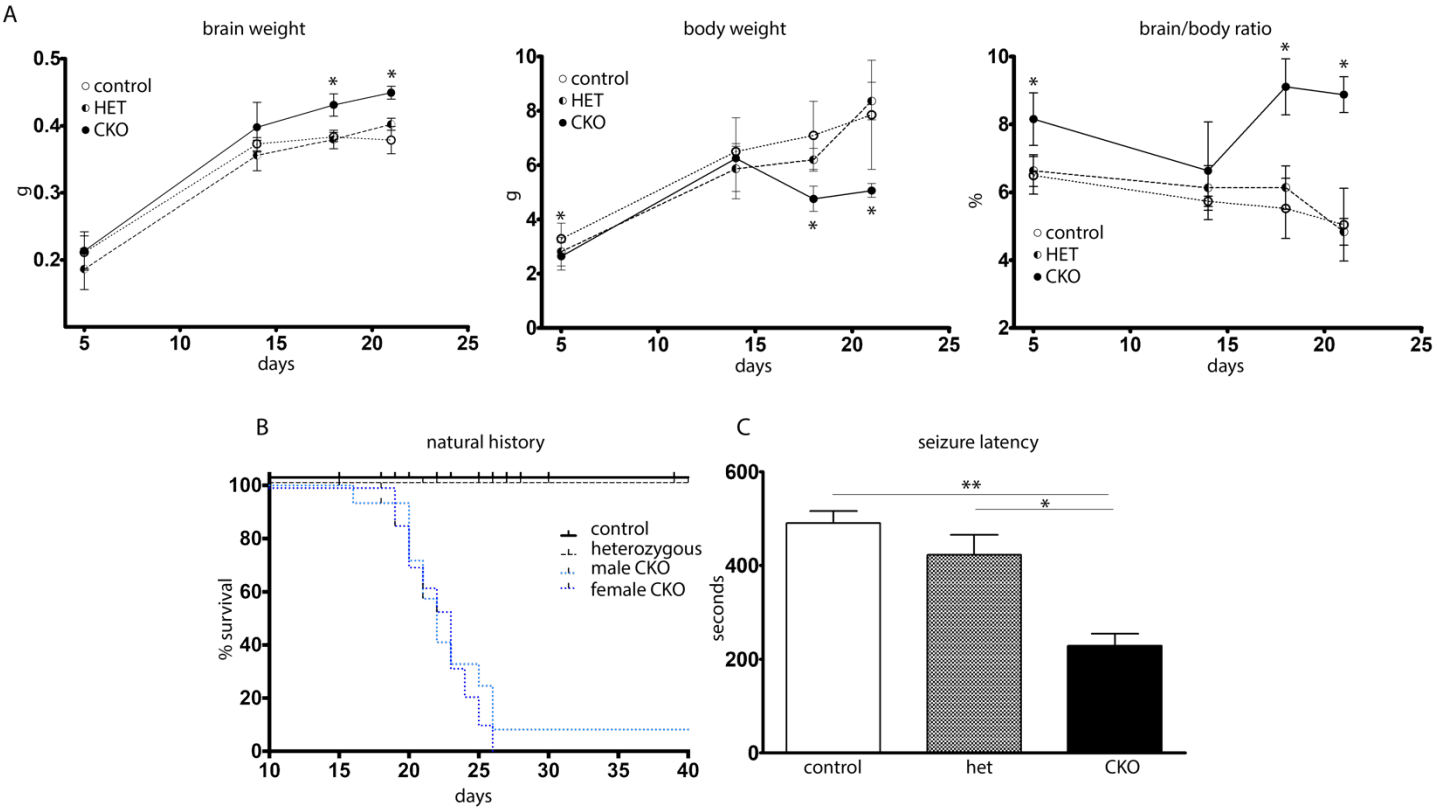

Figure 3-2. *Depdc5-Emx1* CKO mice display changes in gross brain/body weight and demonstrate both seizures and reduced survival.
(A) *Depdc5-Emx1* mice have increased brain weights, are smaller than littermate controls, and cease to gain body weight by P20. CKO mice thus have an increased brain/body weight ratio compared to littermate controls and heterozygotes. *p<.05, two-way ANOVA with Bonferroni's multiple comparisons. n=4-7 controls, n=2-5 heterozygotes, n=3-9 CKOs. (B) Survival was significantly shortened in CKO animals, with only a single CKO animal surviving past P26 ($p<0.0001$ using Log-rank Mantel-Cox test). CKO male: n=17, median survival=22 days; CKO female, n=18, median survival =23 days; compared to control (n=37) and heterozygous (n=28). Tick marks indicate animals that were censored due to sacrifice for biochemical experiments. (C) CKO animals (n=9) showed decreased flurothyl-induced seizure threshold compared to littermate controls (n= 10) and heterozygotes (n=2). *p<.05, **p<.01, one-way ANOVA.

Depdc5-CKO mice have abnormally thickened cortex with cytomegalic neurons

To investigate the etiology for the enlarged brain size in the CKO mouse, cortical histology was examined. Brightfield photomicrographs of H&E stained paraffin sections demonstrated increased thickness of both the hippocampus and overlying cortex (**Figure 3-3A**). As hypothesized following loss of *Depdc5*, a negative regulator of mTORC1, CKO mice had diffusely increased signal intensity of mTORC1 downstream target phosphorylated-S6 (p-S6) (S240/244) (**Figure 3-3B**). Cortical thickness was also significantly increased in CKO mice, consistent with the larger brain size (**Figure 3-3C**). To confirm that the p-S6 positive cells were indeed neuronal, sections were co-stained with the neuronal marker NeuN (**Figure 3-3D**). By P5, cortical neurons were enlarged in the CKO mouse relative to littermate controls, consistent with aberrant mTORC1 activation (**Figure 3-3E**). Immunoblots were performed on cortical lysates from P17-18 mice to evaluate expression of downstream targets of mTOR (p-Akt S473, p-S6 S240/244, and p-S6 S235/236), NPRL2, and GFAP (**Figure 3-3F-G**). After normalization to total S6 protein, phosphorylation of S6 was significantly elevated at both S235/236 and S240/244, consistent with elevated mTORC1 activity. Decreased phosphorylation of Akt (S473) was also evident. Decreased p-Akt has been reported in other models with mTOR hyperactivation and is an expected consequence due to feedback regulation (Carson et al., 2012; Meikle et al., 2008; Yuskaitis et al., 2018). Fellow GATOR1 complex protein NPRL2 showed a decrease, which is consistent with what was seen in the *Depdc5*^{Syn1} CKO mice as well as what was noted in the iPSC and patient-derived neurons described in **Chapter II** (Yuskaitis et al., 2018). Immunofluorescence staining with the layer II-IV marker Cux1 demonstrated an increased number of ectopic Cux1-positive neurons scattered throughout the lower layers (**Figure 3-4**). However, unlike the data from the *Depdc5*^{Syn1} CKO mice, we did not observe increased GFAP in the *Depdc5*^{Emx1} CKO mice, a finding reinforced with immunofluorescence staining for GFAP (**Figure 3-5**).

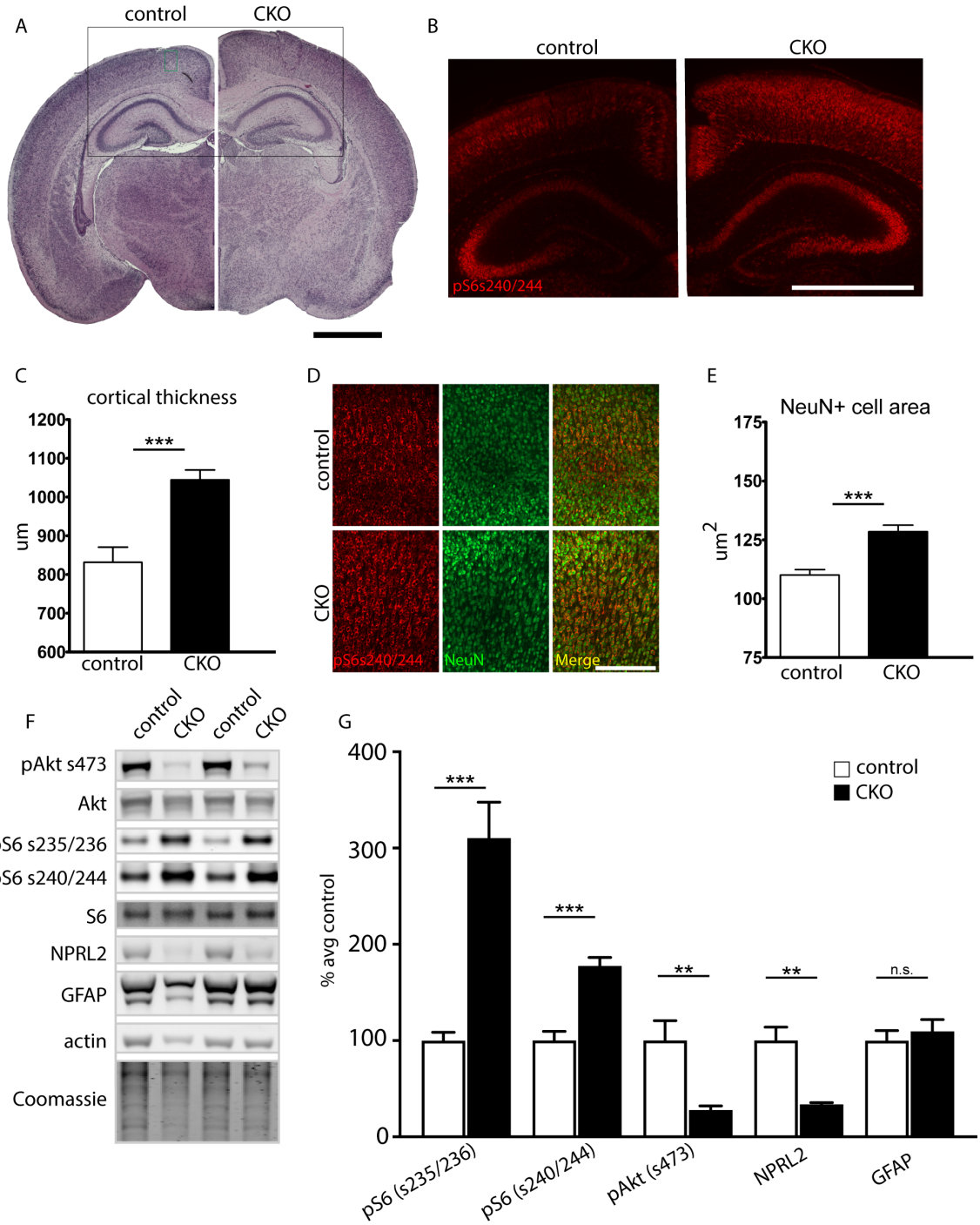

Figure 3-3. Neurohistologic abnormalities in CKO animals.
(A) CKO animals display grossly thickened cortices and hippocampi by P5; hematoxylin and eosin (H&E) stain. Scale bar, 1000 μm. (B) CKO animals show diffusely positive p-S6 (S240/244) immunofluorescence signal intensity (red) in the cortex and hippocampus. Image location indicated by the black box in panel A. Scale bar, 1000 μm. C.) Quantification of cortical width shows increased cortical thickness in CKO animals. Four separate sites were measured and averaged in at least two sections from n=3 animals per genotype. *p<.05, Student's t-test. D-E.) CKO cortical neurons (NeuN, green) are larger with more intense p-S6 (S240/244) signal (red). ***p<.001, Student's t-test, n≥50 neurons per animal from 7 CKOs and 4 littermate controls. Image location indicated by the green box in panel A. Scale bar, 200 μm. F-G.) Representative immunoblot and quantitative analysis of cortical lysates from P17-18 CKO and littermate controls (n=5 mice per genotype). Expression levels were normalized to respective total protein (for pS6 and pAkt) or total protein by Coomassie (for NPRL2 and GFAP), then shown as percent of the average littermate control expression. β-actin is also shown as a loading control. Groups were compared using unpaired t-tests: p-S6 S235/235, p=.0006; p-S6 S240/244, p=.0004; p-Akt S473, p=.009; NPRL2, p=.0015; GFAP, p=.5659. Bars represent mean +/- SEM.

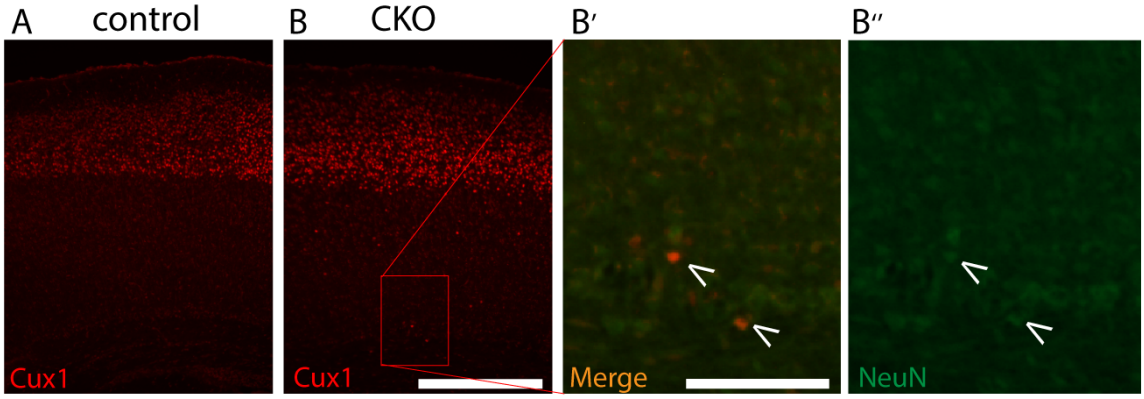

Figure 3-4. Immunofluorescent staining with the layer II-IV marker Cux1 demonstrates a greater number of ectopic neurons present in the CKO than the control.
(A-B) Cortical sections from P5 CKO and littermate control mice stained for layer II-IV marker Cux1 (red). Scale bar, 400 μm. (Inset B') Magnified section co-labeled with the neuronal marker NeuN (green). Scale bar 100 μm. (Inset B") NeuN alone (green). Scale bar 100 μm.

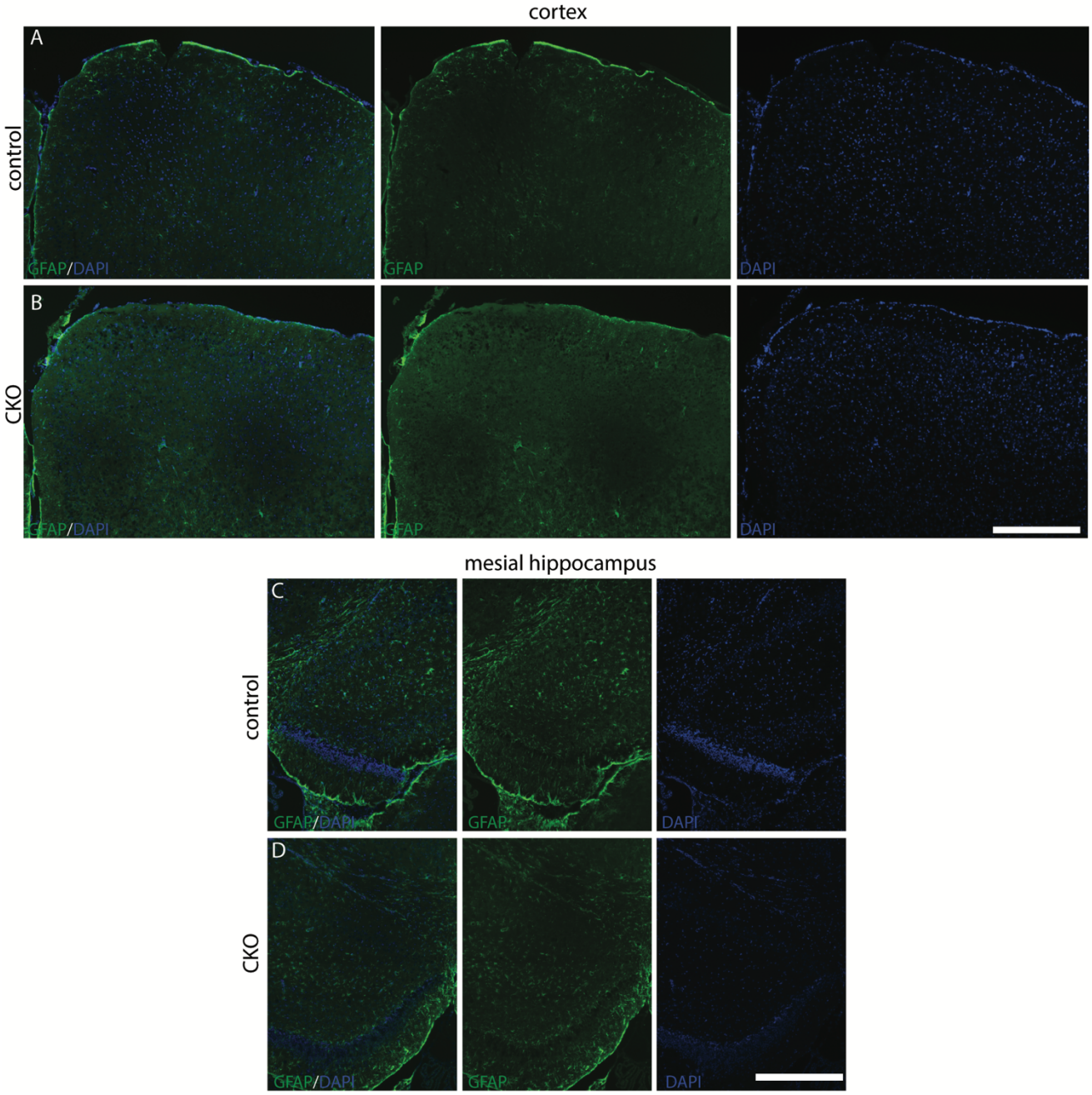

Figure 3-5. CKO mice at P19 do not demonstrate increased astrogliosis.
(A-B) Cortical sections from P19 CKO and littermate control mice stained for astrocytic marker GFAP (green) and nuclei (DAPI). Scale bar, 400 µm. (C-D) Sections from the mesial hippocampus from P19 CKO and littermate control mice stained for astrocytic marker GFAP (green) and nuclei (DAPI). Scale bar, 400 µm.

Depdc5-CKO astrocyte cultures demonstrate increased mTORC1 activation

As noted above, in contrast to published data from the *Depdc5*^{Syn1} mouse model, a marked gliosis, reflected by increased GFAP expression, was not appreciated in the *Depdc5*^{Emx1} CKO, a surprising finding as *Emx1*-Cre targets a population of astrocytes. While this finding may be a function of the young age at which the animals were studied, published data did not demonstrate co-localization of DEPDC5 with astrocytes in human tissue (Dibbens et al., 2013). Given the lack of high-quality antibodies for Depdc5 and challenges in demonstrating astrocytic S6 phosphorylation in mixed cell populations *in vivo*, we generated primary mouse astrocyte cultures for additional characterization. To further address the questions of *Depdc5* expression in astrocytes, we examined mRNA from the astrocyte primary cultures. We found that *Depdc5* mRNA was present in mouse astrocytes and that its expression was significantly reduced in the cultures obtained from the CKO mice. GFAP mRNA expression was not significantly altered in the primary cultures (**Figure 3-6A-B**). To evaluate functional consequences of Depdc5 loss in astrocytes, we characterized mTORC1 activation in cultured astrocytes both during nutrient-plentiful and nutrient-restricted conditions. Immunostaining for phosphorylated S6 (S240/244) in astrocytes suggested increased mTORC1 activation (**Figure 3-6C-H**), a finding confirmed by immunoblot with a slight, but significant increase in S6 phosphorylation in extracts from primary cultures of CKO astrocytes (**Figure 3-6I-L**). Amino acid restriction resulted in a decrease in the level of mTORC1 activation in both control and CKO cells, though the difference in phosphorylation remained the same between control and CKO cells. Consistent with the results from cortical lysates, Akt phosphorylation at S473 was also decreased in the CKO astrocytes (**Figure 3-6M**). While Akt phosphorylation was not changed in the control line following amino acid restriction, it was significantly increased in the CKO cells, consistent with a release of feedback inhibition. In total, these data support that Depdc5 is present and functional in astrocytes.

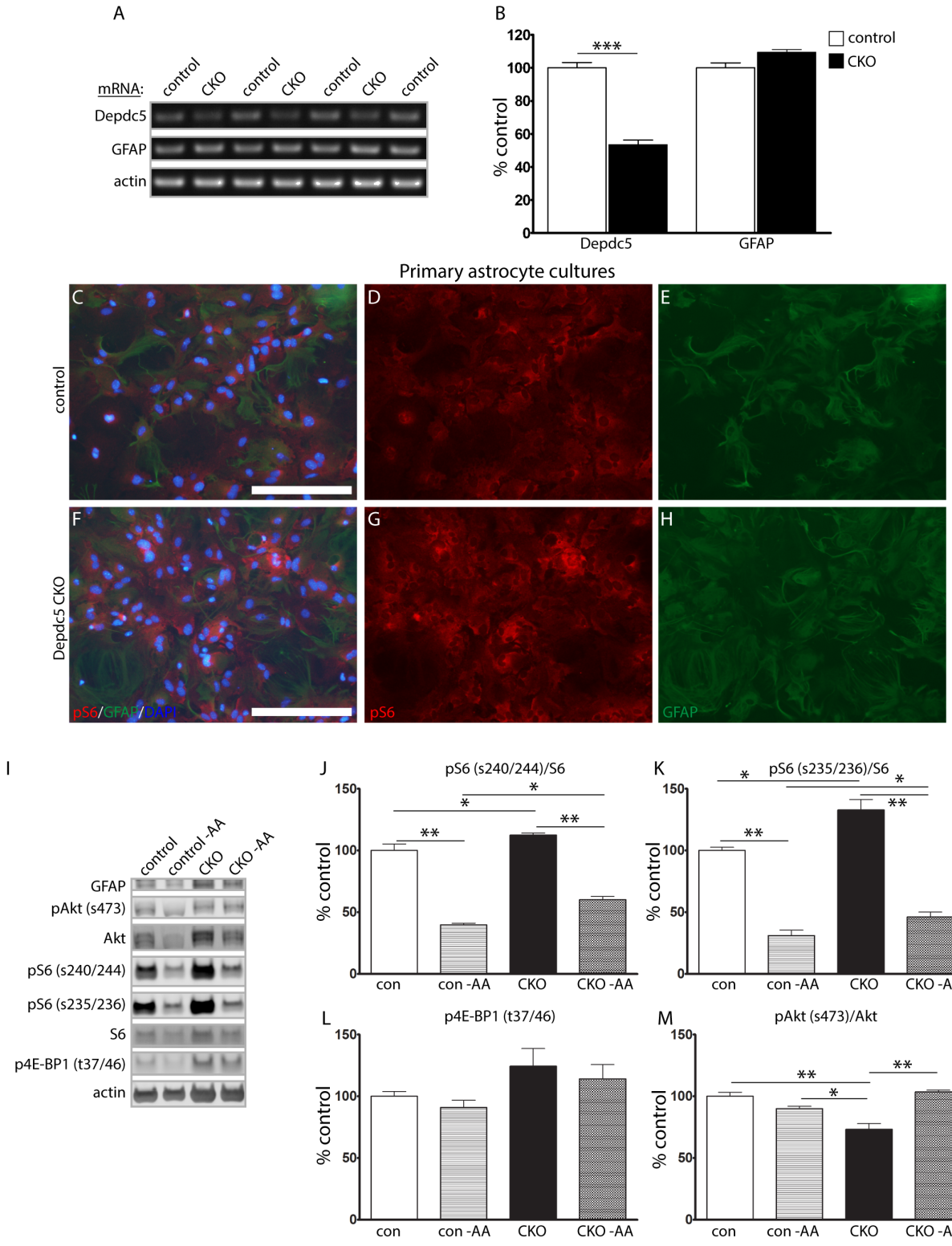

Figure 3-6. Astrocyte cultures from CKO mice display increased mTORC1 activation.
(A-B) Semi-quantitative reverse transcriptase PCR of mRNA extracts from primary astrocyte cultures. Data represent mean +/- SEM. Groups were compared using Student's t-test, independent cultures from n=4 control and n=3 CKO mice. ***p<.001. (C-H) Primary astrocyte cultures from the CKO cortex demonstrate increased p-S6 expression relative to littermate controls. Scale bar, 200 μm. (I-M) Protein immunoblots from primary astrocyte cultures isolated from wild-type and CKO cortex demonstrate increased expression of mTORC1 signaling targets at baseline and when subjected to amino acid deprivation (-AA). Blots were cropped to show relevant bands. Bars represent mean +/- SEM. Groups were compared using two-way ANOVA with Tukey's multiple comparisons, n=3 independent cultures per genotype. *p<.05, **p<.01.

Depdc5-CKO mice show alterations of inhibitory neurotransmission

The thalamocortical circuitry, which includes cortical layer V/VI pyramidal neurons, has been suggested to be involved in generalized epilepsy/seizures in several animal models (Beenhakker and Huguenard, 2009; Kang et al., 2015; McCormick and Contreras, 2001). Additionally, a study in zebrafish suggested that Depdc5 loss of function leads to mTORC1-independent alterations in GABAergic network activity (Swaminathan et al., 2018). Thus, to further define mechanisms that may lead to neuronal excitability and epilepsy in *Depdc5*^{Emx1} CKO mice, we investigated the response of cortical excitatory neurons to GABAergic stimulation.

To characterize GABAergic synaptic transmission in wild-type and CKO mice, miniature inhibitory postsynaptic currents (mIPSCs) were recorded from cortical layer V pyramidal neurons at a -60 mV holding potential (**Figure 3-7A**). Based on observation through diffuse interference contrast microscopy as well as size quantification by immunofluorescence, neurons from *Depdc5*^{Emx1} CKO mice have a larger soma size compared to those from wild-type littermates, a finding reflected in the significantly increased capacitance of CKO neurons (**Figure 3-7B**). mIPSCs in wild-type littermates demonstrated an amplitude of 35.58 ± 4.52 pA, with a frequency of 2.40 ± 0.75 Hz, exhibiting fast rising and slow decaying phases (**Figure 3-7C-D**). Compared with mIPSCs from wild-type littermates, mIPSCs from *Depdc5*^{Emx1} CKO mice showed significantly smaller amplitudes (24.83 ± 2.10 pA) and tended to occur more frequently (4.26 ± 0.86 Hz), though this frequency increase was not statistically significant. The mIPSC amplitude cumulative distribution histogram from CKO mice also showed a left shift toward smaller amplitudes, compared with mIPSCs from WT littermates (k-s test, $p = 0.0001$), suggesting that mIPSCs in layer V pyramidal neurons CKO mice were significantly reduced (data not shown). A significant increase in the rise time and rise time-constant in mIPSC amplitude was seen in CKO mice (**Figure 3-7E-F**), though mIPSC decay time and the decay time-constant were not different (data not shown, p=.35 and .29, respectively). These findings are consistent with postsynaptic mechanisms for decreased mIPSC responses, suggesting a functional impairment in the ability of *Depdc5*-deficient excitatory cortical neurons to respond to GABAergic-mediated inhibition.

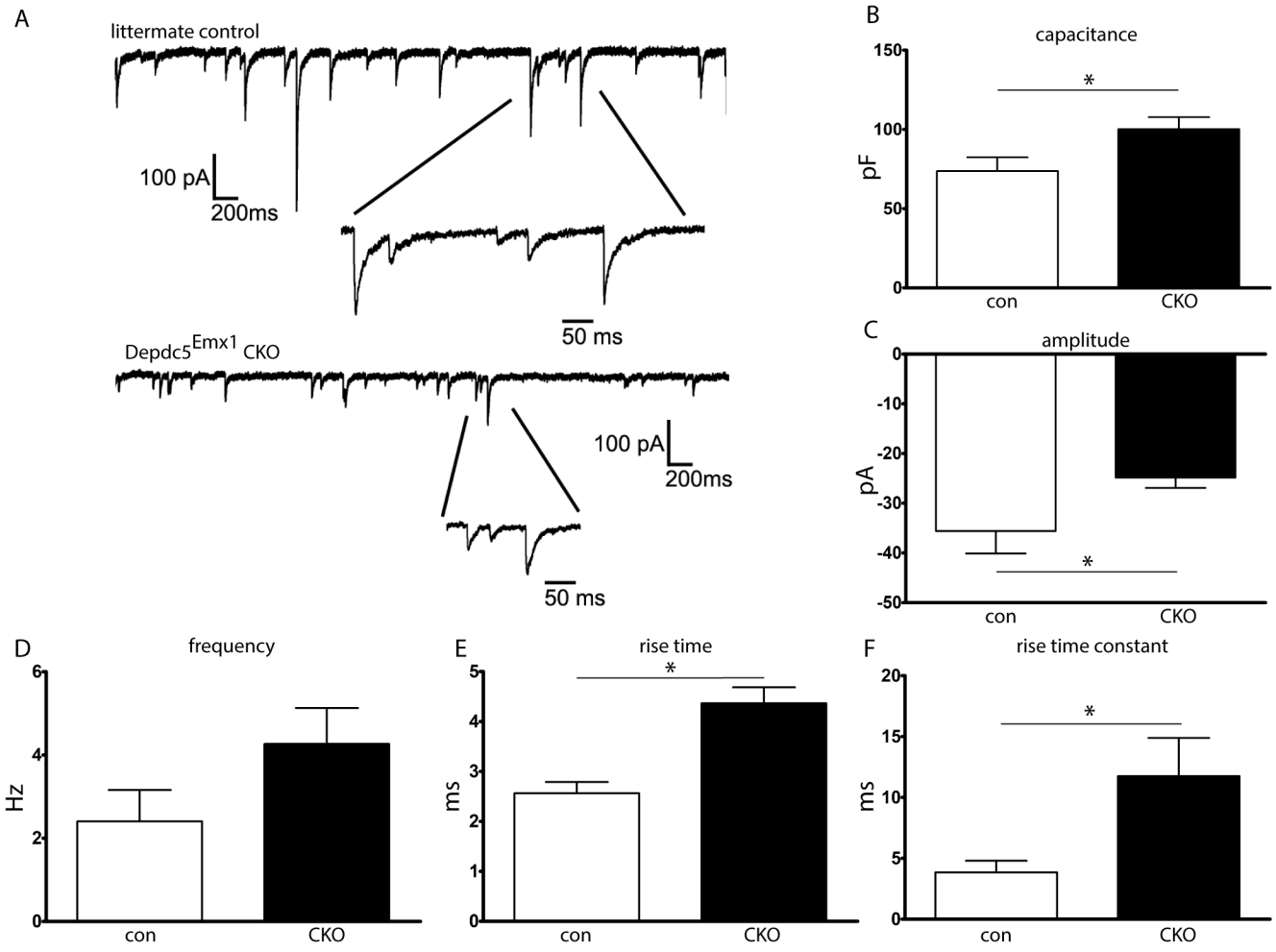

Figure 3-7. Brain slice cultures from CKO mice demonstrate increased capacitance and changes in inhibitory neurocircuitry.

(A) Representative electrophysiologic tracing demonstrating mIPSCs in cortical excitatory neurons. (B) Capacitance was increased in CKO neurons. (C) mIPSC amplitude was decreased in CKO neurons. (D) Frequency of mIPSCs tended to be higher in CKO mice but did not reach statistical significance. (E-F) Both the rise time and rise time constant for mIPSCs were increased in CKO cortical excitatory neurons. n=8-10 neurons from N=3 mice per group. Groups were compared with the Student's t-test, *p<.05.

Rapamycin extends survival of *Depdc5*-CKO mice and reduces seizure frequency, even after withdrawal

Our findings demonstrating macrocephaly with enlarged neurons, altered cortical and hippocampal anatomy, and increased S6 phosphorylation are consistent with previous studies in TSC and Depdc5 mouse models with mTORC1 hyperactivation. To determine the contribution of mTORC1 hyperactivation to premature death in the *Depdc5*^{Emx1} CKO, CKO mice and littermate controls were treated with the mTORC1 inhibitor rapamycin (3 mg/kg, 5 days per week), a protocol that was shown to prevent early death in a *Tsc1* mouse model and rescue myelination in the *Olig2-Tsc2* mouse model (Carson et al., 2015; Carson et al., 2012). Following treatment with rapamycin, 71% of CKO mice survived to 30 days of life, in contrast to untreated or vehicle-treated CKO mice with 5% survival by P26 (**Figure 3-8A**). A witnessed seizure was seen in one of twenty (5%) of the rapamycin-treated CKO mice, a significant reduction from the 25% of untreated or vehicle treated CKO mice demonstrating clinical seizures ($p = <.05$ using Chi-square with Yates correction). The lone rapamycin-treated animal with an observed seizure died prematurely at P22. Cortical extracts confirmed both the marked elevation of S6 phosphorylation prior to treatment and the decrease to near normal levels with rapamycin treatment (**Figure 3-8B-C**). The benefits of rapamycin with respect to mortality were durable despite increased S6 phosphorylation seven days following rapamycin withdrawal at P30. All CKO animals that survived to P30 remained living until the day of sacrifice at P70. CKO animals did have significantly increased brain weights at P70, although the brain-to-body ratio was not significantly different from littermate controls (**Figure 3-8D-F**).

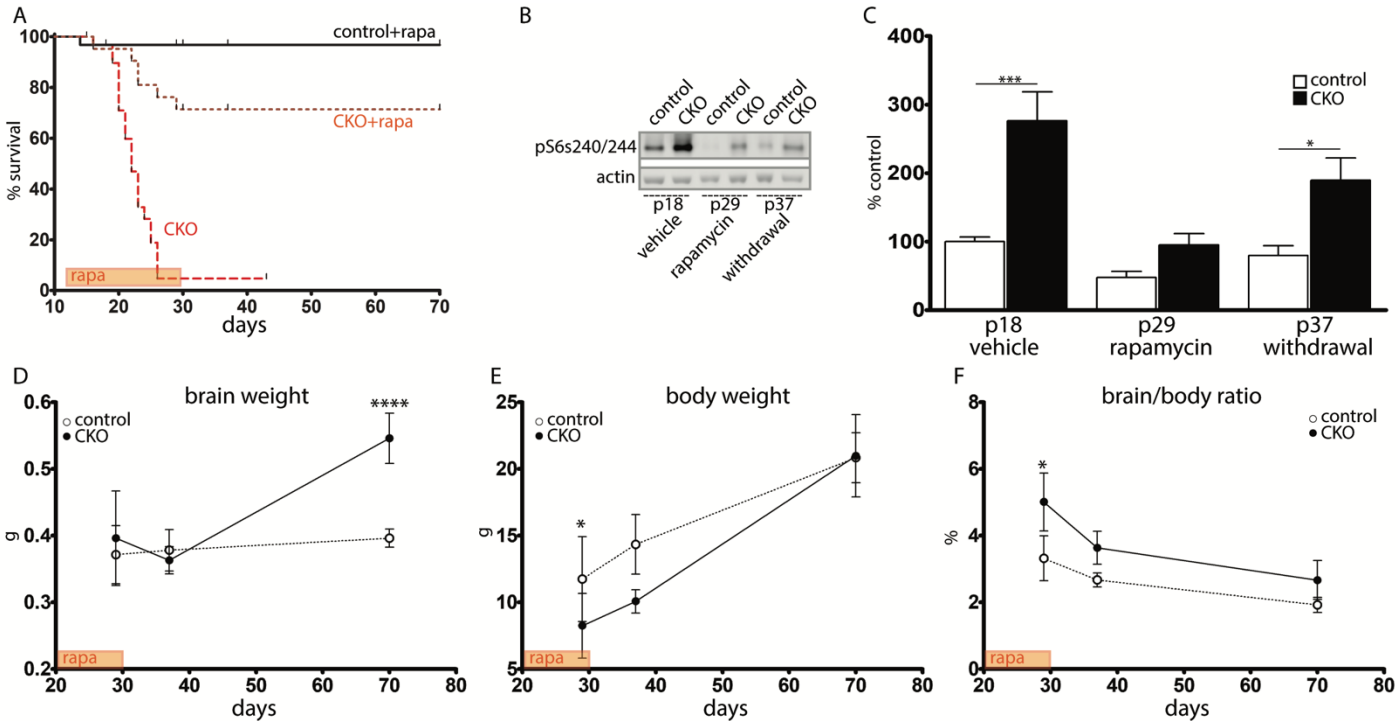

Figure 3-8. Rapamycin treatment prolongs survival even after withdrawal.
(A) Survival after rapamycin ($p<0.0001$ using Log-rank [Mantel-Cox] test). (B) Without treatment, CKO cortical lysates demonstrated increased p-S6 (S240/244) (P18) compared to littermate controls. This was attenuated during rapamycin treatment (P29) and remained attenuated one week after rapamycin withdrawal (P37). (C) Quantification of p-S6 S240/244 expression. n= 4 animals per genotype. *$p<.05$, ***$p<.001$ by 2-way ANOVA with Bonferroni's multiple comparison test. (D-F) Brain weight (D), body weight (E), and brain-to-body ratio (F) immediately after the rapamycin treatment window (P30), 7 days after treatment withdrawal (P37), and 40 days after treatment withdrawal (P70). n=3-6 CKOs and n=4-20 littermate controls. *$p<.05$ by 2-way ANOVA with Bonferroni's multiple comparison test.

Discussion

Mutations in the component proteins of the GATOR1 complex are increasingly appreciated as common causes for focal epilepsies. The association of these mutations with medically-refractory focal epilepsies and SUDEP necessitates a better understanding of the mechanisms by which the loss of these components leads to epilepsy. Herein we describe a novel epileptic mouse model lacking Depdc5 in neuroprogenitor cells.

Experience from the study of mouse models of TSC has demonstrated that mouse models do not recapitulate the human disease completely, including lack of seizures in heterozygous mouse models and lack of focal "tuber-like" structures. Nonetheless, rodent models continue to have value in addressing underlying mechanisms of epilepsy and for designing therapies that may modulate neuronal networks or affect multiple organ systems. Published rodent models have previously and consistently shown that knockout or knockdown of *Depdc5* allows increased mTORC1 activity, increased neuronal size, and dysplastic cortical neurons (Dawson et al., 2020; De Fusco et al., 2020; Hughes et al., 2017; Marsan et al., 2016; Ribierre et al., 2018a; Yuskaitis et al., 2018). Given that homozygous global knockout of *Depdc5* is embryonic lethal and heterozygous mice do not have epilepsy, mouse models with a conditional knockout or with an induced focal second hit have been required for epileptogenesis. Yuskaitis *et al*. demonstrated in the $Depdc5^{Syn1}$ CKO mouse model a lowered seizure threshold, rare spontaneous seizures and premature death (Yuskaitis et al., 2018). By targeting neuroprogenitor cells, we have generated a mouse model with a similar, though more severe phenotype, including a higher incidence of epilepsy and attenuated life span. While we were unable to perform video-EEG recordings due to the small size of the young animals, the relative risk for clinical seizures observed during routine husbandry approached 50% by 25 days of life. This risk is likely an underestimation of total seizure burden given that these were seizures observed during routine handling, however the lack of video-EEG is a limitation of this study. Consistent with this, focused video analysis demonstrated terminal seizures in two of three mice, supporting the likelihood that premature death in this model is due to seizures and that this may serve as a model for investigation of mechanisms of SUDEP. Future studies with video-EEG recordings will be required to fully characterize the association between clinical seizures and SUDEP in our model.

While both *Syn1*-Cre and *Emx1*-Cre result in gene deletion in excitatory neurons, because *Emx1*-Cre targets neuroprogenitor cells, a subset of astrocytes is also targeted. Published data from human tissue failed to definitively show DEPDC5 in astrocytes via immunofluorescence labeling (Dibbens et al., 2013). Without *Depdc5*, astrocytes would have to rely on an alternative method for sensing cellular amino acids (Bar-Peled et al., 2013). While the lack of a quality Depdc5 antibody precluded a direct quantitation of Depdc5 protein in mouse brain or in cultured astrocytes, our data demonstrating mTORC1 hyperactivation in CKO astrocytes and the presence of *Depdc5* mRNA in astrocyte cultures suggest that *Depdc5* is expressed and functional in mouse astrocytes. The contribution of astrocytes to epilepsy is increasingly appreciated (de Lanerolle et al., 2010). Astrocytes perform a variety of functions that can modulate neuronal excitability, including playing a significant role in extracellular potassium regulation. Disruption of these functions or of the ratio of astrocytes to neurons may increase neuronal excitability. It is also possible that non-cell-autonomous effects are occurring in the cortex and contributing to astrocyte dysfunction, however these effects are likely limited in primary astrocyte cultures (Hu et al., 2018). Further studies will be important to determine the contribution of astrocytes and other glial cells to the pathogenesis of *DEPDC5*-related epilepsies.

Our data demonstrate that CKO cortical excitatory neurons have a reduced ability to respond to GABAergic input, which may play a role in neuronal excitability leading to epilepsy. A decrease in mIPSC amplitude, but no significant change in frequency, suggests a postsynaptic mechanism, such as reduced expression or activation of postsynaptic GABA receptors. Ribierre *et al.* reported altered dendritic spine morphology, including spine hypertrophy and increased branching complexity in focal regions of *Depdc5* homozygosity following *in utero* electroporation (Ribierre et al., 2018a). It is possible that similar morphologic alterations are present in the dendritic arbors of $Depdc5^{Emx1}$ CKO mice, impairing the response to presynaptic GABA release. Another possibility involves a potential mTORC1-independent function of *DEPDC5* in regulating fine-branching of the GABAergic network (Swaminathan et al., 2018). While the exact mechanism underlying the decreased response to GABA has not yet been fully determined, our findings may suggest a specific benefit for drug therapies which increased GABA availability.

The finding that inhibition of mTORC1 with rapamycin nearly completely prevented premature death and decreased the incidence of observed seizures in our mouse model strongly supports a primary role for mTORC1 dysregulation. Similar findings concerning premature death were observed following treatment of the $Depdc5^{Syn1}$ mouse with rapamycin

(Yuskaitis et al., 2019). Future studies will be required to better clarify the mechanisms by which transient mTORC1 inhibition is protective in our mouse model. The finding that transient rapamycin treatment (P12 - P30) was able to prevent death and observed seizures for an extended period of time following withdrawal is consistent with the notion that transient mTOR inhibition may be sufficient to modify development and lead to long-lasting benefits with respect to neuronal excitability. Similar findings have been reported following rapamycin withdrawal in TSC mouse models, with extended survival following withdrawal of rapamycin (Armour et al., 2012; Meikle et al., 2008). However, TSC mice given rapamycin until P30 had gradual deterioration following treatment withdrawal (Meikle et al., 2008). While we did not observe clinical deterioration in our mice following rapamycin withdrawal, CKO mice did have an increased brain weight compared to controls at P70, suggesting possible phenotypic re-emergence or progression.

The long-term benefits of early drug treatment with the goal of future seizure prevention are currently being investigated in TSC, the prototypical mTORopathy, using the medication vigabatrin (https://clinicaltrials.gov/ct2/show/NCT02849457). Thus, the concept that seizure prevention during a critical neurodevelopmental window may have lasting consequences for the future development of epilepsy in GATORopathies warrants further consideration. Whether similar long-lasting benefits in our model may result from shorter durations of mTOR inhibition, early seizure prevention with standard antiepileptic medications, or dietary modifications are considerations for future studies.

Materials and Methods

Generation of CKO mouse model

To generate a mouse model of *Depdc5*, mice containing a floxed-stop allele of exon 5 (*Depdc5*$^{tm1c(EUCOMM)Hmgu}$) were obtained from Infrafrontier (EM:10459). As homozygous loss of *Depdc5* is lethal in the embryonic stage (16, 17), to contrast heterozygous versus the homozygous loss of *Depcd5* in cortical neurons, a conditional knockout mouse was generated. To target neuroprogenitor cells, male *Depdc5* mice were crossed to female mice heterozygous for *Depdc5* and *Emx1*-Cre (Jax 005628) and maintained on a C57BL/6 background. This breeding strategy was used due to mitigate risk of germline transmission of *Emx1*.

Mice were housed under normal environmental conditions with a standard 12-hour light-dark cycle and *ad lib* access to water and food. Weekly weights were taken to ensure the maintenance of normal food and water intake. Mice were euthanized under anesthesia for tissue harvesting, methods in accordance with AVMA guidelines. All work was conducted with the approval of the Institutional Animal Care and Use Committee (IACUC) at Vanderbilt University, Nashville, Tennessee (M/17/00125).

Confirmation that pups were born at a Mendelian ratio was determined by counting pups from nineteen consecutive litters. Thereafter, animals were observed daily and weighted weekly or at time of sacrifice. Animals which died were plotted on Kaplan-Meier curves along with animals which were censored for use in experiments. Male and female CKO mice showed no difference in mortality and were used interchangeably in studies. Documentation of seizure incidence was recorded during routine husbandry.

Genotyping

DNA was extracted from mouse tails using the REDExtract-N-Amp Tissue PCR kit according to the manufacturer's instructions (Millipore Sigma #XNAT). Genotyping of the *Depdc5* gene was performed using primers (forward: 5'-TCCAGCTTCAGCTCTCTT-3'; reverse: 5'- AAGCAGCCTATGTACCATTTAT-3') that flank LoxP sites surrounding exon 5, allowing concurrent detection of the wild-type and conditional alleles. Agarose gel electrophoresis was performed, detecting a 701 base pair (bp) band for the wild-type allele, a 981 bp band for the conditional allele, and a 381

bp band for the conditional knockout. The presence of the *Cre* recombinase gene was determined using primers (forward: 5'-GCATTACCGGTCGATGCAACGAGTGATGAG-3'; reverse: 5'-GAGTGAACGAACCTGGTCGAAATCAGTGCG-3') detecting a 408 bp band. Genomic DNA was isolated from astrocytes using a DNeasy kit (Qiagen #69504) and *Cre*-mediated deletion of exon 5 of *Depdc5* was verified by PCR following the genotyping strategy above.

Seizure threshold testing with flurothyl

As described previously, in a blinded manner, P15 mice were placed in a 1.96 L custom built acrylic chamber and allowed to habituate for one minute (37). Following habituation, a 10% solution of the GABA antagonist flurothyl (bis-2,2,2-trifluoroethyl ether, Sigma-Aldrich) in 95% ethanol was dripped at a rate of 100 µL/min onto filter paper suspended above and out of reach of the animal. Latency to seizure, typically a stereotyped clonic-forebrain seizure with rearing followed by tonic-clonic convulsions, was recorded and compared between groups with a one-way ANOVA.

Immunofluorescence

Brain tissues were dissected from *Depdc5* CKO and littermate controls as previously described (37-39). Briefly, animals were anesthetized with ketamine/xylazine and perfused (P5 and older) with ice-cold phosphate buffered saline (PBS) followed by ice-cold 4% paraformaldehyde (PFA) in PBS (pH 7.4). Brains were post-fixed in 4% PFA overnight and cryoprotected in 30% sucrose in PBS prior to sectioning. Brains were frozen in OCT and stored at -80˚ C. 10 um sections were cut using a cryostat.

Immunofluorescence was performed as previously described (40). Briefly, brain sections on slides were post-fixed in 1% PFA, washed in PBS, blocked in 10% goat serum with 0.1% Triton X-100, and primary antibodies were added and incubated overnight at 4C. The next day, slides were washed in PBS and secondary fluorescent antibodies (AlexaFluor, ThermoFisher) were added and allowed to bind for 1 hour. Slides were washed in PBS and coverslipped with mounting medium including DAPI (Vectashield, Vector Labs #H-1200). Negative controls omitting primary antibodies were performed for each experiment.

Photomicrographs were obtained using an AMG EVOS epifluorescence microscope. All images from a given experiment were generated in parallel with constant gain and exposure time. Images analysis was performed with ImageJ and Adobe Photoshop CS5. Minor adjustments of contrast or brightness, as well as cropping, were performed concurrently on control and CKO sections. Experiments were performed in triplicate to ensure reproducibility. Primary antibodies and dilutions are listed in **Table 3-2**.

Cell size

Size of NeuN positive cells was quantified by importing images to ImageJ (NIH, version 1.38) and, in a blinded fashion, cell area was measured in >50 cells per animal from layers 2-4 of the frontal cortex using five independent control littermate and five *Depdc5*$^{Emx1\text{-Cre}}$ CKO mice. Means and standard deviation were calculated and results were compared for statistical significance using Student's *t*-test.

Rapamycin treatment

Rapamycin (LC Laboratories, Woburn, MA) was dissolved at 30 mg/mL in ethanol and diluted with vehicle 0.25% Tween 20/0.25% polyethylene glycol in PBS. *Depdc5*$^{Emx1\text{-Cre}}$ CKO and control littermates were injected with either rapamycin (3 mg/kg) or vehicle i.p. daily Monday-Friday of each week starting at P13-15 (41). All surviving mice were euthanized between P30-70. As nearly all vehicle-treated *Depdc5*$^{Emx1\text{-Cre}}$ CKO mice died by 26 days of life, a vehicle-treated control littermate was euthanized on that same day. All control brains were rapidly removed, weighed, and processed in parallel with brains from *Depdc5*$^{Emx1\text{-Cre}}$ CKO mice. Kaplan-Meier survival curves of *Depdc5*$^{Emx1\text{-Cre}}$ CKO and control mice treated with either rapamycin or vehicle were compared using the log rank test (GraphPad Prism).

Immunoblotting

Mice were anesthetized with isoflurane and tissues rapidly dissected on ice, flash frozen in liquid nitrogen and stored at -80˚ C. Lysate preparation, SDS-PAGE, and immunoblotting were performed as previously described (40). Primary antibodies and dilutions are listed in **Table 3-2**.

Table 3-2. List of primary antibodies.

Antibody	Species	Dilution	Vendor/ Manufacturer	Catalog Number
anti-beta-actin	Rabbit	1:2000 (WB)	Cell Signaling Technology	#4967
anti-beta-actin	Mouse	1:2000 (WB)	Sigma	#A5441
anti-phospho-Akt (Ser473)	Rabbit	1:1000 (WB)	Cell Signaling Technology	#4060
anti-phospho-4E-BP1 (Thr37/46)	Rabbit	1:250 (WB)	Cell Signaling Technology	#2855
anti-4E-BP1 (clone 53H11)	Rabbit	1:500 (WB)	Cell Signaling Technology	#9644
anti-pan-Akt (clone 40D4)	Mouse	1:1000 (WB)	Cell Signaling Technology	#2920S
anti-phospho-S6 (Ser235/236)	Rabbit	1:1000 (WB)	Cell Signaling Technology	#2211
anti-phospho-S6 (Ser240/244)	Rabbit	1:1000-1:2000 (WB); 1:800 (IF)	Cell Signaling Technology	#5364
anti-S6 (clone 54D2)	Mouse	1:500 (WB)	Cell Signaling Technology	#2317S
anti-NPRL2	Rabbit	1:1000 (WB)	Cell Signaling Technology	#37344S
anti-GFAP	Mouse	1:1000 (WB); 1:300 (IF)	Cell Signaling Technology	#3670
anti-NeuN	Mouse	1:1000 (IF)	Abcam	#ab104224
anti-Cux1	Rabbit	1:100 (IF)	Santa Cruz	#SC-13024

Primary mouse astrocyte cultures

Primary mixed glial cultures were prepared from P0 to P2 mouse brains with modification of published protocols (33, 42). Briefly, following euthanasia, cortical tissue was isolated, dissociated and plated into poly-L-lysine (PLL)-coated flasks incubated at 37°C and 8.5% CO_2 in mixed glial culture media (MGCM, DMEM with 10% FBS +pen/strep). Microglia and oligodendrocyte precursors were removed via differential shaking at DIV9. Astrocytes remaining in the T25 flask were washed with PBS and dissociated with 0.25% trypsin in Hanks' balanced salt solution (HBSS). Dissociated cells were re-plated into T-25 flasks or onto PLL-coated 24-well culture dishes until the day of harvest.

For immunoblotting, individual cultures from a single animal represent a single biologic replicate. For amino acid starvation experiments, fresh baseline MGCM or nutrient-limited media consisting of DMEM lacking amino acids

(USBiological D9800-13) was added at time zero. Cells were harvested and lysed for protein after 1.5 hours, then analyzed via immunoblot.

For immunofluorescence microscopy, cells in 24-well dishes were washed with PBS followed by fixation with 4% paraformaldehyde for 10 min. Following PBS washes, cells were labeled as described above prior to imaging with an EVOS fluorescent microscope (AMG).

Semi-quantitative RT-PCR from primary mouse astrocyte cultures

Total RNA was extracted from astrocytes using the RNeasy kit (Qiagen #74134) and QIAShredder columns (Qiagen #79654) according to the manufacturer's instructions. DNA digestion was performed using either on-column DNA digestion (Qiagen #79254). cDNA was synthesized using random primers with the SuperScript VILO cDNA synthesis kit (Invitrogen #11754). A PCR reaction with primers designed to amplify Depdc5, GFAP (224 bp), or Actin (150 bp) was performed using 100 ng of cDNA. Depdc5 (150 bp): F'-5'-GTCCTTTGCTTTTGCAAGTCA-3', R-5'-CCCACGGCCAATATACTGAT-3'. GFAP: F-5'-TCCTGGAACAGCAAAACAAG-3', R-5'- CAGCCTCAGGTTGGTTTCAT-3' (43). Actin: F-5'-CCACCATGTACCCAGGCATT-3', R-5'- GGACTCATCGTACTCCTGC-3'. The reaction was performed as follows using a Bio-Rad T100 thermal cycler: 95°C x 1 minute, repeated 35 times: (95°C x 15 s, 54.5°C x 15 s, 72°C x 2 min), 72°C x 5 min. Following amplification, PCR products were separated on a 1.5% agarose gel. Band densities for Depdc5 and GFAP products were quantified using ImageJ (NIH, version 1.51n) and normalized to Actin, then expressed as % average control. Primary cultures from four separate CKO mice and four littermate controls were analyzed.

Brain slice preparation and whole-cell recordings

Brain slices were prepared using the method previously described in Schofield et al. and Zhou et al. (44, 45) Mice (postnatal 14-18 days old of either gender) were anesthetized with isoflurane. Brains were then surgically removed to prepare coronal slices (300 μm) using a LEICA VT-1200S vibrotome (Leica Inc) in oxygenated (bubbling with 95%O2/5%CO2) ice-cooled dissection solution (4°C) (mM: 2.5 KCl, 0.5 CaCl2, 10 MgSO4, 1.25 NaH2PO4, 24 NaHCO3, 11 Glucose, 214 sucrose). The slices were incubated in a glass chamber containing oxygenated ACSF (mM:

126 NaCl, 2.5 KCl, 2 CaCl2, 2 MgCl2, 26 NaHCO3, 10 glucose, pH 7.4) for 40 min at 35-36°C. The slices were allowed to recover at room temperature for at least 1 hour before recordings.

Whole-cell recordings were carried out with an upright NIKON Eclipse FN-1 IR-DIC microscope and a MultiClamp 700B amplifier and Digidata 1440A (Molecular Devices Inc.). Since the thalamocortical circuitry is involved in epileptogenesis, layer V pyramidal neurons in the somatosensory cortex were chosen for recording (44, 46). Miniature inhibitory postsynaptic currents (mIPSCs) were recorded at -60 mV and isolated by including 10-20 μM NBQX and 1 μM tetrodotoxin (TTX) in the ACSF (flow rate: 1-1.5 ml per min). The internal solution for recordings contained (as per Schofield et al., in mM: 135 CsCl, 10 HEPES, 10 EGTA, 5 QX-314, 5 ATP-Mg (290-295 mOsm, pH = 7.3) with a chloride ion reversal potential close to 0 mV (44). Filled glass electrodes had 3-5 MΩ resistance. Access resistances during recording were continuously monitored and were less than 20-25 MΩ. The access resistances were compensated by 70% and cell capacitance. Unstable recordings with access resistance variation >20% or larger than 25 MΩ were discarded. Junction potentials were compensated for when electrodes were in ACSF. Data were collected using the Clampex program 10.2 (Molecular Devices Inc.) and synaptic currents were filtered at 2 KHz and digitized at 10 KHz. All recordings were made continuously for 20-30 min following the rupture of the membrane (at room temperature, 24°C). mIPSC data were analyzed with Clampfit (Molecular Devices Inc.) using threshold detection (at least 2.5X baseline RMS with no clear synaptic events) (47). Histogram and accumulative graphs were constructed. The network oscillation data were analyzed with both Clampfit (for spike histogram and autocorrelation function) and MATLAB to obtain autocorrelograms. Numerical data were reported as mean ± S.E. and statistical differences were determined by the Student's t-test.

Acknowledgements

The C57BL/6N-Depdc5$^{tm1c(EUCOMM)Hmgu}$ mice were obtained from the MRC Harwell Institute which distributes these mice on behalf of the European Mouse Mutant Archive (www.infrafrontier.eu). The MRC Harwell Institute is also a member of the International Mouse Phenotyping Consortium (IMPC) which funded the generation of the C57BL/6N-Depdc5$^{tm1c(EUCOMM)Hmgu}$ mice. Funding and associated primary phenotypic information may be found at www.mousephenotype.org.

CHAPTER IV

FUTURE DIRECTIONS AND DISCUSSION

Summary

DEPDC5 mutations were identified as a genetic cause of focal epilepsy in 2013. As a negative regulator of mTORC1, *DEPDC5* mutations lead to overactivation of the mTORC1 signaling pathway, which has deleterious effects in the brain, including epilepsy. Since 2013, investigation has begun to determine the specific mechanisms of how *DEPDC5* mutations cause epilepsy in the hopes that new treatments may emerge from a better understanding of disease pathogenesis. Many of these studies have used rodent models. Because animal models differ in the phenotypes demonstrated by animals heterozygous for *Depdc5*, it is important to determine the effects of the heterozygous state in the human brain, considering the vast differences between human and rodent neurodevelopment. At the same time, animal epilepsy models will be needed to test new treatments. We describe a novel genetic mouse model in which 25% of mice develop seizures at a young age, which will be useful for *in vivo* testing of novel therapeutics. The use of patient-derived cells in combination with an animal model provides an ideal strategy for future investigation. In this chapter, I will consider the many questions that remain about the mechanisms of epileptogenesis caused by *DEPDC5* mutations and speculate how the models presented in this dissertation may provide insight.

The role of gene dosage in *DEPDC5*-related epilepsy and potential brain-specific effects

A major finding of the studies in **Chapter II** is that human iPSCs and neurons heterozygous for *DEPDC5* mutation have hyperactivation of mTORC1. Different animal models have demonstrated variability in heterozygous phenotypes, with some animals having a mild phenotype and some having none at all. Taken together with our patient-derived data, this suggests the existence of species-specific or cell type-specific differences in susceptibility to changes in *DEPDC5* gene dosage. A recent report outlined changes in three different states of Depdc5 gene dosage in a mouse: a germline heterozygote (50% protein loss), a heterozygote with 50% protein knockdown (75% protein loss), and a heterozygote with nearly 100% protein knockdown (100% protein loss) (De Fusco et al., 2020). A hyperexcitability phenotype seemed to develop in a dose-dependent effect: heterozygous (50% loss) cells had slight changes in neurite complexity and passive membrane properties, 75% loss caused somewhat increased mEPSC frequency, and near 100% loss further increased

mEPSC frequency in addition to the number of excitatory synapses. This study provides evidence that the effects of DEPDC5 mutation lie on a continuum that is dependent on gene dosage.

Different species and cell types may have varying sensitivities to changes in gene dosage, supporting the need for additional studies in human models. The seizure threshold in mice varies depending on the strain, supporting that different genetic backgrounds result in variability in brain function (Frankel et al., 2001). Indeed, this also highlights the potential limitations of rodent models in studying neurological diseases. The timing of neurogenesis and neuronal migration in humans is quite different than in mice or rats, and synaptogenesis continues well after birth in humans (Pressler and Auvin, 2013). Mice and rats are also lissencephalic, having smooth brain surfaces as opposed to the extensive folding found in the gyrencephalic human brain (Sun and Hevner, 2014). In addition to these differences in brain development and organization, it is possible that DEPDC5 has some species-specific functions. In determining the structure of the GATOR1 complex, DEPDC5 was found to have an unexpected inhibitory binding mode (Shen et al., 2018). The inhibitory mode consists of a strong interaction between DEPDC5 and RagA, which positions the catalytic Arg78 residue of NPRL2 facing away from RagA, interfering with the GAP activity which is needed for suppression of mTORC1 (Shen et al., 2018). This inhibitory mode seems to exist to prevent GATOR1 hyperactivation and is potentially unique to humans, since the critical strip mediating the inhibitory interaction is not well conserved. When a critical-strip-mutant DEPDC5 protein is introduced in yeast, eliminating the inhibitory mode, there is minimal change in GAP activity, suggesting that this mode is not present at least in yeast (Shen et al., 2019). It also raises the possibility that some *DEPDC5* mutations may have a dominant negative effect, if they prevent release of this inhibitory mode. If this binding mode is unique to certain species, it could partially explain some of the species-specific differences in consequences of *DEPDC5* loss.

It is also possible that different susceptibilities to changes in *DEPDC5* gene dosage may exist between cell types. This could help explain why the brain seems particularly sensitive to changes in *DEPDC5* gene dosage. Current evidence suggests that patients with germline mutations in *DEPDC5* have pathology limited to the brain. While *DEPDC5* and *NPRL2* mutations have been associated with various cancers suggesting they function as tumor suppressors, there is no evidence to suggest that patients with epilepsy due to GATOR1 mutations have an increased susceptibility to developing

these cancers (Gao et al., 2012; Huang et al., 2016; Miki et al., 2011; Pang et al., 2019; Tang et al., 2014b). This is in opposition to TSC, in which patients develop neoplasms in multiple organ systems, including cardiac rhabdomyomas, renal angiomyolipomas, and multiple types of skin lesions. mTORC1 is ubiquitously expressed in eukaryotic cells, so why are the effects of germline heterozygous *DEPDC5* mutations limited to the brain? Lethality in animal models null for *Depdc5* suggests that this gene is essential for embryonic development. For example, in addition to cranial dysmorphology in *Depdc5*$^{-/-}$ mice, Hughes et al. (2017) also described gross defects in vascular patterning. Perhaps *DEPDC5* is essential in other body tissues, but tissue-specific compensatory mechanisms exist such that these tissues are able to tolerate lower levels of *DEPDC5* expression. Linking back to the gene dosage hypothesis, it is possible that certain cell types in the brain may be exquisitely sensitive to small changes in *DEPDC5* expression levels. A recent study identified a novel subpopulation of cells, termed caudal late interneuron progenitor (CLIP) cells, that serve as a common cell of origin for both cortical tubers and subependymal nodules (SENs)/subependymal giant cell astrocytomas (SEGAs) due to TSC1/2 mutations (Eichmüller et al., 2020). CLIP cells were found to have low endogenous levels of TSC1/2, with heterozygous loss of function of *TSC2* leading to a disproportional decrease in TSC2 expression, suggesting that these cells are uniquely susceptible to changes in *TSC1/2* gene dosage. It is possible that an analogous cell population with unique vulnerability to changes in *DEPDC5* gene dosage exists in the brain. Eichmüller *et al*. used single cell analysis of iPSC-derived cortical organoids to identify this novel cell population. With our three validated *DEPDC5*$^{+/-}$ patient iPSC lines, we could use these experiments as a framework to compare proportions of progenitor cell types in *DEPDC5*$^{+/-}$ versus wild-type organoids.

It is also possible that the brain is exceptionally reliant on precise regulation of signaling in response to amino acid levels. While glucose serves as the almost sole fuel for the human brain, amino acids serve an important role in the brain because they are the precursors of neurotransmitters. Upstream mechanisms for arginine and leucine sensing in particular have been identified thus far in the mTORC1 pathway (Chantranupong et al., 2016; Wolfson et al., 2016). As a branched-chain amino acid, leucine plays an important role in regulating synthesis of the excitatory neurotransmitter glutamate (Hutson et al., 2001; Murín and Hamprecht, 2008). Leucine can also be metabolized into ketone bodies, the only possible energy source for the brain aside from glucose (Murín and Hamprecht, 2008). Arginine is a precursor for nitric oxide synthesis, which functions as a retrograde neurotransmitter in addition to having roles in intracellular signaling (Moncada et al., 1989; Picon-Pages et al., 2019). Amino acid sensing thus has unique relevance in the brain. The pathogenic effects of

DEPDC5 mutations during neurodevelopment could be a complex picture that is dependent on maternal nutrient availability to the developing fetal brain. However, defects in nutrient sensing due to *DEPDC5* mutations have not been definitively linked to disease pathogenesis. In **Chapter II**, I showed that neurons heterozygous for *DEPDC5* mutation remained sensitive to near-complete nutrient withdrawal. This is in opposition to complete loss or knockdown of *DEPDC5*, which renders cells insensitive to nutrient starvation (Bar-Peled et al., 2013; Hughes et al., 2017; Iffland et al., 2018; Marsan et al., 2016). It is possible that heterozygous cells remain sensitive to severe nutrient withdrawal (amino acid-free DMEM) but may have defects in sensing deficits in specific amino acids. Further experiments with more nuanced starvation media formulations will aid in determining this, as well as the contribution of any identified defects in nutrient sensing to epileptogenesis.

Finally, it is possible that GATOR1 complex proteins have mTORC1-independent roles that are specific to neurons. For example, RNA sequencing of zebrafish with *Depdc5* knockout identified downregulation of many genes associated with GABAergic networks (Swaminathan et al., 2018). Rapamycin did not rescue subsequently identified defects in GAD65/67-positive interneuron neurofilaments, suggesting that this effect is independent of mTORC1. Thus, GATOR1 complex members may have brain-specific roles outside of mTORC1 modulation, for example in transcriptional regulation. Based on these findings in zebrafish, investigating the consequences of *DEPDC5* mutation in human interneurons would be of value. While we examined neurons from a mixed cortical population in **Chapter II**, with the majority consisting of excitatory neurons, differentiation protocols exist to generate relatively pure population of GABAergic interneurons (Maroof et al., 2013; Nicholas et al., 2013). Preliminary results using the protocol described by Maroof *et al*. to generate *DEPDC5*$^{+/-}$ interneurons demonstrated decreased GAD67 expression, suggesting that development of inhibitory synapses may be impaired in these cultures (**Figure 4-1**). However, further experiments are necessary to confirm these results and to place them in a functional context. A conditional mouse model in which *Depdc5* is knocked out from inhibitory interneurons would also be valuable to determine lineage-specific effects *in vivo*.

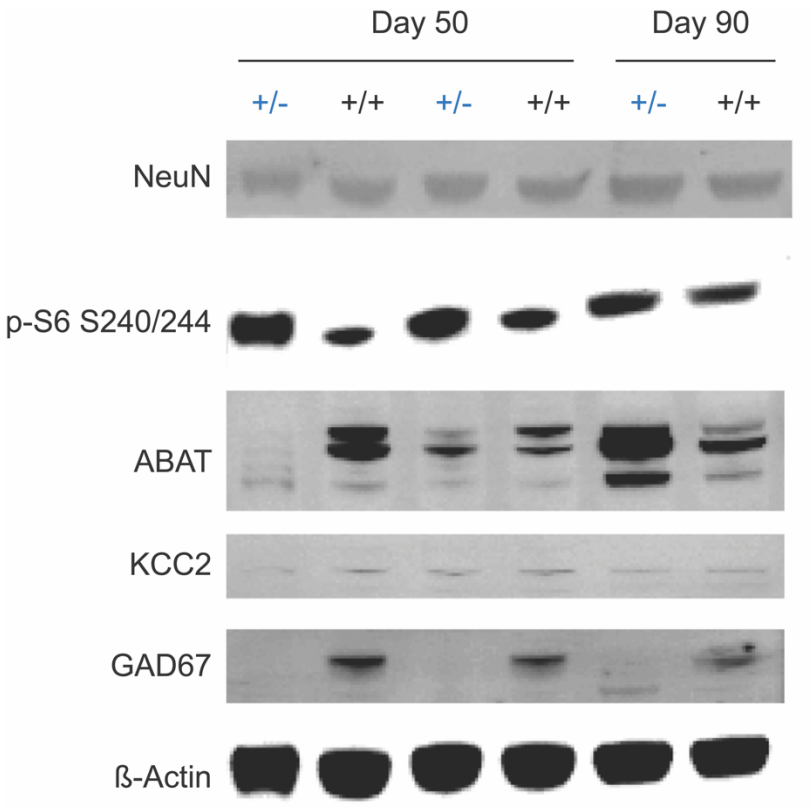

Figure 4-1. Changes in protein expression in GABAergic neurons heterozygous for *DEPDC5* mutation. *DEPDC5*$^{+/-}$ and wild-type GABAergic neuronal lysates were compared at days 50 and 90 of differentiation. Expression levels of p-S6 S240/244 (mTORC1 target), ABAT (GABA transaminase), KCC2 (chloride transporter), and GAD67 (glutamate decarboxylase, enzyme involved in synthesis of GABA) were compared.

Given the increase in genetic screening of epilepsy patients, models to determine the functional consequences of rare or one-off patient variants of unknown significance (VUS) are becoming increasingly important in translational medicine. In **Chapter II**, we studied nonsense *DEPDC5* variants that resulted in premature truncations deleterious to neuronal development, establishing characteristics by which to judge potential pathogenicity of VUS in a human model. Dawson *et al.* recently described a medium-throughput assay that evaluated the ability of patient *DEPDC5* variants transfected into HEK cells to respond to starvation. Variants that were unresponsive to starvation were deemed pathogenic. Only two of the six *DEPDC5* variants tested were deemed pathogenic, F164del and D1556*. The remaining four variants were missense mutations. While certainly more time laborious, corroborating the effects of these six variants in iPSC-derived neurons through the use of CRISPR-Cas9 genomic editing would allow an initial exploration of potential neuronal-specific effects. In combination with the higher-throughput HEK cell based-assay, iPSC-derived neurons could be used to further evaluate patient variants of unknown significance.

Functional evaluation of neurons: alternative differentiation protocols

While our results from Chapter II provide evidence to support an mTORC1 hyperactivation phenotype in *DEPDC5*$^{+/-}$ neurons, our data are not sufficient to make conclusions about how heterozygosity functionally impacts neurons. For this, evaluation of neuronal activity is needed through methods such as whole-cell patch-clamp or multi-well microelectrode array (MEA) recordings. MEAs contain a series of small electrodes that allow the recording of electrical activity from networks of cultured neurons, while whole-cell patch-clamp records from a single neuron at a time. Preliminary data suggests that *DEPDC5*$^{+/-}$ neurons start firing sooner than control neurons after MEA plating (**Figure 4-2**). This could be due to a multitude of reasons, such as accelerated neuronal maturation, enhanced survival following plating, or alterations in excitatory-inhibitory balance. Limitations in our neuronal differentiation protocols precluded a more systematic functional analysis. We used a small molecule-based approach to differentiate neurons from iPSCs. However, drawbacks to small molecule-based protocols exist, including the length of time needed to generate neurons (upwards of several months) as well as the immature quality of neurons generated. When subjected to whole-cell patch-clamp analysis, some neurons do show action potential firing, however when analyzed by multielectrode-array, they do not show robust network bursting. Additionally, without glial cell co-culture, neurons have poor adherence to the surface of the plate, resulting in lifting of cultures after 2-3 weeks on MEA plates and subsequent loss of electrical activity, limiting the ability to longitudinally assess neuronal function during development (**Figure 4-2**). The development of electrically mature neurons is important to be able to appropriately evaluate functional consequences of genetic mutation and can be augmented by several strategies, including co-culture with glial cells and the use of alternative differentiation protocols. Lentiviral-mediated forced expression of target genes, in addition to the inclusion of supportive glial cells in culture, has been shown to generate more electrically mature neurons capable of network bursting activity and represents an ideal strategy going forward (Ho et al., 2016; Zhang et al., 2013). While these protocols can be complex and require considerable optimization, they have the additional benefit of generating electrically mature neurons within weeks, representing a substantial time advantage.

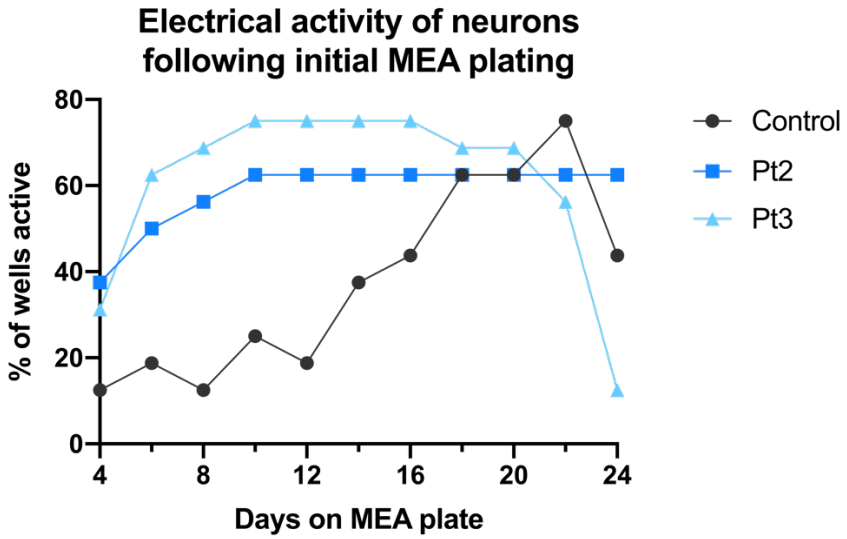

Figure 4-2. Using MEA analysis to assess functional impacts of *DEPDC5* haploinsufficiency.
Neurons from *DEPDC5*$^{+/-}$ patients (Pt2, Pt3) become electrically active more rapidly than control neurons following MEA plating. A decline in number of active wells is evident starting near day 20, corresponding to the time when neurons begin lifting from the wells.

mTORC1 and epileptogenesis: defining specific mechanisms

Accumulating evidence supports a clear role for mTORC1 hyperactivation as causative of disease in *DEPDC5*-related epilepsy. However, the numerous functions regulated by mTORC1 make identification of a clear mechanism challenging. For example, **Chapter II** showed that mTORC1 drives increased neuronal size in *DEPDC5*$^{+/-}$ neurons. Animal models, including our mouse model described in **Chapter III**, demonstrate cortical dyslamination likely due to defects in neuronal migration. As mentioned previously, altered neurite branching, dendritic morphology, or synaptic architecture could also contribute to increased excitability.

A recent report demonstrated synaptic defects in cultured neurons from mice with *Depdc5* knockdown (De Fusco et al., 2020). These defects included increased complexity of dendritic arbors, an increased number of excitatory synapses with a concomitant increase in AMPA receptor expression, and increased frequency of mEPSCs. No changes in mIPSC frequency, the density of inhibitory synapses, or in GABA-β receptor expression were noted. In contrast, our mouse model described in Chapter III displayed reduced mIPSC amplitude and trended toward increased mIPSC frequency. De Fusco *et al*. transduced cultured primary cortical neurons with shRNA to create *Depdc5* knockdown neurons and obtained patch clamp recordings. Our model was a conditional knockout model in which recordings were performed in brain slices,

suggesting two obvious potential differences. First, it is possible that acute knockdown of *Depdc5* has a different effect than mice that developmentally lack *Depdc5*. Additionally, recording from brain slices allows for relative preservation of local circuitry, which may be affected by mTORC1 hyperactivation. Characterization of excitatory properties in brain slices from *Depdc5*^{Emx1} CKO mice is a next step that would be useful for placing the excitatory synaptic changes seen in cultured neurons with *Depdc5* knockdown in the context of the wider brain circuitry. Additionally, iPSC-derived neurons can be used to determine if similar synaptic changes exist in human neurons.

Deficits in lamination and migration are difficult to detect in two-dimensional culture systems, however brain organoids may provide insight. Organoids are three-dimensional, self-organizing collections of cells that can be grown in culture to recapitulate various organs. Brain organoids allow for the complex cytoarchitecture and balance of cell populations in the human brain to be maintained to a better extent than in two-dimensional culture. Because they demonstrate layer patterning, cortical organoids represent an attractive strategy to test how *DEPDC5* mutations may affect lamination in the developing human brain. Organoids can provide snapshots of neurodevelopmental stages and as such their use may also allow for identification of a specific temporal window that is particularly disrupted by *DEPDC5* loss. Organoids represent an especially viable strategy for testing the impacts of a somatic second hit because they can be subjected to single cell targeting/knockout. Indeed, these studies have been done with TSC1/2 mutations (Blair et al., 2018; Eichmüller et al., 2020). One study showed that a second hit mutation in *TSC2* resulted in the development of dysplastic neuron similar to those found in cortical tubers (Blair et al., 2018). Another study found that while some second-hit *TSC2* mutations did develop, they were not essential for the formation of cortical tubers/SENs/SEGAs (Eichmüller et al., 2020). While biallelic inactivation has been identified in several cases of focal cortical dysplasia due to *DEPDC5* mutation, it is hard to imagine that, if a second-hit is absolutely required for the development of FCD, they have only been found in a small subset of patients. Because of this, the dispensable development of biallelic inactivation noted by Eichmüller *et al*. seems an attractive explanation (2020).

A further question is if a second hit in a very small number of cells would be sufficient to cause seizures in a normal brain, or only in a brain that is already experiencing a state of pathologic heterozygosity. For example, it is possible that the differences in passive membrane properties that exist in cytomegalic heterozygous neurons are more permissive for

seizure propagation (De Fusco et al., 2020). MEA experiments with co-cultured homozygous and heterozygous neurons would be useful to determine this. For example, a small amount of fluorescently-labeled *DEPDC5*$^{-/-}$ neurons could be plated on a heterozygous or wild-type background and the effects on network bursting could be evaluated.

The development of a set of isogenic lines would be useful for these purposes. An isogenic control line would also enable us to be more certain that the findings in **Chapter II** are definitively caused by *DEPDC5* mutation. Our preliminary data shows that correcting the 2620C>T mutation in the Patient1 *DEPDC5*$^{+/-}$ line restores wild-type levels of mRNA expression (**Figure 4-3**). The next steps in evaluating this line include validating the cell size phenotypes we described in Chapter II. This line can then be used for further experiments. Combination with an isogenic knockout (-/-) would be most useful.

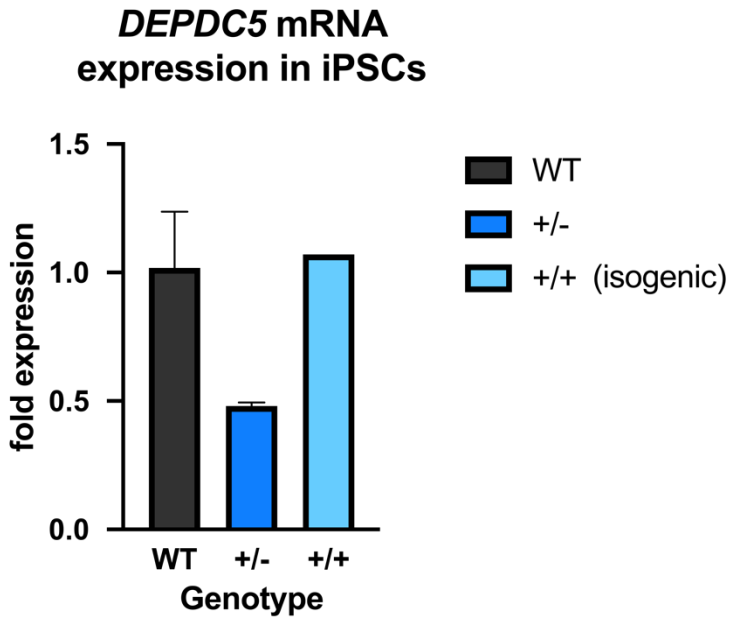

Figure 4-3. Correction of the 2620C>T mutation in iPSCs restores wild-type levels of DEPDC5 mRNA expression. Number of clones: WT, n=4; *DEPDC5*$^{+/-}$, n=2; *DEPDC5*$^{+/+}$ isogenic control, n=1. Bar represents an average of n=3 technical replicates from a single experiment.

Contribution of glial cells to epileptogenesis

Evidence is accumulating to support the role of astrocytes not only as the "support cells" of the brain, but as key participants in crucial roles including the functional activity of the brain (de Lanerolle et al., 2010). For example, astrocytes are important in ion homeostasis, particularly in redistributing extracellular potassium following neuronal firing (Coulter and Steinhäuser, 2015). Yuskaitis *et al*. showed evidence of reactive astrogliosis in a mouse model with conditional knockout of *Depdc5* restricted to neurons and there is additional evidence that neuronal mTORC1 activity regulates the nonreactive state of astrocytes (Yuskaitis et al., 2018; Zhang et al., 2017). It thus seems likely that neuronal loss of *Depdc5* can affect astrocytes, but it is unknown if the effect is reciprocal. The mouse model described in **Chapter III** targets astrocytes for conditional knockout of *Depdc5* in additional to cortical projection neurons, allowing for evaluation of the potential contribution of astrocytes to disease pathogenesis.

Initial immunofluorescence studies did not note expression of *Depdc5* in astrocytes, however co-localization via immunofluorescence may not be the most robust method of determining expression, especially given the poor quality of available DEPDC5 antibodies. Our RT-PCR data suggest that *Depdc5* is expressed in mouse astrocytes, however we were unable to confirm this by immunofluorescence because of this lack available specific Depdc5 antibodies. It is possible that the *Depdc5* expression we noted through the RT-PCR experiments represents *Depdc5* expressed by non-astrocytic cell types, however very few neurons should be present after the shaking protocols used to generate astrocyte cultures.

Because the mTOR signaling pathway is ubiquitously expressed in eukaryotic cells, it would be surprisingly if *DEPDC5* were not expressed in astrocytes. However, if Depdc5 is indeed not expressed in astrocytes, this raises the possibility of a unique amino-acid sensing pathway in astrocytes, since it is presumably still an essential cell function. On a related note, the lysosomal amino acid sensor upstream of mTORC1, SLC38A9, was not found to be present in astrocytes, suggesting there is a precedence for the possibility of cell-type specific pathways (Hellsten et al., 2017). While astrocytes express unique additional solute carriers (SLCs), there is not evidence that they express other unique components upstream of mTORC1, for example the Rag GTPases. This remains an area for further investigation. Protocols also exist to derive astrocytes from iPSCs, representing another potential avenue of study.

Overall, the development of a specific DEPDC5 antibody will be critical going forward. While several reports have published results using a commercially available antibody, we have not found this antibody to be appropriately specific in our hands. Pursuing independent antibody development is certainly a possibility. Other workarounds exist, for example engineering a fluorescently-tagged DEPDC5. This would allow us to conclude definitely whether *DEPDC5* is present in astrocytes, as well as potentially compare levels of expression in neuronal subpopulations.

Therapeutic use of mTOR inhibitors for epilepsy patients

Because patients with mutations in GATOR1 components have a high rate of drug-resistant epilepsy, the development of new therapeutic strategies remains essential. **Chapter II** showed evidence that rapamycin treatment during early neuronal development can rescue the phenotype of neuronal cytomegaly. However, many questions still remain. As mentioned above, it will be first necessary to determine if neuronal cytomegaly is indeed linked to functional changes, then to determine if rescuing cytomegaly relieves these functional changes.

Chapter III showed that treating CKO mice with rapamycin during the window from P12-P30 was sufficient to prolong life and prevent seizures. Only one CKO mouse (5%, 1/20) treated with rapamycin had an observed seizure, compared to 25% (8/32) of vehicle-treated mice. Treatment was effective even though CKO mice displayed evidence of cortical dyslamination and increased cortical thickness by P5, suggesting that even if DEPDC5 loss has developmental consequences, postnatal mTORC1 inhibition may be effective for seizure prevention. In a zebrafish *Depdc5* knockout model, continuous rapamycin treatment was required to prolong survival; if treatment was withdrawn, animals died (Swaminathan et al., 2018). Thus, despite the 40-day durability of rapamycin treatment for a time in our mouse model, it is possible that long-term treatment may be needed to suppress seizures. Indeed, while mice were alive and seizure-free after 40 days of rapamycin withdrawal, by sacrifice at P70, CKO mice did demonstrate an increased brain weight, suggesting the reemergence of an mTORC1 hyperactivation phenotype. In patients with TSC, once rapamycin treatment is discontinued, tumors begin to grow again, suggesting that continuous mTORC1 inhibition is needed to suppress the effects of mutant cells.

Unfortunately, long-term rapamycin has potential consequences, including metabolic derangements such as insulin resistance, potentially because chronic rapamycin can affect mTORC2 (Krueger et al., 2013; Lamming et al., 2012). In mice, long-term rapamycin treatment impaired sleep duration and measures of social interaction and cognitive function (Lu et al., 2015; Saré et al., 2017). Interestingly, mice treated with a sub-therapeutic dose of rapamycin ($1/1000^{th}$ of the treatment dose of 6 mg/kg) still had a minor survival benefit, with 4/16 mice surviving past P30. Because rapamycin is such a potent mTORC1 inhibitor, it is possible that chronic treatment may be accomplished with low doses in order to limit side effects. Doses as low as 0.1 mg/kg show a 50% decrease in p-S6 but a more favorable side-effect profile (Lu et al., 2015). The extent of mTORC1 inhibition necessary for a treatment effect needs to be determined.

Conclusion

Overall, iPSC-derived neurons and cortical organoids provide a unique milieu in which to study the impact of genetic alterations on neurobiology and disease pathogenesis in the human brain. Because species-specific variations exist, human models are most appropriate for determining the contribution of *DEPDC5* haploinsufficiency to disease pathogenesis. Future directions should focus on determining the functional contributions of various phenotypes induced by mTORC1 hyperactivation due to loss of *DEPDC5*.

REFERENCES

Abou-Saleh, H., Zouein, F.A., El-Yazbi, A., Sanoudou, D., Raynaud, C., Rao, C., Pintus, G., Dehaini, H., and Eid, A.H. (2018). The march of pluripotent stem cells in cardiovascular regenerative medicine. Stem Cell Res Ther *9*, 201.

Armour, E.A., Carson, R.P., and Ess, K.C. (2012). Cystogenesis and elongated primary cilia in Tsc1-deficient distal convoluted tubules. Am J Physiol Renal Physiol *303*, F584-592.

Armstrong, L.C., Westlake, G., Snow, J.P., Cawthon, B., Armour, E., Bowman, A.B., and Ess, K.C. (2017). Heterozygous loss of TSC2 alters p53 signaling and human stem cell reprogramming. Hum Mol Genet *26*, 4629-4641.

Bagnall, R.D., Crompton, D.E., Petrovski, S., Lam, L., Cutmore, C., Garry, S.I., Sadleir, L.G., Dibbens, L.M., Cairns, A., Kivity, S.*, et al.* (2016). Exome-based analysis of cardiac arrhythmia, respiratory control, and epilepsy genes in sudden unexpected death in epilepsy. Ann Neurol *79*, 522-534.

Bagnall, R.D., Crompton, D.E., and Semsarian, C. (2017). Genetic Basis of Sudden Unexpected Death in Epilepsy. Front Neurol *8*, 348.

Baldassari, S., Licchetta, L., Tinuper, P., Bisulli, F., and Pippucci, T. (2016). GATOR1 complex: the common genetic actor in focal epilepsies. J Med Genet *53*, 503-510.

Baldassari, S., Picard, F., Verbeek, N.E., van Kempen, M., Brilstra, E.H., Lesca, G., Conti, V., Guerrini, R., Bisulli, F., Licchetta, L.*, et al.* (2019a). The landscape of epilepsy-related GATOR1 variants. Genet Med *21*, 398-408.

Baldassari, S., Ribierre, T., Marsan, E., Adle-Biassette, H., Ferrand-Sorbets, S., Bulteau, C., Dorison, N., Fohlen, M., Polivka, M., Weckhuysen, S.*, et al.* (2019b). Dissecting the genetic basis of focal cortical dysplasia: a large cohort study. Acta Neuropathol *138*, 885-900.

Bar-Peled, L., Chantranupong, L., Cherniack, A.D., Chen, W.W., Ottina, K.A., Grabiner, B.C., Spear, E.D., Carter, S.L., Meyerson, M., and Sabatini, D.M. (2013). A Tumor suppressor complex with GAP activity for the Rag GTPases that signal amino acid sufficiency to mTORC1. Science *340*, 1100-1106.

Bar-Peled, L., Schweitzer, L.D., Zoncu, R., and Sabatini, D.M. (2012). Ragulator is a GEF for the rag GTPases that signal amino acid levels to mTORC1. Cell *150*, 1196-1208.

Baulac, S. (2016). mTOR signaling pathway genes in focal epilepsies. Prog Brain Res *226*, 61-79.

Baulac, S., Ishida, S., Marsan, E., Miquel, C., Biraben, A., Nguyen, D.K., Nordli, D., Cossette, P., Nguyen, S., Lambrecq, V.*, et al.* (2015). Familial focal epilepsy with focal cortical dysplasia due to DEPDC5 mutations. Ann Neurol *77*, 675-683.

Beenhakker, M.P., and Huguenard, J.R. (2009). Neurons that fire together also conspire together: is normal sleep circuitry hijacked to generate epilepsy? Neuron *62*, 612-632.

Beevers, J.E., Caffrey, T.M., and Wade-Martins, R. (2013). Induced pluripotent stem cell (iPSC)-derived dopaminergic models of Parkinson's disease. Biochem Soc Trans *41*, 1503-1508.

Beretta, L., Gingras, A.C., Svitkin, Y.V., Hall, M.N., and Sonenberg, N. (1996). Rapamycin blocks the phosphorylation of 4E-BP1 and inhibits cap-dependent initiation of translation. Embo j *15*, 658-664.

Berkovic, S.F., Serratosa, J.M., Phillips, H.A., Xiong, L., Andermann, E., Diaz-Otero, F., Gomez-Garre, P., Martin, M., Fernandez-Bullido, Y., Andermann, F.*, et al.* (2004). Familial partial epilepsy with variable foci: clinical features and linkage to chromosome 22q12. Epilepsia *45*, 1054-1060.

Bi, W., Glass, I.A., Muzny, D.M., Gibbs, R.A., Eng, C.M., Yang, Y., and Sun, A. (2016). Whole exome sequencing identifies the first STRADA point mutation in a patient with polyhydramnios, megalencephaly, and symptomatic epilepsy syndrome (PMSE). Am J Med Genet A *170*, 2181-2185.

Bisulli, F., Licchetta, L., Baldassari, S., Pippucci, T., and Tinuper, P. (2016). DEPDC5 mutations in epilepsy with auditory features. Epilepsia *57*, 335.

Blair, J.D., Hockemeyer, D., and Bateup, H.S. (2018). Genetically engineered human cortical spheroid models of tuberous sclerosis. Nat Med *24*, 1568-1578.

Bozzi, Y., Casarosa, S., and Caleo, M. (2012). Epilepsy as a Neurodevelopmental Disorder. Frontiers in Psychiatry *3*.

Brodie, M.J. (2010). Antiepileptic drug therapy the story so far. Seizure *19*, 650-655.

Buchmann, I., Milakofsky, L., Harris, N., Hofford, J.M., and Vogel, W.H. (1996). Effect of arginine administration on plasma and brain levels of arginine and various related amino compounds in the rat. Pharmacology *53*, 133-142.

Burger, B.J., Rose, S., Bennuri, S.C., Gill, P.S., Tippett, M.L., Delhey, L., Melnyk, S., and Frye, R.E. (2017). Autistic Siblings with Novel Mutations in Two Different Genes: Insight for Genetic Workups of Autistic Siblings and Connection to Mitochondrial Dysfunction. Front Pediatr *5*, 219.

Cagnetta, R., Frese, C.K., Shigeoka, T., Krijgsveld, J., and Holt, C.E. (2018). Rapid Cue-Specific Remodeling of the Nascent Axonal Proteome. Neuron *99*, 29-46.e24.

Carson, R.P., Kelm, N.D., West, K.L., Does, M.D., Fu, C., Weaver, G., McBrier, E., Parker, B., Grier, M.D., and Ess, K.C. (2015). Hypomyelination following deletion of Tsc2 in oligodendrocyte precursors. Ann Clin Transl Neurol *2*, 1041-1054.

Carson, R.P., Van Nielen, D.L., Winzenburger, P.A., and Ess, K.C. (2012). Neuronal and glia abnormalities in Tsc1-deficient forebrain and partial rescue by rapamycin. Neurobiol Dis *45*, 369-380.

Carvill, G.L., Crompton, D.E., Regan, B.M., McMahon, J.M., Saykally, J., Zemel, M., Schneider, A.L., Dibbens, L., Howell, K.B., Mandelstam, S.*, et al.* (2015). Epileptic spasms are a feature of DEPDC5 mTORopathy. Neurol Genet *1*, e17.

Chambers, S.M., Fasano, C.A., Papapetrou, E.P., Tomishima, M., Sadelain, M., and Studer, L. (2009). Highly efficient neural conversion of human ES and iPS cells by dual inhibition of SMAD signaling. Nat Biotechnol *27*, 275-280.

Chantranupong, L., Scaria, S.M., Saxton, R.A., Gygi, M.P., Shen, K., Wyant, G.A., Wang, T., Harper, J.W., Gygi, S.P., and Sabatini, D.M. (2016). The CASTOR Proteins Are Arginine Sensors for the mTORC1 Pathway. Cell *165*, 153-164.

Chantranupong, L., Wolfson, R.L., Orozco, J.M., Saxton, R.A., Scaria, S.M., Bar-Peled, L., Spooner, E., Isasa, M., Gygi, S.P., and Sabatini, D.M. (2014). The Sestrins interact with GATOR2 to negatively regulate the amino-acid-sensing pathway upstream of mTORC1. Cell Rep *9*, 1-8.

Chen, J., Ou, Y., Yang, Y., Li, W., Xu, Y., Xie, Y., and Liu, Y. (2018). KLHL22 activates amino-acid-dependent mTORC1 signalling to promote tumorigenesis and ageing. Nature *557*, 585-589.

Chung, J., Kuo, C.J., Crabtree, G.R., and Blenis, J. (1992). Rapamycin-FKBP specifically blocks growth-dependent activation of and signaling by the 70 kd S6 protein kinases. Cell *69*, 1227-1236.

Consonni, S.V., Maurice, M.M., and Bos, J.L. (2014). DEP domains: structurally similar but functionally different. Nat Rev Mol Cell Biol *15*, 357-362.

Coulter, D.A., and Steinhäuser, C. (2015). Role of astrocytes in epilepsy. Cold Spring Harb Perspect Med *5*, a022434.

D'Andrea Meira, I., Romão, T.T., Pires do Prado, H.J., Krüger, L.T., Pires, M.E.P., and da Conceição, P.O. (2019). Ketogenic Diet and Epilepsy: What We Know So Far. Front Neurosci *13*, 5-5.

D'Arcangelo, G. (2006). Reelin mouse mutants as models of cortical development disorders. Epilepsy Behav *8*, 81-90.

D'Gama, A.M., Geng, Y., Couto, J.A., Martin, B., Boyle, E.A., LaCoursiere, C.M., Hossain, A., Hatem, N.E., Barry, B.J., Kwiatkowski, D.J., *et al.* (2015). Mammalian target of rapamycin pathway mutations cause hemimegalencephaly and focal cortical dysplasia. Ann Neurol *77*, 720-725.

D'Gama, A.M., Woodworth, M.B., Hossain, A.A., Bizzotto, S., Hatem, N.E., LaCoursiere, C.M., Najm, I., Ying, Z., Yang, E., Barkovich, A.J., *et al.* (2017). Somatic Mutations Activating the mTOR Pathway in Dorsal Telencephalic Progenitors Cause a Continuum of Cortical Dysplasias. Cell Rep *21*, 3754-3766.

Daumke, O., Weyand, M., Chakrabarti, P.P., Vetter, I.R., and Wittinghofer, A. (2004). The GTPase-activating protein Rap1GAP uses a catalytic asparagine. Nature *429*, 197-201.

Dawson, R.E., Nieto Guil, A.F., Robertson, L.J., Piltz, S.G., Hughes, J.N., and Thomas, P.Q. (2020). Functional screening of GATOR1 complex variants reveals a role for mTORC1 deregulation in FCD and focal epilepsy. Neurobiol Dis *134*, 104640.

de Calbiac, H., Dabacan, A., Marsan, E., Tostivint, H., Devienne, G., Ishida, S., Leguern, E., Baulac, S., Muresan, R.C., Kabashi, E., *et al.* (2018). Depdc5 knockdown causes mTOR-dependent motor hyperactivity in zebrafish. Ann Clin Transl Neurol *5*, 510-523.

De Fusco, A., Cerullo, M.S., Marte, A., Michetti, C., Romei, A., Castroflorio, E., Baulac, S., and Benfenati, F. (2020). Acute knockdown of Depdc5 leads to synaptic defects in mTOR-related epileptogenesis. Neurobiol Dis *139*, 104822.

de Lanerolle, N.C., Lee, T.S., and Spencer, D.D. (2010). Astrocytes and epilepsy. Neurotherapeutics *7*, 424-438.

Dehmelt, L., and Halpain, S. (2005). The MAP2/Tau family of microtubule-associated proteins. Genome Biol *6*, 204.

Dibbens, L.M., de Vries, B., Donatello, S., Heron, S.E., Hodgson, B.L., Chintawar, S., Crompton, D.E., Hughes, J.N., Bellows, S.T., Klein, K.M., *et al.* (2013). Mutations in DEPDC5 cause familial focal epilepsy with variable foci. Nat Genet *45*, 546-551.

Dutchak, P.A., Laxman, S., Estill, S.J., Wang, C., Wang, Y., Wang, Y., Bulut, G.B., Gao, J., Huang, L.J., and Tu, B.P. (2015). Regulation of Hematopoiesis and Methionine Homeostasis by mTORC1 Inhibitor NPRL2. Cell Rep *12*, 371-379.

Ebrahimi-Fakhari, D., Wahlster, L., Hoffmann, G.F., and Kolker, S. (2014). Emerging role of autophagy in pediatric neurodegenerative and neurometabolic diseases. Pediatr Res *75*, 217-226.

Eichmüller, O.L., Corsini, N.S., Vértesy, Á., Scholl, T., Gruber, V.-E., Peer, A.M., Chu, J., Novatchkova, M., Paredes, M.F., Feucht, M., *et al.* (2020). Cerebral organoid model reveals excessive proliferation of human caudal late interneuron progenitors in Tuberous Sclerosis Complex. bioRxiv, 2020.2002.2027.967802.

Ellenbroek, B., and Youn, J. (2016). Rodent models in neuroscience research: is it a rat race? Dis Model Mech *9*, 1079-1087.

Evans, M.J., and Kaufman, M.H. (1981). Establishment in culture of pluripotential cells from mouse embryos. Nature *292*, 154-156.

Feldman, M.E., Apsel, B., Uotila, A., Loewith, R., Knight, Z.A., Ruggero, D., and Shokat, K.M. (2009). Active-site inhibitors of mTOR target rapamycin-resistant outputs of mTORC1 and mTORC2. PLoS Biol *7*, e38.

Fernández, V., Llinares-Benadero, C., and Borrell, V. (2016). Cerebral cortex expansion and folding: what have we learned? The EMBO Journal *35*, 1021-1044.

Fidyk, N.J., and Cerione, R.A. (2002). Understanding the catalytic mechanism of GTPase-activating proteins: demonstration of the importance of switch domain stabilization in the stimulation of GTP hydrolysis. Biochemistry *41*, 15644-15653.

Fingar, D.C., Salama, S., Tsou, C., Harlow, E., and Blenis, J. (2002). Mammalian cell size is controlled by mTOR and its downstream targets S6K1 and 4EBP1/eIF4E. Genes & development *16*, 1472-1487.

Fisher, R.S., Acevedo, C., Arzimanoglou, A., Bogacz, A., Cross, J.H., Elger, C.E., Engel, J., Jr., Forsgren, L., French, J.A., Glynn, M.*, et al.* (2014). ILAE official report: a practical clinical definition of epilepsy. Epilepsia *55*, 475-482.

Fisher, R.S., Cross, J.H., French, J.A., Higurashi, N., Hirsch, E., Jansen, F.E., Lagae, L., Moshe, S.L., Peltola, J., Roulet Perez, E.*, et al.* (2017). Operational classification of seizure types by the International League Against Epilepsy: Position Paper of the ILAE Commission for Classification and Terminology. Epilepsia *58*, 522-530.

Frankel, W.N., Taylor, L., Beyer, B., Tempel, B.L., and White, H.S. (2001). Electroconvulsive Thresholds of Inbred Mouse Strains. Genomics *74*, 306-312.

Fukata, Y., Yokoi, N., Miyazaki, Y., and Fukata, M. (2017). The LGI1-ADAM22 protein complex in synaptic transmission and synaptic disorders. Neurosci Res *116*, 39-45.

Gai, Z., Wang, Q., Yang, C., Wang, L., Deng, W., and Wu, G. (2016). Structural mechanism for the arginine sensing and regulation of CASTOR1 in the mTORC1 signaling pathway. Cell Discov *2*, 16051.

Galluzzi, L., Baehrecke, E.H., Ballabio, A., Boya, P., Bravo-San Pedro, J.M., Cecconi, F., Choi, A.M., Chu, C.T., Codogno, P., Colombo, M.I.*, et al.* (2017). Molecular definitions of autophagy and related processes. Embo j *36*, 1811-1836.

Ganley, I.G., Lam du, H., Wang, J., Ding, X., Chen, S., and Jiang, X. (2009). ULK1.ATG13.FIP200 complex mediates mTOR signaling and is essential for autophagy. J Biol Chem *284*, 12297-12305.

Gao, Y., Wang, J., and Fan, G. (2012). NPRL2 is an independent prognostic factor of osteosarcoma. Cancer Biomark *12*, 31-36.

Gaubitz, C., Prouteau, M., Kusmider, B., and Loewith, R. (2016). TORC2 Structure and Function. Trends in Biochemical Sciences *41*, 532-545.

Goldberg, E.M., and Coulter, D.A. (2013). Mechanisms of epileptogenesis: a convergence on neural circuit dysfunction. Nat Rev Neurosci *14*, 337-349.

Gorski, J.A., Talley, T., Qiu, M., Puelles, L., Rubenstein, J.L., and Jones, K.R. (2002). Cortical excitatory neurons and glia, but not GABAergic neurons, are produced in the Emx1-expressing lineage. J Neurosci *22*, 6309-6314.

Gu, X., Orozco, J.M., Saxton, R.A., Condon, K.J., Liu, G.Y., Krawczyk, P.A., Scaria, S.M., Harper, J.W., Gygi, S.P., and Sabatini, D.M. (2017). SAMTOR is an S-adenosylmethionine sensor for the mTORC1 pathway. Science *358*, 813-818.

Guerrini, R., and Parrini, E. (2010). Neuronal migration disorders. Neurobiol Dis *38*, 154-166.

Gupta, S., Ryvlin, P., Faught, E., Tsong, W., and Kwan, P. (2017). Understanding the burden of focal epilepsy as a function of seizure frequency in the United States, Europe, and Brazil. Epilepsia Open *2*, 199-213.

Hara, K., Maruki, Y., Long, X., Yoshino, K., Oshiro, N., Hidayat, S., Tokunaga, C., Avruch, J., and Yonezawa, K. (2002). Raptor, a binding partner of target of rapamycin (TOR), mediates TOR action. Cell *110*, 177-189.

Harrington, L.S., Findlay, G.M., Gray, A., Tolkacheva, T., Wigfield, S., Rebholz, H., Barnett, J., Leslie, N.R., Cheng, S., Shepherd, P.R.*, et al.* (2004). The TSC1-2 tumor suppressor controls insulin-PI3K signaling via regulation of IRS proteins. J Cell Biol *166*, 213-223.

Hellsten, S.V., Eriksson, M.M., Lekholm, E., Arapi, V., Perland, E., and Fredriksson, R. (2017). The gene expression of the neuronal protein, SLC38A9, changes in mouse brain after in vivo starvation and high-fat diet. PLoS One *12*, e0172917.

Hino, O., and Kobayashi, T. (2017). Mourning Dr. Alfred G. Knudson: the two-hit hypothesis, tumor suppressor genes, and the tuberous sclerosis complex. Cancer Sci *108*, 5-11.

Ho, S.M., Hartley, B.J., Tcw, J., Beaumont, M., Stafford, K., Slesinger, P.A., and Brennand, K.J. (2016). Rapid Ngn2-induction of excitatory neurons from hiPSC-derived neural progenitor cells. Methods *101*, 113-124.

Hosokawa, N., Sasaki, T., Iemura, S., Natsume, T., Hara, T., and Mizushima, N. (2009). Atg101, a novel mammalian autophagy protein interacting with Atg13. Autophagy *5*, 973-979.

Hsu, P.P., Kang, S.A., Rameseder, J., Zhang, Y., Ottina, K.A., Lim, D., Peterson, T.R., Choi, Y., Gray, N.S., Yaffe, M.B.*, et al.* (2011). The mTOR-regulated phosphoproteome reveals a mechanism of mTORC1-mediated inhibition of growth factor signaling. Science *332*, 1317-1322.

Hu, S., Knowlton, R.C., Watson, B.O., Glanowska, K.M., Murphy, G.G., Parent, J.M., and Wang, Y. (2018). Somatic Depdc5 deletion recapitulates electroclinical features of human focal cortical dysplasia type IIA. Ann Neurol *84*, 140-146.

Huang, N., Cheng, S., Mi, X., Tian, Q., Huang, Q., Wang, F., Xu, Z., Xie, Z., Chen, J., and Cheng, Y. (2016). Downregulation of nitrogen permease regulator like-2 activates PDK1-AKT1 and contributes to the malignant growth of glioma cells. Mol Carcinog *55*, 1613-1626.

Hughes, J., Dawson, R., Tea, M., McAninch, D., Piltz, S., Jackson, D., Stewart, L., Ricos, M.G., Dibbens, L.M., Harvey, N.L.*, et al.* (2017). Knockout of the epilepsy gene Depdc5 in mice causes severe embryonic dysmorphology with hyperactivity of mTORC1 signalling. Sci Rep *7*, 12618.

Hutson, S.M., Lieth, E., and LaNoue, K.F. (2001). Function of Leucine in Excitatory Neurotransmitter Metabolism in the Central Nervous System. The Journal of Nutrition *131*, 846S-850S.

Iffland, P.H., 2nd, Baybis, M., Barnes, A.E., Leventer, R.J., Lockhart, P.J., and Crino, P.B. (2018). DEPDC5 and NPRL3 modulate cell size, filopodial outgrowth, and localization of mTOR in neural progenitor cells and neurons. Neurobiol Dis *114*, 184-193.

Inoki, K., Li, Y., Zhu, T., Wu, J., and Guan, K.L. (2002). TSC2 is phosphorylated and inhibited by Akt and suppresses mTOR signalling. Nat Cell Biol *4*, 648-657.

Inoue, Y., Nemoto, Y., Murata, R., Tashiro, T., Shakudo, M., Kohno, K., Matsuoka, O., and Mochizuki, K. (1998). CT and MR imaging of cerebral tuberous sclerosis. Brain Dev *20*, 209-221.

Irish, J.M., Myklebust, J.H., Alizadeh, A.A., Houot, R., Sharman, J.P., Czerwinski, D.K., Nolan, G.P., and Levy, R. (2010). B-cell signaling networks reveal a negative prognostic human lymphoma cell subset that emerges during tumor progression. Proc Natl Acad Sci U S A *107*, 12747-12754.

Ishida, S., Picard, F., Rudolf, G., Noe, E., Achaz, G., Thomas, P., Genton, P., Mundwiller, E., Wolff, M., Marescaux, C.*, et al.* (2013). Mutations of DEPDC5 cause autosomal dominant focal epilepsies. Nat Genet *45*, 552-555.

Jacinto, E., Loewith, R., Schmidt, A., Lin, S., Ruegg, M.A., Hall, A., and Hall, M.N. (2004). Mammalian TOR complex 2 controls the actin cytoskeleton and is rapamycin insensitive. Nat Cell Biol *6*, 1122-1128.

Jaworski, J., Spangler, S., Seeburg, D.P., Hoogenraad, C.C., and Sheng, M. (2005). Control of dendritic arborization by the phosphoinositide-3'-kinase-Akt-mammalian target of rapamycin pathway. J Neurosci *25*, 11300-11312.

Jozwiak, J., Jozwiak, S., and Wlodarski, P. (2008). Possible mechanisms of disease development in tuberous sclerosis. Lancet Oncol *9*, 73-79.

Jung, C.H., Jun, C.B., Ro, S.H., Kim, Y.M., Otto, N.M., Cao, J., Kundu, M., and Kim, D.H. (2009). ULK-Atg13-FIP200 complexes mediate mTOR signaling to the autophagy machinery. Mol Biol Cell *20*, 1992-2003.

Kang, J.Q., Shen, W., Zhou, C., Xu, D., and Macdonald, R.L. (2015). The human epilepsy mutation GABRG2(Q390X) causes chronic subunit accumulation and neurodegeneration. Nat Neurosci *18*, 988-996.

Kang, S.A., Pacold, M.E., Cervantes, C.L., Lim, D., Lou, H.J., Ottina, K., Gray, N.S., Turk, B.E., Yaffe, M.B., and Sabatini, D.M. (2013). mTORC1 phosphorylation sites encode their sensitivity to starvation and rapamycin. Science *341*, 1236566.

Kassai, H., Sugaya, Y., Noda, S., Nakao, K., Maeda, T., Kano, M., and Aiba, A. (2014). Selective activation of mTORC1 signaling recapitulates microcephaly, tuberous sclerosis, and neurodegenerative diseases. Cell Rep *7*, 1626-1639.

Kim, D.H., Sarbassov, D.D., Ali, S.M., King, J.E., Latek, R.R., Erdjument-Bromage, H., Tempst, P., and Sabatini, D.M. (2002). mTOR interacts with raptor to form a nutrient-sensitive complex that signals to the cell growth machinery. Cell *110*, 163-175.

Kim, J.S., Ro, S.H., Kim, M., Park, H.W., Semple, I.A., Park, H., Cho, U.S., Wang, W., Guan, K.L., Karin, M.*, et al.* (2015). Sestrin2 inhibits mTORC1 through modulation of GATOR complexes. Sci Rep *5*, 9502.

Klein, K.M., O'Brien, T.J., Praveen, K., Heron, S.E., Mulley, J.C., Foote, S., Berkovic, S.F., and Scheffer, I.E. (2012). Familial focal epilepsy with variable foci mapped to chromosome 22q12: expansion of the phenotypic spectrum. Epilepsia *53*, e151-155.

Korenke, G.C., Eggert, M., Thiele, H., Nurnberg, P., Sander, T., and Steinlein, O.K. (2016). Nocturnal frontal lobe epilepsy caused by a mutation in the GATOR1 complex gene NPRL3. Epilepsia *57*, e60-63.

Kotecha, N., Krutzik, P.O., and Irish, J.M. (2010). Web-based analysis and publication of flow cytometry experiments. Curr Protoc Cytom *Chapter 10*, Unit10.17.

Kowalczyk, M.S., Hughes, J.R., Babbs, C., Sanchez-Pulido, L., Szumska, D., Sharpe, J.A., Sloane-Stanley, J.A., Morriss-Kay, G.M., Smoot, L.B., Roberts, A.E.*, et al.* (2012). Nprl3 is required for normal development of the cardiovascular system. Mamm Genome *23*, 404-415.

Krueger, D.A., Wilfong, A.A., Holland-Bouley, K., Anderson, A.E., Agricola, K., Tudor, C., Mays, M., Lopez, C.M., Kim, M.O., and Franz, D.N. (2013). Everolimus treatment of refractory epilepsy in tuberous sclerosis complex. Ann Neurol *74*, 679-687.

Kuang, L., Hashimoto, K., Huang, E.J., Gentry, M.S., and Zhu, H. (2020). Frontotemporal dementia non-sense mutation of progranulin rescued by aminoglycosides. Hum Mol Genet *29*, 624-634.

Kwon, C.-H., Luikart, B.W., Powell, C.M., Zhou, J., Matheny, S.A., Zhang, W., Li, Y., Baker, S.J., and Parada, L.F. (2006). Pten Regulates Neuronal Arborization and Social Interaction in Mice. *50*, 377-388.

Lakhani, R., Vogel, K.R., Till, A., Liu, J., Burnett, S.F., Gibson, K.M., and Subramani, S. (2014). Defects in GABA metabolism affect selective autophagy pathways and are alleviated by mTOR inhibition. EMBO Mol Med *6*, 551-566.

Lal, D., Reinthaler, E.M., Schubert, J., Muhle, H., Riesch, E., Kluger, G., Jabbari, K., Kawalia, A., Baumel, C., Holthausen, H.*, et al.* (2014). DEPDC5 mutations in genetic focal epilepsies of childhood. Ann Neurol *75*, 788-792.

Lamming, D.W., Ye, L., Katajisto, P., Goncalves, M.D., Saitoh, M., Stevens, D.M., Davis, J.G., Salmon, A.B., Richardson, A., Ahima, R.S.*, et al.* (2012). Rapamycin-induced insulin resistance is mediated by mTORC2 loss and uncoupled from longevity. Science *335*, 1638-1643.

Landfeldt, E., Sejersen, T., and Tulinius, M. (2019). A mini-review and implementation model for using ataluren to treat nonsense mutation Duchenne muscular dystrophy. Acta Paediatr *108*, 224-230.

Laplante, M., and Sabatini, D.M. (2009). An emerging role of mTOR in lipid biosynthesis. Curr Biol *19*, R1046-1052.

Laplante, M., and Sabatini, D.M. (2012). mTOR signaling in growth control and disease. Cell *149*, 274-293.

Lechuga, L., and Franz, D.N. (2019). Everolimus as adjunctive therapy for tuberous sclerosis complex-associated partial-onset seizures. Expert Rev Neurother *19*, 913-925.

Lee, W.S., Stephenson, S.E.M., Howell, K.B., Pope, K., Gillies, G., Wray, A., Maixner, W., Mandelstam, S.A., Berkovic, S.F., Scheffer, I.E*., et al.* (2019). Second-hit DEPDC5 mutation is limited to dysmorphic neurons in cortical dysplasia type IIA. Ann Clin Transl Neurol *6*, 1338-1344.

Li, Y., Cao, J., Chen, M., Li, J., Sun, Y., Zhang, Y., Zhu, Y., Wang, L., and Zhang, C. (2017). Abnormal Neural Progenitor Cells Differentiated from Induced Pluripotent Stem Cells Partially Mimicked Development of TSC2 Neurological Abnormalities. Stem Cell Reports *8*, 883-893.

LiCausi, F., and Hartman, N.W. (2018). Role of mTOR Complexes in Neurogenesis. Int J Mol Sci *19*.

Lin, T.V., Hsieh, L., Kimura, T., Malone, T.J., and Bordey, A. (2016). Normalizing translation through 4E-BP prevents mTOR-driven cortical mislamination and ameliorates aberrant neuron integration. Proc Natl Acad Sci U S A *113*, 11330-11335.

Lipton, J.O., and Sahin, M. (2014). The neurology of mTOR. Neuron *84*, 275-291.

Liu, G.Y., and Sabatini, D.M. (2020). mTOR at the nexus of nutrition, growth, ageing and disease. Nat Rev Mol Cell Biol.

Liu, L., Das, S., Losert, W., and Parent, C.A. (2010). mTORC2 regulates neutrophil chemotaxis in a cAMP- and RhoA-dependent fashion. Dev Cell *19*, 845-857.

Liu, W., Ma, N., Zhao, D., Gao, X., Zhang, X., Yang, L., and Liu, D. (2019). Correlation between the DEPDC5 rs1012068 polymorphism and the risk of HBV-related hepatocellular carcinoma. Clin Res Hepatol Gastroenterol *43*, 446-450.

Livak, K.J., and Schmittgen, T.D. (2001). Analysis of relative gene expression data using real-time quantitative PCR and the 2(-Delta Delta C(T)) Method. Methods *25*, 402-408.

Long, X., Lin, Y., Ortiz-Vega, S., Yonezawa, K., and Avruch, J. (2005). Rheb binds and regulates the mTOR kinase. Curr Biol *15*, 702-713.

Lu, Z., Liu, F., Chen, L., Zhang, H., Ding, Y., Liu, J., Wong, M., and Zeng, L.H. (2015). Effect of Chronic Administration of Low Dose Rapamycin on Development and Immunity in Young Rats. PLoS One *10*, e0135256.

Ma, X.M., and Blenis, J. (2009). Molecular mechanisms of mTOR-mediated translational control. Nat Rev Mol Cell Biol *10*, 307-318.

Magri, L., Cambiaghi, M., Cominelli, M., Alfaro-Cervello, C., Cursi, M., Pala, M., Bulfone, A., Garcia-Verdugo, J.M., Leocani, L., Minicucci, F*., et al.* (2011). Sustained activation of mTOR pathway in embryonic neural stem cells leads to development of tuberous sclerosis complex-associated lesions. Cell Stem Cell *9*, 447-462.

Manifava, M., Smith, M., Rotondo, S., Walker, S., Niewczas, I., Zoncu, R., Clark, J., and Ktistakis, N.T. (2016). Dynamics of mTORC1 activation in response to amino acids. Elife *5*.

Maroof, A.M., Keros, S., Tyson, J.A., Ying, S.W., Ganat, Y.M., Merkle, F.T., Liu, B., Goulburn, A., Stanley, E.G., Elefanty, A.G*., et al.* (2013). Directed differentiation and functional maturation of cortical interneurons from human embryonic stem cells. Cell Stem Cell *12*, 559-572.

Marsan, E., Ishida, S., Schramm, A., Weckhuysen, S., Muraca, G., Lecas, S., Liang, N., Treins, C., Pende, M., Roussel, D*., et al.* (2016). Depdc5 knockout rat: A novel model of mTORopathy. Neurobiol Dis *89*, 180-189.

Martin, C., Meloche, C., Rioux, M.F., Nguyen, D.K., Carmant, L., Andermann, E., Gravel, M., and Cossette, P. (2014). A recurrent mutation in DEPDC5 predisposes to focal epilepsies in the French-Canadian population. Clin Genet *86*, 570-574.

Martina, J.A., Chen, Y., Gucek, M., and Puertollano, R. (2012). MTORC1 functions as a transcriptional regulator of autophagy by preventing nuclear transport of TFEB. Autophagy *8*, 903-914.

McCabe, M.P., Cullen, E.R., Barrows, C.M., Shore, A.N., Tooke, K.I., Laprade, K.A., Stafford, J.M., and Weston, M.C. (2020). Genetic inactivation of mTORC1 or mTORC2 in neurons reveals distinct functions in glutamatergic synaptic transmission. Elife *9*.

McCormick, D.A., and Contreras, D. (2001). On the cellular and network bases of epileptic seizures. Annu Rev Physiol *63*, 815-846.

McMahon, J., Huang, X., Yang, J., Komatsu, M., Yue, Z., Qian, J., Zhu, X., and Huang, Y. (2012). Impaired autophagy in neurons after disinhibition of mammalian target of rapamycin and its contribution to epileptogenesis. J Neurosci *32*, 15704-15714.

Meikle, L., Pollizzi, K., Egnor, A., Kramvis, I., Lane, H., Sahin, M., and Kwiatkowski, D.J. (2008). Response of a neuronal model of tuberous sclerosis to mammalian target of rapamycin (mTOR) inhibitors: effects on mTORC1 and Akt signaling lead to improved survival and function. J Neurosci *28*, 5422-5432.

Meng, J., and Ferguson, S.M. (2018). GATOR1-dependent recruitment of FLCN-FNIP to lysosomes coordinates Rag GTPase heterodimer nucleotide status in response to amino acids. J Cell Biol *217*, 2765-2776.

Miki, D., Ochi, H., Hayes, C.N., Abe, H., Yoshima, T., Aikata, H., Ikeda, K., Kumada, H., Toyota, J., Morizono, T.*, et al.* (2011). Variation in the DEPDC5 locus is associated with progression to hepatocellular carcinoma in chronic hepatitis C virus carriers. Nat Genet *43*, 797-800.

Mohamed, A.R., Bailey, C.A., Freeman, J.L., Maixner, W., Jackson, G.D., and Harvey, A.S. (2012). Intrinsic epileptogenicity of cortical tubers revealed by intracranial EEG monitoring. Neurology *79*, 2249-2257.

Moncada, S., Palmer, R.M., and Higgs, E.A. (1989). Biosynthesis of nitric oxide from L-arginine. A pathway for the regulation of cell function and communication. Biochem Pharmacol *38*, 1709-1715.

Morales-Corraliza, J., Gomez-Garre, P., Sanz, R., Diaz-Otero, F., Gutierrez-Delicado, E., and Serratosa, J.M. (2010). Familial partial epilepsy with variable foci: a new family with suggestion of linkage to chromosome 22q12. Epilepsia *51*, 1910-1914.

Murín, R., and Hamprecht, B. (2008). Metabolic and Regulatory Roles of Leucine in Neural Cells. Neurochemical Research *33*, 279-284.

Nadadhur, A.G., Alsaqati, M., Gasparotto, L., Cornelissen-Steijger, P., van Hugte, E., Dooves, S., Harwood, A.J., and Heine, V.M. (2019). Neuron-Glia Interactions Increase Neuronal Phenotypes in Tuberous Sclerosis Complex Patient iPSC-Derived Models. Stem Cell Reports *12*, 42-56.

Nascimento, F.A., Borlot, F., Cossette, P., Minassian, B.A., and Andrade, D.M. (2015). Two definite cases of sudden unexpected death in epilepsy in a family with a DEPDC5 mutation. Neurol Genet *1*, e28.

Nashef, L., So, E.L., Ryvlin, P., and Tomson, T. (2012). Unifying the definitions of sudden unexpected death in epilepsy. Epilepsia *53*, 227-233.

Nicholas, C.R., Chen, J., Tang, Y., Southwell, D.G., Chalmers, N., Vogt, D., Arnold, C.M., Chen, Y.J., Stanley, E.G., Elefanty, A.G.*, et al.* (2013). Functional maturation of hPSC-derived forebrain interneurons requires an extended timeline and mimics human neural development. Cell Stem Cell *12*, 573-586.

Okita, K., Matsumura, Y., Sato, Y., Okada, A., Morizane, A., Okamoto, S., Hong, H., Nakagawa, M., Tanabe, K., Tezuka, K.*, et al.* (2011). A more efficient method to generate integration-free human iPS cells. Nat Methods *8*, 409-412.

Pang, Y., Xie, F., Cao, H., Wang, C., Zhu, M., Liu, X., Lu, X., Huang, T., Shen, Y., Li, K.*, et al.* (2019). Mutational inactivation of mTORC1 repressor gene DEPDC5 in human gastrointestinal stromal tumors. Proc Natl Acad Sci U S A *116*, 22746-22753.

Park, S.M., Lim, J.S., Ramakrishina, S., Kim, S.H., Kim, W.K., Lee, J., Kang, H.C., Reiter, J.F., Kim, D.S., Kim, H.H.*, et al.* (2018). Brain Somatic Mutations in MTOR Disrupt Neuronal Ciliogenesis, Leading to Focal Cortical Dyslamination. Neuron *99*, 83-97.e87.

Parmigiani, A., Nourbakhsh, A., Ding, B., Wang, W., Kim, Y.C., Akopiants, K., Guan, K.L., Karin, M., and Budanov, A.V. (2014). Sestrins inhibit mTORC1 kinase activation through the GATOR complex. Cell Rep *9*, 1281-1291.

Pende, M., Um, S.H., Mieulet, V., Sticker, M., Goss, V.L., Mestan, J., Mueller, M., Fumagalli, S., Kozma, S.C., and Thomas, G. (2004). S6K1(-/-)/S6K2(-/-) mice exhibit perinatal lethality and rapamycin-sensitive 5'-terminal oligopyrimidine mRNA translation and reveal a mitogen-activated protein kinase-dependent S6 kinase pathway. Mol Cell Biol *24*, 3112-3124.

Peng, M., Yin, N., and Li, M.O. (2017). SZT2 dictates GATOR control of mTORC1 signalling. Nature *543*, 433-437.

Petit, C.S., Roczniak-Ferguson, A., and Ferguson, S.M. (2013). Recruitment of folliculin to lysosomes supports the amino acid-dependent activation of Rag GTPases. J Cell Biol *202*, 1107-1122.

Picard, F., Makrythanasis, P., Navarro, V., Ishida, S., de Bellescize, J., Ville, D., Weckhuysen, S., Fosselle, E., Suls, A., De Jonghe, P.*, et al.* (2014). DEPDC5 mutations in families presenting as autosomal dominant nocturnal frontal lobe epilepsy. Neurology *82*, 2101-2106.

Picon-Pages, P., Garcia-Buendia, J., and Munoz, F.J. (2019). Functions and dysfunctions of nitric oxide in brain. Biochim Biophys Acta Mol Basis Dis *1865*, 1949-1967.

Pierce, J.M.S. (2002). A DISEASE ONCE SACRED. A HISTORY OF THE MEDICAL UNDERSTANDING OF EPILEPSY. Brain *125*, 441-442.

Pinel, J.P., and Rovner, L.I. (1978). Electrode placement and kindling-induced experimental epilepsy. Exp Neurol *58*, 335-346.

Pitkanen, A., Roivainen, R., and Lukasiuk, K. (2016). Development of epilepsy after ischaemic stroke. Lancet Neurol *15*, 185-197.

Pressler, R., and Auvin, S. (2013). Comparison of Brain Maturation among Species: An Example in Translational Research Suggesting the Possible Use of Bumetanide in Newborn. Front Neurol *4*, 36.

Przyborski, S.A., Christie, V.B., Hayman, M.W., Stewart, R., and Horrocks, G.M. (2004). Human embryonal carcinoma stem cells: models of embryonic development in humans. Stem Cells Dev *13*, 400-408.

Ribierre, T., Deleuze, C., Bacq, A., Baldassari, S., Marsan, E., Chipaux, M., Muraca, G., Roussel, D., Navarro, V., Leguern, E.*, et al.* (2018a). Second-hit mosaic mutation in mTORC1 repressor DEPDC5 causes focal cortical dysplasia-associated epilepsy. J Clin Invest *128*, 2452-2458.

Ribierre, T., Deleuze, C., Bacq, A., Baldassari, S., Marsan, E., Chipaux, M., Muraca, G., Roussel, D., Navarro, V., Leguern, E.*, et al.* (2018b). Second-hit mosaic mutation in mTORC1 repressor DEPDC5 causes focal cortical dysplasia–associated epilepsy. The Journal of Clinical Investigation *128*, 2452-2458.

Ricos, M.G., Hodgson, B.L., Pippucci, T., Saidin, A., Ong, Y.S., Heron, S.E., Licchetta, L., Bisulli, F., Bayly, M.A., Hughes, J.*, et al.* (2016). Mutations in the mammalian target of rapamycin pathway regulators NPRL2 and NPRL3 cause focal epilepsy. Ann Neurol *79*, 120-131.

Roux, P.P., Shahbazian, D., Vu, H., Holz, M.K., Cohen, M.S., Taunton, J., Sonenberg, N., and Blenis, J. (2007). RAS/ERK signaling promotes site-specific ribosomal protein S6 phosphorylation via RSK and stimulates cap-dependent translation. J Biol Chem *282*, 14056-14064.

Roy, A., Skibo, J., Kalume, F., Ni, J., Rankin, S., Lu, Y., Dobyns, W.B., Mills, G.B., Zhao, J.J., Baker, S.J., *et al.* (2015). Mouse models of human PIK3CA-related brain overgrowth have acutely treatable epilepsy. eLife *4*.

Rozengurt, E., Soares, H.P., and Sinnet-Smith, J. (2014). Suppression of feedback loops mediated by PI3K/mTOR induces multiple overactivation of compensatory pathways: an unintended consequence leading to drug resistance. Mol Cancer Ther *13*, 2477-2488.

Rudack, T., Xia, F., Schlitter, J., Kötting, C., and Gerwert, K. (2012). Ras and GTPase-activating protein (GAP) drive GTP into a precatalytic state as revealed by combining FTIR and biomolecular simulations. Proceedings of the National Academy of Sciences *109*, 15295-15300.

Rushing, G.V., Brockman, A.A., Bollig, M.K., Leelatian, N., Mobley, B.C., Irish, J.M., Ess, K.C., Fu, C., and Ihrie, R.A. (2019). Location-dependent maintenance of intrinsic susceptibility to mTORC1-driven tumorigenesis. Life Sci Alliance *2*.

Ryvlin, P., Nashef, L., Lhatoo, S.D., Bateman, L.M., Bird, J., Bleasel, A., Boon, P., Crespel, A., Dworetzky, B.A., Høgenhaven, H., *et al.* (2013). Incidence and mechanisms of cardiorespiratory arrests in epilepsy monitoring units (MORTEMUS): a retrospective study. The Lancet Neurology *12*, 966-977.

Sabatini, D.M. (2017). Twenty-five years of mTOR: Uncovering the link from nutrients to growth. Proc Natl Acad Sci U S A *114*, 11818-11825.

Sabatini, D.M., Erdjument-Bromage, H., Lui, M., Tempst, P., and Snyder, S.H. (1994). RAFT1: a mammalian protein that binds to FKBP12 in a rapamycin-dependent fashion and is homologous to yeast TORs. Cell *78*, 35-43.

Salmon, A.B. (2015). About-face on the metabolic side effects of rapamycin. Oncotarget *6*, 2585-2586.

Sancak, Y., Bar-Peled, L., Zoncu, R., Markhard, A.L., Nada, S., and Sabatini, D.M. (2010). Ragulator-Rag complex targets mTORC1 to the lysosomal surface and is necessary for its activation by amino acids. Cell *141*, 290-303.

Sancak, Y., Peterson, T.R., Shaul, Y.D., Lindquist, R.A., Thoreen, C.C., Bar-Peled, L., and Sabatini, D.M. (2008). The Rag GTPases bind raptor and mediate amino acid signaling to mTORC1. Science *320*, 1496-1501.

Sancak, Y., Thoreen, C.C., Peterson, T.R., Lindquist, R.A., Kang, S.A., Spooner, E., Carr, S.A., and Sabatini, D.M. (2007). PRAS40 is an insulin-regulated inhibitor of the mTORC1 protein kinase. Mol Cell *25*, 903-915.

Sarbassov, D.D., Ali, S.M., Kim, D.H., Guertin, D.A., Latek, R.R., Erdjument-Bromage, H., Tempst, P., and Sabatini, D.M. (2004). Rictor, a novel binding partner of mTOR, defines a rapamycin-insensitive and raptor-independent pathway that regulates the cytoskeleton. Curr Biol *14*, 1296-1302.

Sarbassov, D.D., Ali, S.M., Sengupta, S., Sheen, J.H., Hsu, P.P., Bagley, A.F., Markhard, A.L., and Sabatini, D.M. (2006). Prolonged rapamycin treatment inhibits mTORC2 assembly and Akt/PKB. Mol Cell *22*, 159-168.

Sarbassov, D.D., Guertin, D.A., Ali, S.M., and Sabatini, D.M. (2005). Phosphorylation and regulation of Akt/PKB by the rictor-mTOR complex. Science *307*, 1098-1101.

Sardiello, M., Palmieri, M., di Ronza, A., Medina, D.L., Valenza, M., Gennarino, V.A., Di Malta, C., Donaudy, F., Embrione, V., Polishchuk, R.S., *et al.* (2009). A gene network regulating lysosomal biogenesis and function. Science *325*, 473-477.

Saré, R.M., Song, A., Loutaev, I., Cook, A., Maita, I., Lemons, A., Sheeler, C., and Smith, C.B. (2017). Negative Effects of Chronic Rapamycin Treatment on Behavior in a Mouse Model of Fragile X Syndrome. Front Mol Neurosci *10*, 452.

Saxton, R.A., Knockenhauer, K.E., Wolfson, R.L., Chantranupong, L., Pacold, M.E., Wang, T., Schwartz, T.U., and Sabatini, D.M. (2016). Structural basis for leucine sensing by the Sestrin2-mTORC1 pathway. Science *351*, 53-58.

Saxton, R.A., and Sabatini, D.M. (2017). mTOR Signaling in Growth, Metabolism, and Disease. Cell *169*, 361-371.

Scerri, T., Riseley, J.R., Gillies, G., Pope, K., Burgess, R., Mandelstam, S.A., Dibbens, L., Chow, C.W., Maixner, W., Harvey, A.S.*, et al.* (2015). Familial cortical dysplasia type IIA caused by a germline mutation in DEPDC5. Ann Clin Transl Neurol *2*, 575-580.

Scheffer, I.E., Berkovic, S., Capovilla, G., Connolly, M.B., French, J., Guilhoto, L., Hirsch, E., Jain, S., Mathern, G.W., Moshe, S.L.*, et al.* (2017). ILAE classification of the epilepsies: Position paper of the ILAE Commission for Classification and Terminology. Epilepsia *58*, 512-521.

Scheffer, I.E., Heron, S.E., Regan, B.M., Mandelstam, S., Crompton, D.E., Hodgson, B.L., Licchetta, L., Provini, F., Bisulli, F., Vadlamudi, L.*, et al.* (2014). Mutations in mammalian target of rapamycin regulator DEPDC5 cause focal epilepsy with brain malformations. Ann Neurol *75*, 782-787.

Settembre, C., Zoncu, R., Medina, D.L., Vetrini, F., Erdin, S., Erdin, S., Huynh, T., Ferron, M., Karsenty, G., Vellard, M.C.*, et al.* (2012). A lysosome-to-nucleus signalling mechanism senses and regulates the lysosome via mTOR and TFEB. Embo j *31*, 1095-1108.

Shah, O.J., Wang, Z., and Hunter, T. (2004). Inappropriate activation of the TSC/Rheb/mTOR/S6K cassette induces IRS1/2 depletion, insulin resistance, and cell survival deficiencies. Curr Biol *14*, 1650-1656.

Shahi, P.K., Hermans, D., Sinha, D., Brar, S., Moulton, H., Stulo, S., Borys, K.D., Capowski, E., Pillers, D.M., Gamm, D.M.*, et al.* (2019). Gene Augmentation and Readthrough Rescue Channelopathy in an iPSC-RPE Model of Congenital Blindness. Am J Hum Genet *104*, 310-318.

Shahjalal, H.M., Abdal Dayem, A., Lim, K.M., Jeon, T.I., and Cho, S.G. (2018). Generation of pancreatic β cells for treatment of diabetes: advances and challenges. Stem Cell Res Ther *9*, 355.

Shen, K., Huang, R.K., Brignole, E.J., Condon, K.J., Valenstein, M.L., Chantranupong, L., Bomaliyamu, A., Choe, A., Hong, C., Yu, Z.*, et al.* (2018). Architecture of the human GATOR1 and GATOR1-Rag GTPases complexes. Nature *556*, 64-69.

Shen, K., Valenstein, M.L., Gu, X., and Sabatini, D.M. (2019). Arg-78 of Nprl2 catalyzes GATOR1-stimulated GTP hydrolysis by the Rag GTPases. J Biol Chem *294*, 2970-2975.

Shi, Y., Kirwan, P., and Livesey, F.J. (2012a). Directed differentiation of human pluripotent stem cells to cerebral cortex neurons and neural networks. Nature Protocols *7*, 1836-1846.

Shi, Y., Kirwan, P., and Livesey, F.J. (2012b). Directed differentiation of human pluripotent stem cells to cerebral cortex neurons and neural networks. Nat Protoc *7*, 1836-1846.

Sim, J.C., Scerri, T., Fanjul-Fernandez, M., Riseley, J.R., Gillies, G., Pope, K., van Roozendaal, H., Heng, J.I., Mandelstam, S.A., McGillivray, G.*, et al.* (2016). Familial cortical dysplasia caused by mutation in the mammalian target of rapamycin regulator NPRL3. Ann Neurol *79*, 132-137.

Sokolov, A.M., Seluzicki, C.M., Morton, M.C., and Feliciano, D.M. (2018). Dendrite growth and the effect of ectopic Rheb expression on cortical neurons. Neurosci Lett *671*, 140-147.

Sun, T., and Hevner, R.F. (2014). Growth and folding of the mammalian cerebral cortex: from molecules to malformations. Nat Rev Neurosci *15*, 217-232.

Sveinsson, O., Andersson, T., Carlsson, S., and Tomson, T. (2017). The incidence of SUDEP: A nationwide population-based cohort study. Neurology *89*, 170-177.

Swaminathan, A., Hassan-Abdi, R., Renault, S., Siekierska, A., Riché, R., Liao, M., De Witte, P.A.M., Yanicostas, C., Soussi-Yanicostas, N., Drapeau, P.*, et al.* (2018). Non-canonical mTOR-Independent Role of DEPDC5 in Regulating GABAergic Network Development. Current Biology *28*, 1924-1937.e1925.

Takahashi, K., and Yamanaka, S. (2006). Induction of pluripotent stem cells from mouse embryonic and adult fibroblast cultures by defined factors. Cell *126*, 663-676.

Tang, G., Gudsnuk, K., Kuo, S.H., Cotrina, M.L., Rosoklija, G., Sosunov, A., Sonders, M.S., Kanter, E., Castagna, C., Yamamoto, A.*, et al.* (2014a). Loss of mTOR-dependent macroautophagy causes autistic-like synaptic pruning deficits. Neuron *83*, 1131-1143.

Tang, Y., Jiang, L., and Tang, W. (2014b). Decreased expression of NPRL2 in renal cancer cells is associated with unfavourable pathological, proliferation and apoptotic features. Pathol Oncol Res *20*, 829-837.

Thijs, R.D., Surges, R., O'Brien, T.J., and Sander, J.W. (2019). Epilepsy in adults. Lancet *393*, 689-701.

Thomson, J.A., Itskovitz-Eldor, J., Shapiro, S.S., Waknitz, M.A., Swiergiel, J.J., Marshall, V.S., and Jones, J.M. (1998). Embryonic stem cell lines derived from human blastocysts. Science *282*, 1145-1147.

Thoreen, C.C., Kang, S.A., Chang, J.W., Liu, Q., Zhang, J., Gao, Y., Reichling, L.J., Sim, T., Sabatini, D.M., and Gray, N.S. (2009). An ATP-competitive mammalian target of rapamycin inhibitor reveals rapamycin-resistant functions of mTORC1. J Biol Chem *284*, 8023-8032.

Thoreen, C.C., and Sabatini, D.M. (2009). Rapamycin inhibits mTORC1, but not completely. Autophagy *5*, 725-726.

Thurman, D.J., Hesdorffer, D.C., and French, J.A. (2014). Sudden unexpected death in epilepsy: assessing the public health burden. Epilepsia *55*, 1479-1485.

Tsai, M.H., Chan, C.K., Chang, Y.C., Yu, Y.T., Chuang, S.T., Fan, W.L., Li, S.C., Fu, T.Y., Chang, W.N., Liou, C.W.*, et al.* (2017). DEPDC5 mutations in familial and sporadic focal epilepsy. Clin Genet *92*, 397-404.

Tsun, Z.Y., Bar-Peled, L., Chantranupong, L., Zoncu, R., Wang, T., Kim, C., Spooner, E., and Sabatini, D.M. (2013). The folliculin tumor suppressor is a GAP for the RagC/D GTPases that signal amino acid levels to mTORC1. Mol Cell *52*, 495-505.

Urbanska, M., Gozdz, A., Swiech, L.J., and Jaworski, J. (2012). Mammalian target of rapamycin complex 1 (mTORC1) and 2 (mTORC2) control the dendritic arbor morphology of hippocampal neurons. J Biol Chem *287*, 30240-30256.

van Kranenburg, M., Hoogeveen-Westerveld, M., and Nellist, M. (2015). Preliminary functional assessment and classification of DEPDC5 variants associated with focal epilepsy. Hum Mutat *36*, 200-209.

Van Loo, K.M.J., and Becker, A.J. (2020). Transcriptional Regulation of Channelopathies in Genetic and Acquired Epilepsies. Frontiers in Cellular Neuroscience *13*.

Wang, S., Tsun, Z.Y., Wolfson, R.L., Shen, K., Wyant, G.A., Plovanich, M.E., Yuan, E.D., Jones, T.D., Chantranupong, L., Comb, W.*, et al.* (2015). Metabolism. Lysosomal amino acid transporter SLC38A9 signals arginine sufficiency to mTORC1. Science *347*, 188-194.

Weckhuysen, S., Marsan, E., Lambrecq, V., Marchal, C., Morin-Brureau, M., An-Gourfinkel, I., Baulac, M., Fohlen, M., Kallay Zetchi, C., Seeck, M.*, et al.* (2016). Involvement of GATOR complex genes in familial focal epilepsies and focal cortical dysplasia. Epilepsia *57*, 994-1003.

Wei, Y., and Lilly, M.A. (2014). The TORC1 inhibitors Nprl2 and Nprl3 mediate an adaptive response to amino-acid starvation in Drosophila. Cell Death Differ *21*, 1460-1468.

Wei, Y., Reveal, B., Cai, W., and Lilly, M.A. (2016). The GATOR1 Complex Regulates Metabolic Homeostasis and the Response to Nutrient Stress in Drosophila melanogaster. G3 (Bethesda) *6*, 3859-3867.

Weston, M.C., Chen, H., and Swann, J.W. (2014). Loss of mTOR repressors Tsc1 or Pten has divergent effects on excitatory and inhibitory synaptic transmission in single hippocampal neuron cultures. Front Mol Neurosci *7*, 1.

Wilson, J.V., and Reynolds, E.H. (1990). Texts and documents. Translation and analysis of a cuneiform text forming part of a Babylonian treatise on epilepsy. Med Hist *34*, 185-198.

Winden, K.D., Sundberg, M., Yang, C., Wafa, S.M.A., Dwyer, S., Chen, P.F., Buttermore, E.D., and Sahin, M. (2019). Biallelic Mutations in TSC2 Lead to Abnormalities Associated with Cortical Tubers in Human iPSC-Derived Neurons. J Neurosci *39*, 9294-9305.

Wolfson, R.L., Chantranupong, L., Saxton, R.A., Shen, K., Scaria, S.M., Cantor, J.R., and Sabatini, D.M. (2016). Sestrin2 is a leucine sensor for the mTORC1 pathway. Science *351*, 43-48.

Wolfson, R.L., Chantranupong, L., Wyant, G.A., Gu, X., Orozco, J.M., Shen, K., Condon, K.J., Petri, S., Kedir, J., Scaria, S.M.*, et al.* (2017). KICSTOR recruits GATOR1 to the lysosome and is necessary for nutrients to regulate mTORC1. Nature *543*, 438-442.

Wolfson, R.L., and Sabatini, D.M. (2017). The Dawn of the Age of Amino Acid Sensors for the mTORC1 Pathway. Cell Metab *26*, 301-309.

Wyant, G.A., Abu-Remaileh, M., Wolfson, R.L., Chen, W.W., Freinkman, E., Danai, L.V., Vander Heiden, M.G., and Sabatini, D.M. (2017). mTORC1 Activator SLC38A9 Is Required to Efflux Essential Amino Acids from Lysosomes and Use Protein as a Nutrient. Cell *171*, 642-654.e612.

Xie, G.X., and Palmer, P.P. (2007). How regulators of G protein signaling achieve selective regulation. J Mol Biol *366*, 349-365.

Yang, H., Rudge, D.G., Koos, J.D., Vaidialingam, B., Yang, H.J., and Pavletich, N.P. (2013). mTOR kinase structure, mechanism and regulation. Nature *497*, 217-223.

Yates, J.R., Maclean, C., Higgins, J.N., Humphrey, A., le Marechal, K., Clifford, M., Carcani-Rathwell, I., Sampson, J.R., and Bolton, P.F. (2011). The Tuberous Sclerosis 2000 Study: presentation, initial assessments and implications for diagnosis and management. Arch Dis Child *96*, 1020-1025.

York, G.K., and Steinberg, D.A. (2007). An Introduction to the Life and Work of John Hughlings Jackson: Introduction. Med Hist Suppl, 3-34.

Yu, Y., Yoon, S.O., Poulogiannis, G., Yang, Q., Ma, X.M., Villen, J., Kubica, N., Hoffman, G.R., Cantley, L.C., Gygi, S.P.*, et al.* (2011). Phosphoproteomic analysis identifies Grb10 as an mTORC1 substrate that negatively regulates insulin signaling. Science *332*, 1322-1326.

Yuskaitis, C.J., Jones, B.M., Wolfson, R.L., Super, C.E., Dhamne, S.C., Rotenberg, A., Sabatini, D.M., Sahin, M., and Poduri, A. (2018). A mouse model of DEPDC5 -related epilepsy: Neuronal loss of Depdc5 causes dysplastic and ectopic neurons, increased mTOR signaling, and seizure susceptibility. Neurobiology of Disease *111*, 91-101.

Yuskaitis, C.J., Rossitto, L.-A., Gurnani, S., Bainbridge, E., Poduri, A., and Sahin, M. (2019). Chronic mTORC1 inhibition rescues behavioral and biochemical deficits resulting from neuronal Depdc5 loss in mice. Human Molecular Genetics.

Zainal Abidin, N., Haq, I.J., Gardner, A.I., and Brodlie, M. (2017). Ataluren in cystic fibrosis: development, clinical studies and where are we now? Expert Opin Pharmacother *18*, 1363-1371.

Zhang, C.S., Jiang, B., Li, M., Zhu, M., Peng, Y., Zhang, Y.L., Wu, Y.Q., Li, T.Y., Liang, Y., Lu, Z.*, et al.* (2014). The lysosomal v-ATPase-Ragulator complex is a common activator for AMPK and mTORC1, acting as a switch between catabolism and anabolism. Cell Metab *20*, 526-540.

Zhang, Y., Pak, C., Han, Y., Ahlenius, H., Zhang, Z., Chanda, S., Marro, S., Patzke, C., Acuna, C., Covy, J.*, et al.* (2013). Rapid single-step induction of functional neurons from human pluripotent stem cells. Neuron *78*, 785-798.

Zhang, Y., Xu, S., Liang, K.Y., Li, K., Zou, Z.P., Yang, C.L., Tan, K., Cao, X., Jiang, Y., Gao, T.M.*, et al.* (2017). Neuronal mTORC1 Is Required for Maintaining the Nonreactive State of Astrocytes. J Biol Chem *292*, 100-111.

Zhou, J., Blundell, J., Ogawa, S., Kwon, C.H., Zhang, W., Sinton, C., Powell, C.M., and Parada, L.F. (2009a). Pharmacological Inhibition of mTORC1 Suppresses Anatomical, Cellular, and Behavioral Abnormalities in Neural-Specific Pten Knock-Out Mice. Journal of Neuroscience *29*, 1773-1783.

Zhou, Y.D., Lee, S., Jin, Z., Wright, M., Smith, S.E., and Anderson, M.P. (2009b). Arrested maturation of excitatory synapses in autosomal dominant lateral temporal lobe epilepsy. Nat Med *15*, 1208-1214.